

Chapter-3

RESULTS AND DISCUSSION

The results of geochemical and isotopic studies carried out in samples from various formations of the Vindhyan Supergroup in Rajasthan are presented in this chapter. Attempts have been made to interpret these results in terms of their implications for the sources of the sediments and for the tectonic evolution of the Vindhyan Basin during the Proterozoic Eon. Apart for our own results, geochemical data from other sources, especially those for the basement and older rocks surrounding the basin, have also been used in discussion.

3.1 Results

3.1.1 Geochemical Data

The data for major element and trace element contents, radiogenic isotopic ratios, stable isotopic ratios in carbonates and U-Pb dating of zircon are presented in various tables in the following pages. The data tables are arranged according to the stratigraphic order of the groups and formations. Concentrations of major elements are presented in 'wt%' of their oxides, whereas those of trace elements are in 'ppm'. Sr and Nd isotopic ratios measured in our samples are presented as $^{87}\text{Sr}/^{86}\text{Sr}_m$ and $^{143}\text{Nd}/^{144}\text{Nd}_m$. Since the variations in $^{143}\text{Nd}/^{144}\text{Nd}$ are extremely low, we make use of the $\epsilon_{\text{Nd}}(0)$ parameter which is defined as:

$$\varepsilon_{Nd}(0) = \left[\frac{\left(\frac{^{143}Nd}{^{144}Nd} \right)_s^p}{\left(\frac{^{143}Nd}{^{144}Nd} \right)_{CHUR}^p} - 1 \right] \times 10^4$$

$$\varepsilon_{Nd}(T) = \left[\frac{\left(\frac{^{143}Nd}{^{144}Nd} \right)_s^T}{\left(\frac{^{143}Nd}{^{144}Nd} \right)_{CHUR}^T} - 1 \right] \times 10^4$$

where subscript 's' and 'CHUR', respectively stand for sample and Chondritic Uniform Reservoir and superscript 'p' and 'T' stand for present day and at T years respectively. The present day $^{143}Nd/^{144}Nd$ ratio in the CHUR is 0.512638 (Depaolo and Wasserburg, 1976).

The Sm-Nd model dates, calculated for the various Vindhyan formations, are also presented in the tables with respect to CHUR and depleted mantle (DM). The model dates T_{CHUR} and T_{DM} respectively are calculated using the following relations,

$$T_{CHUR} = (1/\lambda) \ln \left[1 + \frac{\left(\frac{^{143}Nd}{^{144}Nd} \right)_s - \left(\frac{^{143}Nd}{^{144}Nd} \right)_{CHUR}}{\left(\frac{^{147}Sm}{^{144}Nd} \right)_s - \left(\frac{^{147}Sm}{^{144}Nd} \right)_{CHUR}} \right]$$

$$T_{DM} = (1/\lambda) \ln \left[1 + \frac{\left(\frac{^{143}Nd}{^{144}Nd} \right)_s - \left(\frac{^{143}Nd}{^{144}Nd} \right)_{DM}}{\left(\frac{^{147}Sm}{^{144}Nd} \right)_s - \left(\frac{^{147}Sm}{^{144}Nd} \right)_{DM}} \right]$$

where $(^{143}\text{Nd}/^{144}\text{Nd})_{\text{CHUR}} = 0.512638$ and $(^{147}\text{Sm}/^{144}\text{Nd})_{\text{CHUR}} = 0.1967$; after DePalo & Wasserburg (1976) and $(^{143}\text{Nd}/^{144}\text{Nd})_{\text{DM}} = 0.513114$ and $(^{147}\text{Sm}/^{144}\text{Nd})_{\text{DM}} = 0.222$; after Michard et al. (1985).

The parameter $f_{\text{Sm}/\text{Nd}}$, presented in the tables was calculated using the following relationship:

$$f_{\frac{\text{Sm}}{\text{Nd}}} = \left[\frac{\left(\frac{^{147}\text{Sm}}{^{144}\text{Nd}} \right)_S}{\left(\frac{^{147}\text{Sm}}{^{144}\text{Nd}} \right)_{\text{CHUR}}} - 1 \right]$$

For normalization of data we have utilized data for various hypothetical reservoirs such as CHUR, Primitive Mantle (PM), Post Archean Average Australian Sedimentary Rocks (PAAS) and Upper Continental Crust (UCC). The sources of these data are from McDonough & Sun (1995), McLennan et al. (1989) and Taylor and McLennan (1985), respectively. Table 3.1 through 3.5 present the geochemical data for Pre-Vindhyan rocks and various formations of the Vindhyan Supergroup in Rajasthan.

3.1.2 U-Pb analytical data for detrital zircons

Detrital zircons from the Sawa Sandstone Formation from Chittorgarh area were dated using U-Pb method on a SHRIMP-II. The analytical data: concentration of U, Th, Pb and various isotopic ratios are presented in Table 3.6. Table 3.6 also presents the $^{207}\text{Pb}/^{206}\text{Pb}$ apparent ages and percent discordance of the data.

3.1.3 $\delta^{13}\text{C}$ and $\delta^{18}\text{O}$ data from limestones

The stable isotopic compositions of C and O from the two limestone formations are presented in form of the change in the isotopic ratios of C and O in comparison to

those in the Pee Dee Belemnite (PDB) standard. The stable isotope data are presented as $\delta^{13}\text{C}$ and $\delta^{18}\text{O}$ in permil. These are defined as follows:

$$\delta^{13}\text{C}_{PDB} = \left[\frac{\left(\frac{^{13}\text{C}}{^{12}\text{C}} \right)_{\text{Sample}}}{\left(\frac{^{13}\text{C}}{^{12}\text{C}} \right)_{PDB}} - 1 \right] * 1000$$

$$\delta^{18}\text{O}_{PDB} = \left[\frac{\left(\frac{^{18}\text{O}}{^{16}\text{O}} \right)_{\text{Sample}}}{\left(\frac{^{18}\text{O}}{^{16}\text{O}} \right)_{PDB}} - 1 \right] * 1000$$

During the analyses of our samples measurements were also done routinely for an international standard, NBS-19, from the International Atomic Energy Agency (IAEA) and for a local laboratory standard, the Makarana Marble (MMB), which were pre-calibrated against PDB. The results for the standards are presented in Table 3.7.

The $\delta^{13}\text{C}$ and $\delta^{18}\text{O}$ data for the Lakheri Limestone Formation are presented in Table 3.8. The Balwan Limestone Formation was sampled in more detailed fashion considering its stratigraphic position within the Vindhyan Supergroup. The results of C and O isotope analyses for this formation are given in Table 3.9.

3.1.4 $^{87}\text{Sr}/^{86}\text{Sr}$ data from limestones

For Sr isotopic stratigraphy samples of the Lakheri Limestone and the Balwan Limestone formations were selected based on their $\delta^{13}\text{C}$ and $\delta^{18}\text{O}$ compositions and trace element contents. The trace elements ratios (Table 3.10), such as Mn/Sr, were used as a proxy for alteration and samples with lowest values of Mn/Sr were analysed for $^{87}\text{Sr}/^{86}\text{Sr}$. These samples essentially represent least altered carbonate components in the whole rock samples. The $^{87}\text{Sr}/^{86}\text{Sr}$ ratio data are presented in Table 3.11.

Table 3.1: Geochemical data for Pre-Vindhyan rocks and basal volcanics of the Vindhyan near Chittorgarh.

	<i>CGB07-03 Berach Granite</i>	<i>CGB07-06 Berach Granite</i>	<i>CHITTOR-09-23B Metavolcanics</i>	<i>CGB07-08 Metavolcanics</i>	<i>CHITTOR-09-26 Khairmalla</i>	<i>CHITTOR-09-25 Khairmalla</i>	<i>CHITTOR-09-24 Metavolcanics</i>
SiO ₂	61.10	56.66	47.82	42.06	61.86	55.13	44.71
TiO ₂	0.43	0.66	0.74	1.36	0.12	0.55	1.73
Al ₂ O ₃	13.95	12.25	13.04	9.80	3.28	13.90	10.72
Fe ₂ O ₃	3.61	4.99	8.58	14.98	bdl	5.38	14.51
MnO	0.02	0.06	0.04	0.11	0.03	0.09	0.15
MgO	2.48	2.62	3.33	9.27	10.85	5.52	5.36
CaO	0.22	1.72	0.35	2.60	11.58	1.71	8.45
Na ₂ O	bdl	2.38	bdl	0.29	bdl	2.89	1.77
K ₂ O	6.63	3.86	4.93	3.72	2.25	2.76	0.97
P ₂ O ₅	0.09	0.18	0.11	0.17	0.07	0.18	0.21
LOI	1.67	1.99	3.87	4.38		3.19	1.91
TOTAL	90.21	87.35	82.81	88.73	105.44	91.29	90.49
Rb	259	103	301	109	53.9	151	36.2
Sr	17.1	142	145	133	112	237	220
Ba	1172	1206	390	1624	313	816	235
Y	14.3	15.0	19.3	18.9	1.92	1bdl	23.65
Zr	125	63.4	123	137	18.1	98.8	89.0
Hf	4.05	1.99	3.45	3.79	0.56	2.59	2.61
Nb	12.6	12.9	13.0	10.0	1.66	5.85	8.90
Ta	0.84	0.86	1.01	0.61	0.15	0.41	0.49
Th	31.6	6.44	21.9	3.07	5.44	11.9	2.71
U	4.02	2.10	2.96	0.52	0.39	1.91	0.54
La	16.9	31.0	55.1	20.7	9.66	38.2	17.5
Ce	31.9	63.1	107	42.1	16.27	71.5	38.0
Pr	2.76	7.29	11.8	4.45	1.63	7.71	5.14
Nd	12.8	31.8	41.8	21.9	4.95	27.4	21.7
Sm	2.50	5.68	8.65	4.75	0.89	5.48	5.27
Eu	0.51	1.26	1.34	1.98	0.21	1.15	1.61
Gd	2.70	4.49	6.57	4.85	0.64	3.93	5.53
Tb	0.44	0.58	0.72	0.74	0.05	0.40	0.80
Dy	2.82	3.02	4.17	4.44	0.40	2.19	5.23
Ho	0.58	0.57	0.76	0.84	0.07	0.37	0.96
Er	1.73	1.58	2.44	2.20	0.23	1.16	2.86
Tm	0.27	0.23	0.34	0.30	0.03	0.15	0.36
Yb	2.03	1.68	2.40	2.11	0.23	1.11	2.39
Lu	0.29	0.23	0.36	0.28	0.04	0.17	0.34
Sc	0.02	3.98	18.6	37.18	bdl	8.36	28.37
V	bdl	18.01	88.5	360	3.17	73.4	291
Cr	bdl	bdl	111	166	bdl	18.4	66.0
Co	bdl	4.53	27.1	43.1	0.94	11.8	41.6
Ni	bdl	0.29	43.5	44.34	bdl	7.36	34.88
Pb	21.9	11.1	6.24	93.1	3.84	6.25	4.14
Cs			9.17		0.82	2.85	1.58
⁸⁷ Sr/ ⁸⁶ Sr _m	1.05362	0.76331	1.96917	0.75992	0.85778	0.74595	0.71769
¹⁴³ Nd/ ¹⁴⁴ Nd _m	0.510999	0.511091	0.511291		0.510919	0.510964	0.512015
ε _{Nd} (0)	-32.0	-30.2	-26.3		-33.5	-32.7	-12.2
T _{CHUR}	3.16	2.65	2.86		2.97	3.35	1.90
T _{DM}	3.08	2.69	2.85		2.94	3.22	2.22
f _{SmNd}	-0.40	-0.45	-0.36	-0.33	-0.45	-0.38	-0.25

Table 3.2: Geochemical data for samples from various formations of the Semri Group.

	<i>CHITTOR-09-20</i> <i>Khardeola SST</i>	<i>CGB07-11</i> <i>Bhadesar QTZ</i>	<i>CGB07-12</i> <i>Bhadesar QTZ</i>	<i>CGB07-04</i> <i>Quartzite</i>	<i>CGB07-07</i> <i>Bhadesar QTZ</i>
SiO ₂	79.41	97.66	75.98	90.67	85.09
TiO ₂	0.04	0.09	0.04	0.18	0.08
Al ₂ O ₃	1.44	0.00	3.29	4.54	0.00
Fe ₂ O ₃	1.30	0.41	0.12	0.11	1.96
MnO	0.02	0.00	0.02	0.00	0.01
MgO		0.02	0.18	0.00	0.40
CaO		0.00	0.02	0.25	0.23
Na ₂ O		0.00	0.19	0.00	0.00
K ₂ O	0.05	0.00	4.21	1.46	0.67
P ₂ O ₅		0.02	0.01	0.00	0.30
LOI	0.44	0.19	0.74	0.81	0.66
TOTAL	82.70	98.39	84.79	98.01	89.40
Rb	1.63		107.48	42.21	
Sr	89.18		30.52	4.13	
Ba	20.90		627.20	157.50	
Y	3.15		1.19	1.29	
Zr	38.73		29.55	9.30	
Hf	1.08		0.82	0.32	
Nb	0.52		0.85	0.28	
Ta	0.04		0.07	0.05	
Th	2.32		9.15	1.27	
U	0.64		1.13	2.55	
La	9.93		6.52	4.89	
Ce	20.48		12.34	8.00	
Pr	2.27		0.52	bdl	
Nd	7.77		4.74	2.71	
Sm	1.60		0.59	0.32	
Eu	0.24		0.19	0.07	
Gd	1.11		0.38	0.23	
Tb	0.11		0.04	0.03	
Dy	0.69		0.18	0.15	
Ho	0.13		0.04	0.04	
Er	0.42		0.13	0.14	
Tm	0.06		0.02	0.02	
Yb	0.41		0.18	0.17	
Lu	0.07		0.03	0.02	
Sc	0.68		bdl	bdl	
V	17.43		6.78	bdl	
Cr	4.46		bdl	bdl	
Co	0.00		bdl	0.80	
Ni	4.36		bdl	bdl	
Pb	2.26		19.85	9.54	
Cs	0.14				
⁸⁷ Sr/ ⁸⁶ Sr _m	0.73557		0.92481	0.92304	
¹⁴³ Nd/ ¹⁴⁴ Nd _m	0.511579		0.511658	0.510928	
$\epsilon_{Nd}(0)$	-20.7		-19.1	-33.4	
T _{CHUR}	2.23		1.22	2.07	
T _{DM}	2.39		1.50	2.20	
f _{Sm/Nd}	-0.37		-0.62	-0.64	

QTZ: Quartzite; SST: Sandstone; SH: Shale and LST: Limestone

Table 3.2 continued...

	CGB07-14 Bhagwanpura LST		CGB07-05 Bhagwanpura LST		CGB07-13 Bhagwanpura LST	
SiO ₂	16.65		9.39		14.13	
TiO ₂	0.11		0.11		0.12	
Al ₂ O ₃	0.00		0.00		0.00	
Fe ₂ O ₃	0.97		1.67		1.28	
MnO	0.03		0.20		0.04	
MgO	12.79		1.04		13.64	
CaO	36.38		63.76		38.75	
Na ₂ O	0.00		0.00		0.00	
K ₂ O	0.77		0.00		0.81	
P ₂ O ₅	0.03		0.07		0.03	
LOI	-		-		-	
TOTAL	67.73		76.24		68.80	
	Sil.	Carb.	Sil.	Carb.		
Rb				1.01		
Sr				290.90		
Ba				8.32		
Y				21.73		
Zr				bdl		
Hf				0.01		
Nb				bdl		
Ta				bdl		
Th				0.19		
U				bdl		
La				29.46		
Ce				38.26		
Pr				3.43		
Nd				17.17		
Sm				3.61		
Eu				2.23		
Gd				4.13		
Tb				0.52		
Dy				2.80		
Ho				0.55		
Er				1.43		
Tm				0.19		
Yb				1.31		
Lu				0.17		
Sc				bdl		
V				bdl		
Cr				4.78		
Co				1.71		
Ni				0.80		
Pb				5.87		
Cs						
⁸⁷ Sr/ ⁸⁶ Sr _m	0.81884	0.71446	0.75906	0.75906		
¹⁴³ Nd/ ¹⁴⁴ Nd _m		0.511412	0.511241	0.511241		
ε _{Nd(0)}		-23.9	-27.3	-27.3		
T _{CHUR}		2.68	3.04	3.04		
T _{DM}		2.72	2.99	2.99		
f _{Sm/Nd}	-0.35		-0.35	-0.35		

Table 3.2 continued..

	CGB07-09 Khardeola SH	CGB07-10 Khardeola SH	CGB07-02 Sawa Grit	CGB07-15 Sawa SST	CGB07-16 Sawa SST
SiO ₂	56.39	55.90	100.15	74.17	86.95
TiO ₂	0.69	0.69	0.08	0.66	0.01
Al ₂ O ₃	23.34	22.98	0.28	8.13	0.00
Fe ₂ O ₃	5.66	5.62	0.38	3.50	0.20
MnO	0.02	0.02	0.00	0.01	0.01
MgO	1.54	1.53	0.04	0.00	0.07
CaO	0.15	0.15	0.00	0.21	0.08
Na ₂ O	0.29	0.30	0.00	0.00	0.17
K ₂ O	6.12	6.09	0.11	1.32	0.00
P ₂ O ₅	0.08	0.08	0.02	0.00	0.00
LOI	2.92	3.18	0.86	1.48	0.53
TOTAL	97.19	96.52	101.92	89.47	88.02
Rb	263.60	302.50		35.57	6.87
Sr	43.64	40.19		0.99	Bdl
Ba	580.30	416.80		62.25	13.92
Y	35.93	26.49		16.68	0.62
Zr	121.30	106.90		195.00	12.86
Hf	3.63	3.31		5.49	0.44
Nb	14.08	12.84		5.29	0.06
Ta	1.27	1.11		0.31	0.01
Th	26.19	24.63		14.56	1.97
U	4.73	3.72		1.98	0.69
La	47.56	60.25		12.13	2.54
Ce	90.09	105.30		22.73	4.20
Pr	9.82	12.49		2.20	Bdl
Nd	38.85	47.17		11.70	1.68
Sm	7.37	8.57		2.56	0.21
Eu	1.40	1.62		0.62	0.03
Gd	7.26	7.37		3.21	0.13
Tb	1.07	0.95		0.49	0.02
Dy	6.46	5.06		2.83	0.05
Ho	1.28	0.96		0.54	0.02
Er	3.53	2.61		1.49	0.05
Tm	0.51	0.36		0.21	0.01
Yb	3.53	2.67		1.55	0.10
Lu	0.48	0.36		0.22	0.02
Sc	14.50	15.85		0.92	bdl
V	69.33	77.45		14.73	bdl
Cr	90.42	100.10		8.76	bdl
Co	15.62	6.41		0.02	bdl
Ni	27.43	24.94		2.34	bdl
Pb	14.81	8.16		11.62	10.84
Cs					
⁸⁷ Sr/ ⁸⁶ Sr _m	1.07899	0.99102		0.88497	0.82709
¹⁴³ Nd/ ¹⁴⁴ Nd _m	0.511314	0.51143		0.511439	0.511481
ε _{Nd(0)}	-25.8	-23.6		-23.4	-22.6
T _{CHUR}	2.43	2.14		2.80	1.44
T _{DM}	2.53	2.31		2.81	1.68
f _{Sm/Nd}	-0.42	-0.44		-0.33	-0.62

<i>Table 3.2 continued.</i>					
	<i>CHITTOR-09-21 Sawa (Palri) SH</i>	<i>CGB07-17 Binota Shale</i>	<i>CHITTOR-09-19 Binota Shale</i>	<i>CGB07-23 NimbaheraSH</i>	<i>CGB07-24 Nimbahera SH</i>
SiO ₂	58.45	73.43	61.04	65.46	54.59
TiO ₂	0.75	0.51	0.70	0.76	0.98
Al ₂ O ₃	12.41	6.57	13.13	15.05	24.43
Fe ₂ O ₃	3.72	1.28	5.29	3.41	4.73
MnO	0.02	0.02	0.02	0.04	0.02
MgO	0.44	0.80	0.44	0.69	0.91
CaO		0.58	-0.08	0.18	0.21
Na ₂ O	0.35	0.19	0.30	0.53	0.72
K ₂ O	3.00	2.46	3.15	2.95	3.92
P ₂ O ₅	0.02	0.37	0.01	0.03	0.03
LOI	3.83	2.81	3.89	3.21	4.57
TOTAL	82.99	89.02	87.90	92.29	95.09
Rb	185.45	113.75		167.05	
Sr	165.50	187.10		61.14	
Ba	378.00	351.90		438.80	
Y	26.56	26.77		20.15	
Zr	192.20	101.50		151.00	
Hf	5.12	3.21		4.69	
Nb	5.20	7.85		14.94	
Ta	0.37	0.60		1.14	
Th	19.54	11.31		21.00	
U	3.46	6.77		3.32	
La	55.80	14.56		47.14	
Ce	120.40	28.80		106.30	
Pr	12.82	4.14		10.00	
Nd	46.59	22.81		37.06	
Sm	9.79	5.54		6.43	
Eu	1.48	1.13		1.13	
Gd	7.25	4.96		5.24	
Tb	0.85	0.71		0.72	
Dy	5.16	4.33		4.06	
Ho	0.96	0.93		0.81	
Er	3.15	2.85		2.36	
Tm	0.44	0.46		0.36	
Yb	3.19	3.59		2.70	
Lu	0.48	0.53		0.38	
Sc	15.23	8.30		10.72	
V	109.30	373.70		73.84	
Cr	54.75	41.86		52.35	
Co	8.69	4.29		4.91	
Ni	17.67	47.37		3.89	
Pb	17.83	22.73		19.61	
Cs	8.52				
⁸⁷ Sr/ ⁸⁶ Sr _m	0.82945	0.74781		0.82574	
¹⁴³ Nd/ ¹⁴⁴ Nd _m	0.51169	0.511975		0.511645	
$\epsilon_{Nd}(0)$	-18.5	-12.9		-19.4	
T _{CHUR}	2.07	2.02		1.65	
T _{DM}	2.28	2.30		1.91	
$f_{Sm/Nd}$	-0.35	-0.25		-0.47	

Table 3.2 continued..

	CGB07-18 Nimbahera LST	CGB07-19 Suket SH	CGB07-22A Suket SH	CGB07-22B Suket SH
SiO ₂	23.41	65.13	64.44	73.15
TiO ₂	0.13	0.70	0.62	0.62
Al ₂ O ₃	0.00	6.59	9.66	7.02
Fe ₂ O ₃	0.95	7.52	6.17	3.68
MnO	0.03	0.02	0.00	0.00
MgO	0.63	1.18	0.75	0.56
CaO	56.29	0.21	0.07	0.04
Na ₂ O	0.08	0.20	0.00	0.00
K ₂ O	0.76	1.32	1.50	1.22
P ₂ O ₅	0.34	0.03	0.02	0.03
LOI		3.03	2.60	1.95
TOTAL	82.61	85.91	85.82	88.28
Rb	6.61	68.47		
Sr	239.90	16.90		
Ba	39.78	203.20		
Y	16.46	14.68		
Zr	bdl	154.70		
Hf	0.06	4.83		
Nb	bdl	6.38		
Ta	bdl	0.56		
Th	5.10	13.77		
U	0.28	2.41		
La	16.85	19.03		
Ce	29.68	36.99		
Pr	2.72	3.64		
Nd	14.87	16.63		
Sm	2.84	3.19		
Eu	0.56	0.63		
Gd	2.96	3.18		
Tb	0.43	0.49		
Dy	2.67	2.94		
Ho	0.54	0.58		
Er	1.48	1.64		
Tm	0.21	0.25		
Yb	1.44	1.93		
Lu	0.19	0.27		
Sc	0.83	4.50		
V	bdl	33.91		
Cr	bdl	18.92		
Co	3.02	5.69		
Ni	5.96	20.49		
Pb	29.28	14.07		
Cs				
⁸⁷ Sr/ ⁸⁶ Sr _m	0.71033	0.81791	0.82299	0.81018
¹⁴³ Nd/ ¹⁴⁴ Nd _m	0.511881	0.511795	0.510894	0.51176
E _{Nd} (0)	-14.8	-16.4	-34.0	-17.1
T _{CHUR}	1.42	1.59	3.27	0.98
T _{DM}	1.76	1.89	3.17	1.28
f _{Sm/Nd}	-0.41	-0.41	-0.41	-0.69

Table 3.3: Geochemical data for samples from the Kaimur Group.

	CGB07-20 Kaimur SST	CGB07-21 Kaimur SST
SiO ₂	97.47	95.43
TiO ₂	0.02	0.10
Al ₂ O ₃		
Fe ₂ O ₃	0.14	0.44
MnO	0.01	
MgO	0.03	0.03
CaO	0.10	
Na ₂ O	0.16	
K ₂ O		
P ₂ O ₅	0.01	0.02
LOI	0.29	0.29
TOTAL	98.24	96.31
Rb		2.19
Sr		5.76
Ba		12.45
Y		1.68
Zr		24.23
Hf		0.40
Nb		0.17
Ta		0.01
Th		0.97
U		0.18
La		10.58
Ce		25.48
Pr		0.58
Nd		7.54
Sm		0.76
Eu		0.11
Gd		0.50
Tb		0.05
Dy		0.16
Ho		0.04
Er		0.12
Tm		0.02
Yb		0.15
Lu		0.02
Sc		bdl
V		bdl
Cr		bdl
Co		bdl
Ni		bdl
Pb		1.58
Cs		
⁸⁷ Sr/ ⁸⁶ Sr _m		0.72875
¹⁴³ Nd/ ¹⁴⁴ Nd _m		0.511703
ε _{Nd} (0)		-18.2
T _{CHUR}		1.05
T _{DM}		1.33
f _{Sm/Nd}		-0.69
SST: Sandstone		

Table 3.4: Geochemical data for samples from various formations of the Rewa Group.

	CHITTO-09-02 Panna SH	CHITTOR-09-16 Panna SH	CHITTOR-09-17 Panna SH	CHITTOR-09-18 Panna SH	CHITTOR-09-11 Panna SH
SiO ₂	42.56	59.14	55.28	62.57	61.16
TiO ₂	0.66	0.59	0.92	0.68	1.01
Al ₂ O ₃	11.54	8.00	12.14	11.20	12.89
Fe ₂ O ₃	8.23	5.25	6.92	3.33	8.31
MnO	0.25	0.02	0.06	0.02	0.07
MgO	1.64	0.55	1.34	0.53	2.62
CaO	29.36				1.96
Na ₂ O					
K ₂ O	3.13	2.11	3.14	3.54	3.60
P ₂ O ₅	0.08	0.03	0.12	0.03	0.07
LOI	-	2.54	6.73	6.37	4.75
TOTAL	97.45	78.25	86.64	88.26	96.43
Rb	154.85		318.17		
Sr	203.90		427.37		
Ba	496.30		1245.06		
Y	25.10		60.61		
Zr	83.61		655.68		
Hf	2.61		6.11		
Nb	6.24		22.55		
Ta	0.51		0.83		
Th	13.62		18.03		
U	2.00		3.07		
La	29.81		106.88		
Ce	60.56		216.63		
Pr	8.31		8.21		
Nd	31.71		29.51		
Sm	7.19		6.27		
Eu	1.36		1.01		
Gd	6.59		5.01		
Tb	0.86		0.64		
Dy	5.31		4.07		
Ho	0.95		0.76		
Er	2.89		2.44		
Tm	0.39		0.34		
Yb	2.69		2.49		
Lu	0.40		0.38		
Sc	12.33		39.05		
V	65.16		217.62		
Cr	40.79		162.87		
Co	13.89		189.47		
Ni	26.47		269.33		
Pb	7.39		59.62		
Cs	15.55		9.75		
⁸⁷ Sr/ ⁸⁶ Sr _m	0.78567		0.89992		
¹⁴³ Nd/ ¹⁴⁴ Nd _m	0.511859		0.511765		
ε _{Nd} (0)	-15.2		-17.0		
T _{CHUR}	1.99		1.95		
T _{DM}	2.25		2.19		
f _{Sm/Nd}	-0.30		-0.35		

SST: Shale; SST: Sandstone and LST: Limestone

Table 3.4 continued..

	CHITTOR-09-15 Panna SH	BUNDI-09-08 Indergarh SST	CHITTOR-09-03 Indergarh SST	CHITTOR-09-05 Jhiri/Panna SH	CHITTOR-09-06 Jhiri SH
SiO ₂	62.77	75.44	73.27	61.61	64.70
TiO ₂	0.72	0.08		0.99	0.77
Al ₂ O ₃	9.09	2.00	1.08	13.13	10.55
Fe ₂ O ₃	3.30		4.95	5.68	3.52
MnO	0.04	0.02	0.16	0.02	0.03
MgO	0.53			1.65	1.31
CaO				0.11	1.82
Na ₂ O					0.20
K ₂ O	2.77	0.56	0.12	5.70	4.42
P ₂ O ₅	0.02		0.03	0.03	0.05
LOI	2.63	0.40	1.15	4.07	3.50
TOTAL	81.88	78.51	80.74	92.99	90.88
Rb	132.80	14.00	2.77		176.20
Sr	153.70	125.00	128.20		166.90
Ba	290.30	27.14	76.64		368.50
Y	17.62	2.46	1.99		20.46
Zr	206.30	58.72	14.86		234.80
Hf	6.23	1.72	0.43		6.74
Nb	9.76	0.25	0.13		7.87
Ta	0.75	0.01	0.02		0.62
Th	17.19	2.48	1.27		17.02
U	2.93	0.66	0.40		2.98
La	39.04	9.02	12.05		33.08
Ce	97.76	21.87	27.41		67.32
Pr	10.41	2.42	3.51		8.03
Nd	38.42	8.77	13.47		29.15
Sm	8.06	1.98	2.91		6.22
Eu	1.15	0.29	0.47		1.01
Gd	5.61	1.15	1.92		5.11
Tb	0.66	0.11	0.14		0.66
Dy	4.06	0.73	0.67		4.26
Ho	0.75	0.14	0.10		0.80
Er	2.47	0.44	0.27		2.55
Tm	0.35	0.07	0.03		0.35
Yb	2.56	0.50	0.23		2.54
Lu	0.39	0.08	0.04		0.39
Sc	8.90	0.34	0.70		11.59
V	61.10	6.08	4.15		66.32
Cr	36.19	0.00	0.00		38.06
Co	12.24	0.00	0.32		14.54
Ni	16.65	0.00	0.00		21.29
Pb	27.27	1.01	1.31		16.16
Cs	8.47	0.32	0.17		8.16
⁸⁷ Sr/ ⁸⁶ Sr _m	0.81198	0.75932	0.71890		0.84885
¹⁴³ Nd/ ¹⁴⁴ Nd _m	0.511727		0.511888		0.511755
E _{Nd(0)}	-17.8		-14.6		-17.2
T _{CHUR}	1.98		1.72		1.98
T _{DM}	2.21		2.04		2.22
f _{Sm/Nd}	-0.36		-0.34		-0.34

Table 3.4 continued..

	BUNDI-09-12 Jhiri SH	BUNI-09-11 Taragarh SST	LAK07-16 Taragarh SST	BUNDI-09-14 Taragarh SST
SiO ₂	63.73	97.37	93.2	93.02
TiO ₂	0.88	0.41	0.21	0.00
Al ₂ O ₃	14.15	1.68	3.89	1.32
Fe ₂ O ₃	7.34		0.17	
MnO	0.02	0.02	0.01	0.02
MgO	1.47	0.00		
CaO	0.31			
Na ₂ O				
K ₂ O	3.33	0.29	0.11	0.09
P ₂ O ₅	0.08	0.01	0.03	
LOI	3.54	0.72	1.07	0.20
TOTAL	94.84	100.50	98.68	94.65
Rb	413.85	16.25	4.78	2.59
Sr	581.85	144.70	147.30	133.60
Ba	830.31	18.58	176.50	54.42
Y	70.56	12.33	5.18	2.38
Zr	558.28	276.50	89.71	16.55
Hf	5.80	9.01	2.68	0.53
Nb	25.26	2.00	1.25	0.19
Ta	1.02	0.04	0.08	0.02
Th	21.51	11.58	5.72	1.28
U	3.10	2.22	1.27	0.33
La	125.70	18.38	7.42	4.08
Ce	258.47	38.95	15.98	9.42
Pr	11.38	5.53	1.91	1.50
Nd	41.25	20.52	7.03	5.98
Sm	8.90	4.49	1.76	1.37
Eu	1.42	0.69	0.43	0.23
Gd	7.33	3.67	1.66	1.00
Tb	0.92	0.44	0.18	0.11
Dy	5.68	2.72	1.24	0.68
Ho	1.03	0.51	0.23	0.12
Er	3.25	1.66	0.78	0.34
Tm	0.45	0.23	0.12	0.04
Yb	3.16	1.68	0.90	0.29
Lu	0.47	0.26	0.15	0.05
Sc	40.07	0.07	1.00	0.00
V	263.82	0.74	18.30	0.00
Cr	187.47	3.80	1.35	0.00
Co	43.26	0.00	0.00	0.00
Ni	87.30	0.00	0.91	0.00
Pb	11.60	2.46	1.49	4.03
Cs	16.27	0.54	0.23	0.13
⁸⁷ Sr/ ⁸⁶ Sr _m	0.78285		0.74155	1.05282
¹⁴³ Nd/ ¹⁴⁴ Nd _m	0.511733		0.511841	0.511879
ε _{Nd} (0)	-17.7		-15.5	-14.8
T _{CHUR}	2.08		1.26	1.11
T _{DM}	2.29		1.60	1.45
f _{SmNd}	-0.56		-0.49	-0.53

Table 3.5: Geochemical data for samples from various formations of the Bhandar Group.

	GANDOLI-1 Lakheri LST	CHITTOR-09-07 Ganurgarh SH	BUNDI-09-10 Ganurgarh SH	LAK07-01 Ganurgarh SH	GANDOLI-3 Lakheri LST	GANDOLI-2 Lakheri LST
SiO ₂	34.85	58.43	68.90	79.75	32.67	31.66
TiO ₂	0.36	1.37	0.93	0.65	0.38	0.30
Al ₂ O ₃	5.47	15.43	16.39	9.11	5.48	4.53
Fe ₂ O ₃	3.61	9.58	4.15	3.59	4.95	3.69
MnO	0.41	0.02	0.03	0.07	0.38	0.45
MgO	0.88	2.89	1.66	1.00	0.83	0.82
CaO	42.01	0.14		0.39	38.78	47.21
Na ₂ O			0.12	0.15		
K ₂ O	1.40	5.00	3.15	1.40	1.49	1.12
P ₂ O ₅	0.05	0.12	0.02	0.02	0.07	0.06
LOI		5.16	4.37	3.77		
TOTAL	89.04	98.14	99.71	99.90	85.02	89.84
Rb	11.29	221.05	194.90	80.55		
Sr	798.40	172.20	193.50	168.30		
Ba	6720.00	361.00	346.50	501.90		
Y	129.90	27.08	18.64	16.49		
Zr	0.10	186.50	181.50	177.00		
Hf	0.03	5.09	5.54	5.34		
Nb	0.00	15.45	12.61	4.96		
Ta	0.00	1.07	1.01	0.38		
Th	27.21	17.73	22.89	15.87		
U	0.71	3.36	4.52	3.79		
La	42.83	25.75	48.71	26.95		
Ce	97.40	54.64	95.31	59.53		
Pr	10.40	7.31	11.53	7.25		
Nd	48.72	30.12	39.01	26.01		
Sm	13.82	7.40	7.38	5.43		
Eu	3.48	1.50	0.92	0.82		
Gd	15.28	6.80	4.77	4.31		
Tb	2.13	0.89	0.58	0.57		
Dy	13.19	5.72	4.03	3.76		
Ho	2.33	1.04	0.81	0.69		
Er	6.82	3.26	2.76	2.25		
Tm	0.86	0.44	0.40	0.32		
Yb	5.97	3.05	2.95	2.31		
Lu	0.86	0.45	0.45	0.35		
Sc	28.39	20.41	14.51	6.46		
V	12.75	130.40	93.02	63.44		
Cr	19.53	67.65	68.03	28.64		
Co	33.81	14.18	11.98	14.22		
Ni	82.88	30.00	34.65	17.54		
Pb	15.25	9.66	16.97	34.67		
Cs	0.52	12.83	11.57	3.81		
⁸⁷ Sr/ ⁸⁶ Sr _m		0.86238	0.79315	0.76140		
¹⁴³ Nd/ ¹⁴⁴ Nd _m		0.51175	0.51161	0.511762		
E _{Nd(0)}		-17.3	-20.1	-17.1		
T _{CHUR}		2.80	1.30	1.19		
T _{DM}		2.81	1.57	1.49		
f _{SmNd}		-0.24	-0.61	-0.57		

SST: Sandstone; SH: Shale and LST: Limestone

Table 3.5 continued..					
	GANDOLI-12 Lakheri LST	GANDOLI-11 Lakheri LST	GANDOLI-7 Lakheri LST	GANDOLI-5 Lakheri LST	GANDOLI-4 Lakheri LST
SiO ₂	22.97	24.09	23.41	31.73	34.11
TiO ₂	0.06	0.07	0.11	0.27	0.33
Al ₂ O ₃	1.72	1.94	2.19	4.38	5.28
Fe ₂ O ₃	1.13	1.52	1.79	2.92	3.71
MnO	0.12	0.14	0.32	0.47	0.41
MgO	0.46	0.62	0.62	0.75	0.85
CaO	67.33	70.66	63.22	47.43	43.64
Na ₂ O					
K ₂ O	0.36	0.36	0.41	1.10	1.33
P ₂ O ₅	0.12	0.12	0.07	0.05	0.05
LOI				-	
TOTAL	94.27	99.52	92.15	89.08	89.69
				Sil.	Carb.
Rb				25.28	1.12
Sr				14.69	19.36
Ba				587.50	65.59
Y				1.24	2.14
Zr				6.54	0.33
Hf				0.67	0.03
Nb				1.57	
Ta				0.18	0.00
Th				2.26	1.31
U				0.60	0.08
La				2.35	0.83
Ce				3.64	1.46
Pr				1.72	0.94
Nd				5.65	4.43
Sm				1.06	1.23
Eu				0.25	0.28
Gd				0.91	1.39
Tb				0.11	0.19
Dy				0.75	1.21
Ho				0.15	0.22
Er				0.52	0.65
Tm				0.08	0.08
Yb				0.55	0.59
Lu				0.09	0.09
Sc				0.52	0.57
V				3.40	
Cr				2.25	
Co				1.03	0.48
Ni				2.86	1.25
Pb				1.60	1.40
Cs				1.42	0.11
⁸⁷ Sr/ ⁸⁶ Sr _m				0.78300	
¹⁴³ Nd/ ¹⁴⁴ Nd _m				0.51160	
ε _{Nd} (0)				-20.2	
T _{CHUR}				1.30	
T _{DM}				1.57	
f _{Sm/Nd}				-0.62	

Table 3.5 continued..

	SATUR-12 Lakheri LST	GANDOLI-13 Lakheri LST	BUNDI-09-09 Samaria SH	BUND-09I-13 Samaria SH	CHITTOR-09-13 Samaria SH
SiO ₂	10.00	24.12	72.00	63.66	52.95
TiO ₂	0.12	0.07	0.24	0.79	0.88
Al ₂ O ₃	2.39	1.63	7.64	12.52	16.59
Fe ₂ O ₃	1.21	0.65	1.57	4.17	4.96
MnO	0.06	0.11	0.02	0.07	0.02
MgO	0.52	0.45	1.17	1.38	1.38
CaO	69.57	70.24		0.18	0.02
Na ₂ O					
K ₂ O	0.69	0.33	1.65	4.12	6.04
P ₂ O ₅	0.07	0.04	0.01	0.06	0.05
LOI	-		1.87	11.24	5.68
TOTAL	84.62	97.64	86.15	98.19	88.58
	Sil.	Carb.			
Rb	9.06	1.25			522.40
Sr	11.02	16.31			180.80
Ba	5.20	2.19			494.00
Y	0.19	0.31			37.79
Zr	1.96	0.23			140.00
Hf	0.20	0.02			3.96
Nb	0.45				13.10
Ta	0.05	0.00			1.05
Th	0.27	0.46			29.20
U	0.25	0.09			7.57
La	0.16	0.38			68.66
Ce	0.32	0.82			135.50
Pr	0.12	0.36			15.51
Nd	0.41	1.33			56.31
Sm	0.09	0.29			11.92
Eu	0.02	0.04			1.64
Gd	0.08	0.25			9.06
Tb	0.01	0.03			1.09
Dy	0.11	0.21			7.04
Ho	0.03	0.04			1.33
Er	0.09	0.12			4.30
Tm	0.01	0.02			0.59
Yb	0.10	0.10			4.05
Lu	0.02	0.02			0.60
Sc	0.10	0.07			25.34
V	0.98				158.80
Cr	0.67				108.30
Co	0.01	0.06			3.67
Ni	0.13	0.34			40.16
Pb	0.42	0.50			7.36
Cs	0.51	0.13			26.07
⁸⁷ Sr/ ⁸⁶ Sr _m	0.73810				0.96337
¹⁴³ Nd/ ¹⁴⁴ Nd _m	0.511777				0.511843
ε _{Nd} (0)	-16.8				-15.5
T _{CHUR}	1.25				1.76
T _{DM}	1.56				2.05
f _{Sm/Nd}	-0.53				-0.35

Table 3.5 continued..					
	SATUR07-22 Samaria-LST	SATUR07-01 Samaria SH	SATUR07-21 Samaria SH	BUNDI-09-01 Samaria SH	BUNDI-09-02 Samaria SH
SiO ₂	17.21	64.57	55.02	38.61	55.37
TiO ₂	0.02	0.92	0.76	0.44	0.74
Al ₂ O ₃	1.49	15.35	11.89	7.36	15.66
Fe ₂ O ₃	4.76	4.93	5.98	7.37	7.22
MnO	0.11	0.02	0.05	0.27	0.05
MgO	18.62	2.30	2.36	1.31	1.41
CaO	45.66	0.38	16.79	36.43	4.02
Na ₂ O					
K ₂ O	0.42	5.18	3.55	1.41	4.14
P ₂ O ₅	0.01	0.16	0.15	0.09	0.04
LOI	-	4.47	3.41	24.85	9.80
TOTAL	88.3	98.27	99.95	118.14	98.45
Rb		272.20			260.40
Sr		137.50			195.40
Ba		387.60			1320.00
Y		29.15			24.37
Zr		160.20			104.20
Hf		4.31			3.24
Nb		17.15			11.07
Ta		1.24			0.88
Th		21.72			26.61
U		3.03			1.80
La		50.15			51.93
Ce		98.34			103.90
Pr		12.31			12.25
Nd		45.89			43.42
Sm		10.11			8.70
Eu		1.60			1.28
Gd		8.19			6.31
Tb		1.01			0.77
Dy		6.08			5.02
Ho		1.07			0.94
Er		3.36			3.06
Tm		0.45			0.43
Yb		3.13			3.04
Lu		0.45			0.45
Sc		18.09			16.01
V		94.87			63.42
Cr		76.25			49.94
Co		10.80			14.60
Ni		41.80			29.53
Pb		6.61			12.88
Cs		12.15			15.72
⁸⁷ Sr/ ⁸⁶ Sr _m		1.02725			0.82376
¹⁴³ Nd/ ¹⁴⁴ Nd _m		0.511829			0.511734
ε _{Nd(0)}		-15.8			-17.6
T _{CHUR}		1.14			1.82
T _{DM}		1.47			2.08
f _{Sm/Nd}		-0.55			-0.38

Table 3.5 continued...

	Satur-23 Bundi Hill SST	LAK07-14 Black SH	CHITOR-09-11 Black SH	CHITTOR-09-12 Black SH	CHITTOR-09-9 Black SH	CHITTOR-09-8 Black SH
SiO ₂	95.37	65.19	61.16	65.15	59.92	44.81
TiO ₂	0.26	0.92	1.01	0.55	1.22	0.63
Al ₂ O ₃	1.93	15.98	12.89	12.00	16.88	9.83
Fe ₂ O ₃	0.53	3.59	8.31	3.70	8.65	5.10
MnO	0.02	0.03	0.07	0.03	0.03	0.14
MgO		1.56	2.62	0.98	2.99	8.26
CaO	0.02		1.96	0.02	0.22	15.92
Na ₂ O		0.32				
K ₂ O	0.16	3.35	3.60	3.70	4.95	2.86
P ₂ O ₅	0.07	0.01	0.07	0.02	0.07	0.04
LOI	1.13	8.20	4.75	4.04	4.79	-
TOTAL	99.49	99.15	96.43	90.19	99.71	87.58
Rb	6.54			213.60	212.05	
Sr	79.59			182.40	112.10	
Ba	193.20			329.30	328.90	
Y	10.09			22.57	25.96	
Zr	207.50			125.60	163.00	
Hf	6.16			3.71	4.67	
Nb	3.78			6.94	15.72	
Ta	0.28			0.61	1.19	
Th	6.34			17.05	20.99	
U	1.91			3.36	3.33	
La	12.39			33.81	29.42	
Ce	28.43			68.48	73.23	
Pr	3.96			8.27	9.46	
Nd	15.28			29.94	36.34	
Sm	3.22			6.35	7.93	
Eu	0.55			1.07	1.33	
Gd	2.55			5.12	6.63	
Tb	0.33			0.66	0.87	
Dy	2.19			4.39	5.61	
Ho	0.41			0.84	1.04	
Er	1.34			2.75	3.32	
Tm	0.19			0.38	0.46	
Yb	1.43			2.66	3.20	
Lu	0.22			0.40	0.47	
Sc	2.76			13.34	19.98	
V	7.92			78.58	127.60	
Cr	8.96			49.22	79.91	
Co	0.11			10.32	20.18	
Ni	0.43			32.84	29.54	
Pb	1.73			32.71	10.25	
Cs	0.20			13.35	14.25	
⁸⁷ Sr/ ⁸⁶ Sr _m	0.75253			0.86776	1.07818	
¹⁴³ Nd/ ¹⁴⁴ Nd _m	0.511891			0.511723	0.511798	
ε _{Nd(0)}	-14.6			-17.8	-16.4	
T _{CHUR}	1.02			2.03	1.97	
T _{DM}	1.36			2.25	2.22	
f _{SmNd}	-0.57			-0.35	-0.33	

Table 3.5 continued.

	LAK07-09 Black SH	LAK07-02 Black SH (Sirbu-SH)	LAK07-10 Black SH	LAK07-11 Black SH	LAK07-12 Grey SH	LAK07-13 Black SH
SiO ₂	62.42	65.62	65.04	73.83	74.61	69.07
TiO ₂	0.96	0.92	0.85	0.86	0.87	0.92
Al ₂ O ₃	17.3	15.9	16.06	13.25	14.25	15.89
Fe ₂ O ₃	3.84	4.13	4.46	3.00	3.46	4.49
MnO	0.03	0.03	0.03	0.07	0.03	0.04
MgO	1.63	1.70	1.72	1.61	1.53	1.72
CaO				0.51		
Na ₂ O	0.09	0.50	0.13	0.93	0.53	0.75
K ₂ O	3.79	3.25	3.53	2.31	2.78	2.89
P ₂ O ₅	0.02	0.03	0.02	0.01	0.01	0.03
LOI	8.28	10.2	6.52	4.72	3.30	5.00
TOTAL	98.35	102.32	98.36	101.10	101.37	100.79
Rb		214.25				
Sr		177.50				
Ba		360.90				
Y		31.14				
Zr		165.40				
Hf		5.22				
Nb		14.40				
Ta		1.14				
Th		22.61				
U		4.97				
La		49.75				
Ce		105.30				
Pr		14.48				
Nd		55.10				
Sm		11.50				
Eu		1.56				
Gd		8.00				
Tb		1.07				
Dy		7.01				
Ho		1.31				
Er		4.13				
Tm		0.55				
Yb		3.74				
Lu		0.54				
Sc		16.21				
V		100.00				
Cr		75.04				
Co		11.48				
Ni		29.79				
Pb		23.31				
Cs		16.65				
⁸⁷ Sr/ ⁸⁶ Sr _m		0.80083				
¹⁴³ Nd/ ¹⁴⁴ Nd _m		0.511725				
ε _{Nd(0)}		-17.8				
T _{CHUR}		1.23				
T _{DM}		1.53				
f _{Sm/Nd}		-0.57				

Table 3.5 continued...

	BUNDI-09-05 Shikaoda SST	BUNDI-09-3 Balwan LST	BUNDI-9-04 Balwan LST	BUNDI-09-06 Dholpur SH	BUNDI-09-07 Dholpur SH	
SiO ₂	98.06	11.86	7.40	81.21	70.32	
TiO ₂	0.01	0.12		0.41	0.87	
Al ₂ O ₃	1.51	2.77	1.11	6.20	14.1	
Fe ₂ O ₃	0.16	1.90	1.65	3.47	3.39	
MnO	0.02	0.25	0.15	0.28	0.02	
MgO		0.57	12.9	0.91	1.34	
CaO		74.73	50.0	1.69	0.00	
Na ₂ O						
K ₂ O	0.22	0.55	0.08	1.06	3.12	
P ₂ O ₅	0.00	0.01		0.03	0.02	
LOI	0.35			3.52	3.47	
TOTAL	100.32	92.75	73.32	98.78	96.66	
		Sil.	Carb.			
Rb	7.35	8.66	0.97	2.19	54.23	176.20
Sr	97.61	10.52	11.52	99.19	162.90	184.00
Ba	13.43	6.72	20.84	53.32	521.40	252.10
Y	4.04	0.14	0.58	0.00	16.73	22.94
Zr	38.00	0.34	0.06	0.00	181.60	192.40
Hf	1.09	0.05	0.01	0.00	5.31	5.86
Nb	0.70	0.30		0.03	5.07	11.51
Ta	0.06	0.04		0.01	0.52	0.91
Th	3.24	0.09	0.28	0.00	10.82	20.34
U	0.76	0.20	0.03	3.96	2.53	3.55
La	10.01	0.29	0.38	0.44	18.22	40.20
Ce	23.28	0.32	0.57	0.00	41.27	81.60
Pr	2.50	0.26	0.43	0.17	5.11	9.99
Nd	9.11	1.05	1.91	0.70	19.60	35.39
Sm	1.94	0.23	0.45	0.14	4.76	7.18
Eu	0.26	0.04	0.09	0.02	0.94	1.08
Gd	1.29	0.20	0.46	0.08	4.86	5.48
Tb	0.13	0.02	0.06	0.00	0.68	0.73
Dy	0.82	0.18	0.37	0.03	4.21	4.86
Ho	0.15	0.04	0.07	0.01	0.72	0.92
Er	0.48	0.12	0.19	0.01	2.15	3.00
Tm	0.07	0.02	0.02	0.00	0.29	0.42
Yb	0.47	0.10	0.14	0.00	2.04	2.98
Lu	0.07	0.02	0.02	0.00	0.30	0.45
Sc	0.12	0.01	0.03	0.00	5.83	12.30
V	7.67	1.29		6.85	26.02	76.40
Cr	2.61	0.86		0.17	21.22	58.64
Co	0.03	0.14	0.11	17.53	15.24	7.44
Ni	0.00	0.68	0.61	2.34	14.62	30.25
Pb	1.55	1.56	1.49	27.58	14.93	12.53
Cs	0.26	0.71	0.07	0.12	5.83	11.48
⁸⁷ Sr/ ⁸⁶ Sr _m	0.72537	0.86464		0.70818	0.80527	0.77186
¹⁴³ Nd/ ¹⁴⁴ Nd _m	0.511773	0.511642			0.511683	0.511908
ε _{Nd(0)}	-16.9	-19.4			-18.6	-14.2
T _{CHUR}	1.19	1.49			1.27	1.12
T _{DM}	1.50	1.77			1.55	1.48
f _{Sm/Nd}	-0.56	-0.52			-0.58	-0.50

Labels-Spot	U	Th	ThU	± ThU	Pb*	204Pb	204Pb (ppb)	206Pb	± 206Pb	f (206)	206Pb*	± 206Pb	207Pb*	235U	235U	± 235U	238U	238U	± 238U	206Pb*	206Pb*	207Pb/206Pb	± 207Pb/206Pb	206Pb*	206Pb*	207Pb/206Pb	± 207Pb/206Pb	Apparent Age	± 207Pb/206Pb	% DISC	
9017-98.1	215.27	139.49	0.689	0.014	120	1	1.59E-05	2.86E-05	2.70E-04	0.186	1.54E-03	11.090	0.207	0.476	0.465	0.169	8.40E-03	0.979	6.50E-04	2546.9	6.45	1.4									
9017-99.1	101.97	114.79	1.163	0.024	61	0	1.00E-05	1.00E-05	1.70E-04	0.319	3.60E-03	10.596	0.227	0.465	0.165	8.99E-03	0.944	1.18E-03	2509.3	12.04	1.9										
9017-99.1	142.89	61.51	0.446	0.009	61	6	1.24E-04	9.51E-06	2.19E-03	0.123	4.45E-03	7.225	0.166	0.391	0.134	7.17E-03	0.860	1.69E-03	2149.4	20.86	0.9										
9017-94.1	143.94	89.96	0.646	0.015	52	3	7.68E-05	1.39E-03	1.39E-03	0.190	2.98E-03	5.027	0.104	0.322	0.113	5.87E-03	0.928	8.80E-04	1850.2	14.06	2.7										
9017-98.1	152.08	124.3	0.844	0.017	88	0	7.52E-06	1.60E-05	1.39E-04	0.236	2.94E-03	11.258	0.271	0.478	0.171	1.09E-02	0.975	9.10E-04	2568.6	8.98	1.9										
9017-100.1	146.51	43.79	0.309	0.007	50	1	3.55E-05	2.28E-05	6.20E-04	0.089	1.97E-03	5.250	0.101	0.329	0.116	5.78E-03	0.956	6.10E-04	1892.6	10.28	3.2										
9017-102.1	103.92	50.74	0.504	0.011	62	2	3.54E-05	2.41E-05	6.10E-04	0.132	2.95E-03	14.085	0.264	0.522	0.196	8.26E-03	0.974	8.40E-04	2791.0	7.04	2.9										
9017-103.1	305.08	162.7	0.517	0.011	167	2	1.48E-05	8.25E-06	2.60E-04	0.145	9.00E-04	11.084	0.207	0.484	0.166	8.79E-03	0.988	4.90E-04	2519.6	4.91	-1										
9017-109.1	105.36	69.11	0.678	0.015	55	2	4.48E-05	3.68E-05	7.80E-04	0.190	2.77E-03	9.933	0.184	0.453	0.159	8.10E-03	0.952	9.60E-04	2445.8	10.26	1.5										
9017-111.1	154.75	83.93	0.580	0.012	82	2	3.23E-05	2.11E-05	5.60E-04	0.166	1.55E-03	10.805	0.204	0.468	0.168	8.24E-03	0.966	8.30E-04	2633.1	8.3	2.3										
9017-113.1	95.35	123.46	1.403	0.029	59	4	1.16E-04	3.45E-05	1.98E-03	0.384	5.64E-03	10.328	0.207	0.462	0.162	8.57E-03	0.962	8.90E-04	2479.7	9.26	1.3										
Bojunda05-02 (N 24° 50.431'; E 74° 35.626')																															
9018-2.1	241.66	139.08	0.585	0.012	82	8	1.29E-04	3.12E-05	2.18E-03	0.177	1.72E-03	4.602	0.091	0.307	0.109	5.37E-03	0.930	8.00E-04	1776.3	13.48	3										
9018-4.1	74.48	97.33	1.350	0.031	46	4	1.33E-04	4.59E-05	2.30E-03	0.362	4.60E-03	10.760	0.215	0.470	0.166	8.24E-03	0.925	1.27E-03	2518.3	12.86	1.4										
9018-3.1	67.46	105.13	1.610	0.036	45	4	1.31E-04	4.22E-05	2.28E-03	0.458	7.62E-03	11.009	0.245	0.471	0.169	9.13E-03	0.921	1.48E-03	2551.2	14.73	2.4										
9018-6.1	104.85	63.42	0.625	0.013	32	3	1.11E-04	3.79E-05	1.99E-03	0.179	4.40E-03	3.880	0.088	0.277	0.102	5.29E-03	0.892	1.05E-03	1654.4	19.25	4.8										
9018-7.1	72.26	79.95	1.143	0.024	43	2	6.85E-05	2.83E-05	1.19E-03	0.317	4.31E-03	10.931	0.235	0.470	0.169	8.65E-03	0.910	1.51E-03	2545.5	15.12	2.5										
9018-8.1	266.53	115.77	0.466	0.010	93	4	4.80E-05	1.34E-05	8.39E-04	0.134	1.19E-03	5.323	0.100	0.336	0.115	5.94E-03	0.973	5.00E-04	1877.0	7.86	0.5										
9018-37.1	119.63	77.41	0.669	0.014	40	4	1.23E-04	3.07E-05	2.19E-03	0.190	4.15E-03	4.401	0.092	0.301	0.106	5.69E-03	0.942	7.50E-04	1734.0	13.01	2.2										
9018-28.1	215.67	94.79	0.454	0.010	75	1	1.98E-05	2.44E-05	3.40E-04	0.192	1.46E-03	5.148	0.100	0.326	0.115	5.72E-03	0.945	7.30E-04	1874.9	11.56	3.1										
9018-33.1	160.19	115.89	0.748	0.016	52	6	1.42E-04	3.39E-05	2.47E-03	0.209	2.27E-03	4.056	0.086	0.288	0.102	5.29E-03	0.922	8.40E-04	1865.6	15.33	2.2										
9018-35.1	258.48	122.89	0.491	0.010	79	3	4.12E-05	1.56E-05	7.10E-04	0.140	1.36E-03	4.042	0.075	0.285	0.103	4.89E-03	0.969	4.80E-04	1674.2	8.59	3.3										
9018-13.1	147.8	73.09	0.511	0.012	80	1	2.03E-05	2.56E-05	3.60E-04	0.144	2.72E-03	11.218	0.244	0.479	0.170	8.69E-03	0.890	1.70E-03	2555.7	16.83	1.3										
9018-12.1	171.27	149.84	0.904	0.019	99	1	1.76E-05	2.49E-05	3.00E-04	0.250	1.77E-03	11.007	0.223	0.473	0.169	8.42E-03	0.926	1.31E-03	2546.8	13.03	2										
9018-17.1	160.06	63.38	0.409	0.009	84	1	1.00E-05	1.00E-05	1.70E-04	0.109	1.08E-03	11.336	0.292	0.474	0.173	1.08E-02	0.931	1.64E-03	2590.3	15.89	3.4										
9018-22.1	136.11	134.92	1.024	0.022	79	1	2.23E-05	1.71E-05	3.90E-04	0.291	7.93E-03	10.885	0.466	0.462	0.168	1.49E-02	0.796	4.47E-03	2536.8	45.37	3.6										
9018-50.1	66.18	102.74	1.604	0.034	26	0	1.00E-05	1.00E-05	1.70E-04	0.454	4.78E-03	4.181	0.100	0.294	0.103	5.59E-03	0.855	1.29E-03	1663.3	23.16	1.4										
9018-51.1	63.78	33.7	0.546	0.012	36	2	6.32E-05	3.25E-05	1.10E-03	0.147	2.86E-03	12.473	0.335	0.499	0.181	9.71E-03	0.801	2.93E-03	2665.4	27.06	2.1										
9018-48.1	289.42	147.72	0.527	0.011	101	3	4.13E-05	1.30E-05	7.20E-04	0.150	2.44E-03	5.007	0.095	0.322	0.113	5.67E-03	0.965	5.70E-04	1842.2	9.11	2.2										
9018-43.1	207.57	138.53	0.689	0.014	68	3	6.00E-05	1.92E-05	1.04E-03	0.194	1.68E-03	4.261	0.096	0.294	0.105	5.21E-03	0.869	1.21E-03	1713.8	21.31	2.9										
9018-50.1.2	56.88	87.16	1.583	0.072	23	1	7.49E-05	5.46E-05	1.30E-03	0.473	1.01E-02	4.181	0.103	0.291	0.104	5.79E-03	0.866	1.29E-03	1700.2	22.98	3.1										
9018-51.1.2	64.95	34.55	0.550	0.012	37	1	3.04E-05	4.96E-05	5.30E-04	0.150	3.16E-03	12.813	0.276	0.502	0.182	1.01E-02	0.958	1.15E-03	2671.6	10.47	1.8										
9018-48.1.2	262.24	145.31	0.532	0.011	97	0	3.09E-06	1.97E-05	5.00E-05	0.155	1.47E-03	4.914	0.100	0.316	0.113	6.00E-03	0.967	5.90E-04	1946.5	9.52	4.2										
9018-43.1.2	214.06	143.63	0.693	0.014	71	2	3.12E-05	2.92E-05	5.40E-04	0.204	3.75E-03	4.324	0.096	0.296	0.106	5.69E-03	0.911	9.80E-04	1730.2	17.06	3.4										
9018-42.1	162.75	89.82	0.570	0.012	54	2	4.40E-05	2.27E-05	7.60E-04	0.172	2.51E-03	4.426	0.092	0.301	0.107	5.79E-03	0.952	6.00E-04	1742.7	10.43	2.7										
9018-38.1	56.53	40.16	0.734	0.017	17	2	1.76E-04	1.41E-04	3.05E-03	0.212	6.32E-03	3.702	0.120	0.270	0.100	5.08E-03	0.873	2.41E-03	1616.0	45.81	4.8										

Labels-Spot	U (ppm)	Th (ppm)	Th/U ± 1σ	Pb* (ppm)	204Pb (ppb)	204Pb/206Pb	± 2σ Pb/206Pb	f (206) ²⁰⁶	206Pb*	± 2σ Pb/206Pb*	207Pb*	± 2σ Pb/206Pb*	208Pb*	± 2σ Pb/206Pb*	207Pb/206Pb	± 2σ Pb/206Pb	208Pb/206Pb	± 2σ Pb/206Pb	Apparent Age	± 2σ Pb/206Pb	% DISC				
9018-38.1	56.63	59.03	0.638	0.014	52	0	7.76E-06	3.36E-05	1.30E-04	0.173	3.18E-03	10.985	235U	± 2σ Pb/206Pb*	207Pb/206Pb	± 2σ Pb/206Pb*	208Pb*	± 2σ Pb/206Pb*	207Pb/206Pb	± 2σ Pb/206Pb	208Pb/206Pb	± 2σ Pb/206Pb	Apparent Age	± 2σ Pb/206Pb	% DISC
9018-29.1	255.32	178.06	0.720	0.015	140	2	2.19E-05	7.63E-05	3.80E-04	0.202	2.25E-03	10.615	235U	± 2σ Pb/206Pb*	207Pb/206Pb	± 2σ Pb/206Pb*	208Pb*	± 2σ Pb/206Pb*	207Pb/206Pb	± 2σ Pb/206Pb	208Pb/206Pb	± 2σ Pb/206Pb	Apparent Age	± 2σ Pb/206Pb	% DISC
9018-83.1	114.86	52.18	0.469	0.010	37	1	4.20E-05	3.93E-05	7.30E-04	0.135	2.46E-03	4.461	235U	± 2σ Pb/206Pb*	207Pb/206Pb	± 2σ Pb/206Pb*	208Pb*	± 2σ Pb/206Pb*	207Pb/206Pb	± 2σ Pb/206Pb	208Pb/206Pb	± 2σ Pb/206Pb	Apparent Age	± 2σ Pb/206Pb	% DISC
9018-87.1	108.85	58.04	0.562	0.013	39	3	9.53E-05	2.98E-05	1.85E-03	0.165	2.21E-03	5.115	235U	± 2σ Pb/206Pb*	207Pb/206Pb	± 2σ Pb/206Pb*	208Pb*	± 2σ Pb/206Pb*	207Pb/206Pb	± 2σ Pb/206Pb	208Pb/206Pb	± 2σ Pb/206Pb	Apparent Age	± 2σ Pb/206Pb	% DISC
9018-58.1	205.06	68.03	0.343	0.007	124	2	2.54E-05	1.68E-05	4.40E-04	0.093	1.03E-03	15.324	235U	± 2σ Pb/206Pb*	207Pb/206Pb	± 2σ Pb/206Pb*	208Pb*	± 2σ Pb/206Pb*	207Pb/206Pb	± 2σ Pb/206Pb	208Pb/206Pb	± 2σ Pb/206Pb	Apparent Age	± 2σ Pb/206Pb	% DISC
9018-82.1	248.94	76.49	0.317	0.007	84	0	5.97E-06	1.79E-05	1.00E-04	0.093	1.54E-03	5.116	235U	± 2σ Pb/206Pb*	207Pb/206Pb	± 2σ Pb/206Pb*	208Pb*	± 2σ Pb/206Pb*	207Pb/206Pb	± 2σ Pb/206Pb	208Pb/206Pb	± 2σ Pb/206Pb	Apparent Age	± 2σ Pb/206Pb	% DISC
9018-84.1	201.1	47.41	0.244	0.006	70	3	4.86E-05	1.60E-05	8.40E-04	0.072	1.16E-03	5.807	235U	± 2σ Pb/206Pb*	207Pb/206Pb	± 2σ Pb/206Pb*	208Pb*	± 2σ Pb/206Pb*	207Pb/206Pb	± 2σ Pb/206Pb	208Pb/206Pb	± 2σ Pb/206Pb	Apparent Age	± 2σ Pb/206Pb	% DISC
9018-85.1	44.19	33.77	0.789	0.021	16	2	1.91E-04	7.54E-05	3.32E-03	0.223	5.45E-03	5.003	235U	± 2σ Pb/206Pb*	207Pb/206Pb	± 2σ Pb/206Pb*	208Pb*	± 2σ Pb/206Pb*	207Pb/206Pb	± 2σ Pb/206Pb	208Pb/206Pb	± 2σ Pb/206Pb	Apparent Age	± 2σ Pb/206Pb	% DISC
9018-87.1	204.38	74.78	0.378	0.008	70	2	4.18E-05	1.91E-05	7.20E-04	0.105	2.02E-03	5.191	235U	± 2σ Pb/206Pb*	207Pb/206Pb	± 2σ Pb/206Pb*	208Pb*	± 2σ Pb/206Pb*	207Pb/206Pb	± 2σ Pb/206Pb	208Pb/206Pb	± 2σ Pb/206Pb	Apparent Age	± 2σ Pb/206Pb	% DISC
9018-86.1	116.33	55.73	0.495	0.010	59	1	1.94E-05	2.31E-05	3.40E-04	0.144	1.71E-03	10.037	235U	± 2σ Pb/206Pb*	207Pb/206Pb	± 2σ Pb/206Pb*	208Pb*	± 2σ Pb/206Pb*	207Pb/206Pb	± 2σ Pb/206Pb	208Pb/206Pb	± 2σ Pb/206Pb	Apparent Age	± 2σ Pb/206Pb	% DISC
9018-71.1	166.02	70.54	0.439	0.010	58	4	7.94E-05	2.18E-05	1.38E-03	0.127	1.52E-03	5.234	235U	± 2σ Pb/206Pb*	207Pb/206Pb	± 2σ Pb/206Pb*	208Pb*	± 2σ Pb/206Pb*	207Pb/206Pb	± 2σ Pb/206Pb	208Pb/206Pb	± 2σ Pb/206Pb	Apparent Age	± 2σ Pb/206Pb	% DISC
9018-72.1	164.91	88.74	0.619	0.013	68	1	2.97E-05	1.85E-05	5.10E-04	0.181	2.70E-03	4.948	235U	± 2σ Pb/206Pb*	207Pb/206Pb	± 2σ Pb/206Pb*	208Pb*	± 2σ Pb/206Pb*	207Pb/206Pb	± 2σ Pb/206Pb	208Pb/206Pb	± 2σ Pb/206Pb	Apparent Age	± 2σ Pb/206Pb	% DISC
9018-76.1	88.17	83.97	0.984	0.021	30	1	5.72E-05	8.87E-05	9.90E-04	0.285	6.14E-03	4.005	235U	± 2σ Pb/206Pb*	207Pb/206Pb	± 2σ Pb/206Pb*	208Pb*	± 2σ Pb/206Pb*	207Pb/206Pb	± 2σ Pb/206Pb	208Pb/206Pb	± 2σ Pb/206Pb	Apparent Age	± 2σ Pb/206Pb	% DISC
9018-78.1	76.91	101.1	1.358	0.029	48	3	9.05E-05	4.28E-05	1.57E-03	0.379	3.91E-03	10.643	235U	± 2σ Pb/206Pb*	207Pb/206Pb	± 2σ Pb/206Pb*	208Pb*	± 2σ Pb/206Pb*	207Pb/206Pb	± 2σ Pb/206Pb	208Pb/206Pb	± 2σ Pb/206Pb	Apparent Age	± 2σ Pb/206Pb	% DISC
9018-80.1	108.14	101.88	0.971	0.020	42	2	8.04E-05	3.10E-05	1.39E-03	0.277	4.36E-03	5.190	235U	± 2σ Pb/206Pb*	207Pb/206Pb	± 2σ Pb/206Pb*	208Pb*	± 2σ Pb/206Pb*	207Pb/206Pb	± 2σ Pb/206Pb	208Pb/206Pb	± 2σ Pb/206Pb	Apparent Age	± 2σ Pb/206Pb	% DISC
9018-82.1	131.32	104.97	0.826	0.017	73	2	3.04E-05	2.03E-05	5.30E-04	0.228	2.35E-03	10.805	235U	± 2σ Pb/206Pb*	207Pb/206Pb	± 2σ Pb/206Pb*	208Pb*	± 2σ Pb/206Pb*	207Pb/206Pb	± 2σ Pb/206Pb	208Pb/206Pb	± 2σ Pb/206Pb	Apparent Age	± 2σ Pb/206Pb	% DISC
9018-87.1	209.02	140.27	0.693	0.014	115	1	1.78E-05	1.59E-05	3.10E-04	0.196	1.54E-03	10.879	235U	± 2σ Pb/206Pb*	207Pb/206Pb	± 2σ Pb/206Pb*	208Pb*	± 2σ Pb/206Pb*	207Pb/206Pb	± 2σ Pb/206Pb	208Pb/206Pb	± 2σ Pb/206Pb	Apparent Age	± 2σ Pb/206Pb	% DISC
9018-89.1	193.88	123.32	0.657	0.014	62	0	8.63E-06	1.71E-05	1.50E-04	0.187	2.09E-03	4.280	235U	± 2σ Pb/206Pb*	207Pb/206Pb	± 2σ Pb/206Pb*	208Pb*	± 2σ Pb/206Pb*	207Pb/206Pb	± 2σ Pb/206Pb	208Pb/206Pb	± 2σ Pb/206Pb	Apparent Age	± 2σ Pb/206Pb	% DISC
9018-90.1	258.46	34.66	0.139	0.003	77	3	4.59E-05	2.66E-05	7.90E-04	0.037	1.13E-03	4.573	235U	± 2σ Pb/206Pb*	207Pb/206Pb	± 2σ Pb/206Pb*	208Pb*	± 2σ Pb/206Pb*	207Pb/206Pb	± 2σ Pb/206Pb	208Pb/206Pb	± 2σ Pb/206Pb	Apparent Age	± 2σ Pb/206Pb	% DISC
9018-91.1	82.02	37.89	0.477	0.010	46	4	1.05E-04	3.47E-05	1.83E-03	0.130	3.45E-03	12.717	235U	± 2σ Pb/206Pb*	207Pb/206Pb	± 2σ Pb/206Pb*	208Pb*	± 2σ Pb/206Pb*	207Pb/206Pb	± 2σ Pb/206Pb	208Pb/206Pb	± 2σ Pb/206Pb	Apparent Age	± 2σ Pb/206Pb	% DISC
9018-96.1	142.51	85.61	0.621	0.014	44	5	1.30E-04	4.44E-05	2.25E-03	0.162	2.35E-03	4.155	235U	± 2σ Pb/206Pb*	207Pb/206Pb	± 2σ Pb/206Pb*	208Pb*	± 2σ Pb/206Pb*	207Pb/206Pb	± 2σ Pb/206Pb	208Pb/206Pb	± 2σ Pb/206Pb	Apparent Age	± 2σ Pb/206Pb	% DISC
9018-97.1	126.03	175.61	1.439	0.030	54	1	3.26E-05	2.95E-05	5.70E-04	0.405	3.09E-03	5.153	235U	± 2σ Pb/206Pb*	207Pb/206Pb	± 2σ Pb/206Pb*	208Pb*	± 2σ Pb/206Pb*	207Pb/206Pb	± 2σ Pb/206Pb	208Pb/206Pb	± 2σ Pb/206Pb	Apparent Age	± 2σ Pb/206Pb	% DISC
9018-106.1	193.65	101.78	0.543	0.012	64	3	5.27E-06	2.19E-05	9.10E-04	0.159	1.59E-03	4.445	235U	± 2σ Pb/206Pb*	207Pb/206Pb	± 2σ Pb/206Pb*	208Pb*	± 2σ Pb/206Pb*	207Pb/206Pb	± 2σ Pb/206Pb	208Pb/206Pb	± 2σ Pb/206Pb	Apparent Age	± 2σ Pb/206Pb	% DISC
9018-110.1	74.89	64.89	0.891	0.019	29	1	3.92E-05	4.32E-05	6.80E-04	0.254	4.20E-03	5.094	235U	± 2σ Pb/206Pb*	207Pb/206Pb	± 2σ Pb/206Pb*	208Pb*	± 2σ Pb/206Pb*	207Pb/206Pb	± 2σ Pb/206Pb	208Pb/206Pb	± 2σ Pb/206Pb	Apparent Age	± 2σ Pb/206Pb	% DISC

Spot name follows the convention x-y-z; where x = sample number, y = grain number and z = spot number. Multiple analyses in an individual spot are labeled as x-y.z.z

Uncertainties reported at 1σ (absolute) and are calculated by numerical propagation of all known sources of error

²⁰⁶Pb refers to mole fraction of total ²⁰⁶Pb that is due to common Pb, calculated using the ²⁰⁶Pb-method;

common Pb composition used is the surface blank (4/6: 0.05770; 7/6: 0.895500; 8/6: 2.13840)

* refers to radiogenic Pb (corrected for common Pb)

Discordance relative to origin = 100 * (1 - (²⁰⁶Pb/²⁰⁶Pb age) / (²⁰⁷Pb/²⁰⁶Pb age))

Calibration standard 6286; U = 910 ppm; Age = 559 Ma; ²¹⁰Pb/²³⁸U = 0.09059

Error in ²⁰⁶Pb/²⁰⁶Pb calibration 1.0 - 1.7% depending on analytical session

UO/ZrO 5.83660; Pb⁷/UO₂ 0.10335, Error 1.70

Th/U calibration: F = 0.03900*UO + 0.85600

Table 3.7: $\delta^{13}\text{C}$ and $\delta^{18}\text{O}$ of the international standard NBS-19 and the local standard MMB.

	$\delta^{13}\text{C}_{\text{PDB}} (\text{‰})$	$\pm 1\sigma$	$\delta^{18}\text{O}_{\text{PDB}} (\text{‰})$	$\pm 1\sigma$
NBS-19				
Recommended	1.95	0.05	-2.20	0.10
Measured (n=20)	1.97	0.05	-2.31	0.09
MMB				
Recommended	3.90	0.05	-10.70	0.10
Measured (n=20)	3.87	0.05	-10.79	0.10

Table 3.8: C and O isotopic compositions in samples from the Lakheri Limestone.

Sample	Depth (m)	$\delta^{13}\text{C}_{\text{PDB}} (\text{‰})$	$\delta^{18}\text{O}_{\text{PDB}} (\text{‰})$
Gandoli-1	0	1.22	-12.22
Gandoli-2	0.1	1.13	-12.05
Gandoli-4	0.5	1.23	-12.16
Gandoli-5	0.9	1.2	-12.52
Gandoli-6	3	-0.23	-10.36
Gandoli-10	13	1.66	-11.9
Gandoli-11	25	5.96	-10.24
Gandoli-18	60	4.12	-9.26
Gandoli-21	76	5.97	-8.36
Gandoli-23	86	4.13	-11.64

Table 3.9: C and O isotopic compositions in samples from the Balwan Limestone.

Sr. No.	Sample	$\delta^{13}\text{C}_{\text{PDB}}$ (‰)	$\delta^{18}\text{O}_{\text{PDB}}$ (‰)
1	BWK-10-1	0.03	-8.43
2	BWK-10-2	3.33	-8.22
3	BWK-10-3A	3.96	-9.98
4	BWK-10-3B	4.18	-8.17
5	BWK-10-4	2.08	-8.94
6	BWK-10-5	4.50	-8.08
7	BWK-10-6	4.05	-4.17
8	BWK-10-7	3.72	-2.69
9	BWK-10-8	-0.64	-3.25
10	BWK-10-9	2.63	-2.34
11	BWK-10-13B	-0.17	-2.42
12	BWK-10-14	-0.75	-5.60
13	BWK-10-15	0.09	-4.26
14	BWK-10-16	3.30	-4.17
15	BUNDI-09-04	3.66	-2.63
16	BWK-10-20	4.13	-9.31
17	BWK-10-21	3.91	-10.70
18	BWK-10-22	1.36	-5.92
19	BWK-10-23	-0.38	-5.10
20	BWK-10-24	0.47	-2.76
21	BWK-10-25	3.83	-8.21
22	BWK-10-26	4.14	-4.79
23	BWK-10-27A	4.41	-5.72
24	BWK-10-28	3.92	-4.79
25	BWK-10-29	1.45	-5.39
26	BWK-10-30	1.56	-5.88
27	BWK-10-31	6.63	-3.71
28	BWK-10-32	3.95	-7.36
29	BWK-10-33	2.84	-5.14
30	BWK-10-34	3.41	-9.60
31	BWK-10-35A	-3.72	-9.00
32	BWK-10-35A-II	-3.65	-6.62
33	BWK-10-35B	-3.43	-7.78
34	BWK-10-36	1.55	-2.79
35	BWK-10-37	1.37	-2.05
36	BWK-10-39	2.50	-3.78
37	BWK-10-40	3.61	-8.58
38	BWK-10-41	4.50	-6.88
39	BWK-10-43	1.13	-6.93
40	BWK-10-44	4.05	-6.09
41	BWK-10-45	4.10	-7.93
42	BWK-10-46	1.53	-6.49
43	BWK-10-47	3.08	-4.02
44	BWK-10-48	0.90	-3.97
45	BWK-10-50	2.16	-5.37
46	BWK-10-51	4.19	-5.79
47	BWK-10-52	2.82	-5.58
48	BWK-10-53	3.27	-6.63
49	BWK-10-55	-2.84	-5.34
50	BWK-10-56	-3.06	-3.29
51	BWK-10-57	1.87	-1.23
52	BWK-10-60	3.98	-5.56
53	BWK-10-61	3.80	-4.87
54	BWK-10-62	2.62	-4.38
55	BWK-10-63	3.94	-6.26
56	BWK-10-64	3.97	-7.10
57	BWK-10-65	4.15	-6.19
58	BWK-10-66	4.17	-6.84
59	BWK-10-67	4.27	-7.88
60	BWK-10-68	-0.58	-2.30
61	BWK-10-69	-1.32	-5.00
62	BWK-10-70	2.50	-2.47
63	BWK-10-71	-0.58	-3.95
64	BWK-10-72	-0.51	-5.70
65	BWK-10-73	-4.93	-10.00
66	BWK-10-73-2	-0.82	-2.32
67	BWK-10-73-3	-1.46	-3.53
68	BWK-10-74	-3.48	-8.51
69	BWK-10-75	-0.57	-3.28

70	BWK-10-76	0.20	-2.35
71	BWK-10-77	-0.79	-5.92
72	BWK-10-78	1.21	-3.37
73	BWK-10-79	0.35	-3.40
74	BWK-10-80	0.59	-2.98
75	BWK-10-81	0.05	-3.67
76	BWK-10-82	1.17	-2.60
77	BWK-10-83	0.39	-5.74
78	BWK-10-84	1.15	-2.62
79	BWK-10-85	0.70	-2.70
80	BWK-10-86	0.68	-1.37
81	BWK-10-87	-0.80	-5.97
82	BWK-10-88	1.33	-4.21
83	BWK-10-89	0.39	-3.33
84	BWK-10-90	1.57	-3.23
85	BWK-10-92	-2.33	-5.48
86	BWK-10-93	-3.08	-5.58
87	BWK-10-94	-3.38	-5.99
88	BWK-10-95	-3.55	-5.09
89	BWK-10-96	2.83	-3.10
90	BWK-10-96-R	3.10	-3.14
91	BWK-10-97	-0.48	-4.66
92	BWK-10-98	2.30	-3.56
93	BWK-10-99	-0.96	-4.46

Table 3.10: Trace element data for selected samples from the Balwan Limestone.

	Mn/Sr	(Sr/Ca) $\times 10^{-4}$	(Mg/Ca) $\times 10^{-3}$	(Fe/Ca) $\times 10^{-3}$
BWK-10-1	35.54	3.49	21.40	28.49
BWK-10-2	9.05	6.51	43.73	31.45
BWK-10-3	5.17	7.01	29.48	15.65
BWK-10-4	16.94	4.27	37.73	27.44
BUNDI-09-04	11.03	7.42	1203.84	35.76
BWK-10-5	4.82	8.39	80.53	3.68
BWK-10-8	87.79	2.49	36.46	48.59
BWK-10-9	88.25	6.05	973.24	68.14
BWK-10-13B	28.71	9.88	1382.01	62.71
BWK-10-15	9.33	7.68	832.27	31.31
BWK-10-20	5.41	8.33	26.81	12.28
BWK-10-21	4.35	8.31	31.66	10.19

Table 3.11: Sr isotopic ratio data for carbonate components from limestone formations of the Upper Vindhyaans.

	Sample	$^{87}\text{Sr}/^{86}\text{Sr}$	2 sigma	$(^{87}\text{Sr}/^{86}\text{Sr})^{\text{norm}}$
Balwan Limestone	BWK-10-1	0.72599	0.00006	0.72601
	BWK-10-2	0.71430	0.00002	0.71432
	BWK-10-3A	0.71571	0.00002	0.71573
	BWK-10-3B	0.71449	0.00008	0.71451
	BWK-10-4	0.72814	0.00009	0.72816
	BWK-10-5	0.70674	0.00001	0.70676
	BWK-10-6	0.70828	0.00002	0.70830
	BWK-10-13B	0.70903	0.00001	0.70905
	BWK-10-20	0.70682	0.00002	0.70684
	BWK-10-21	0.71031	0.00002	0.71033
Lakheri Limestone	Gandoli--3	0.71520	0.00003	0.71522
	Gandoli--4	0.71885	0.00006	0.71887
	Gandoli--6	0.71556	0.00004	0.71558
	Gandoli--8	0.71526	0.00001	0.71528
	Gandoli--10	0.71312	0.00002	0.71314
	Gandoli--11	0.71078	0.00003	0.71080
	Gandoli--18	0.71884	0.00008	0.71886
	Gandoli--23	0.71803	0.00003	0.71805

$(^{87}\text{Sr}/^{86}\text{Sr})_{\text{norm}} = ^{87}\text{Sr}/^{86}\text{Sr}$ ratio normalized with respect to a value of 0.71025 of the international standard NBS 987. The long term average of this value for our lab is 0.71023.

3.2 Discussion

3.2.1 Pre-Vindhyan rocks

To understand the provenance and evolution of a sedimentary basin it is necessary to document the possible source rocks in the vicinity of the basin. In the Rajasthan sector of the Vindhyan, the possible source rocks are the various pre-Vindhyan igneous, metamorphic and sedimentary rocks of the Aravalli mountain ranges. The nature of contact between the Vindhyan and the pre-Vindhyan in the area south/southeast and in the north-east of Chittorgarh is not very well defined due to post-Vindhyan tectonic activities, which have eliminated the primary signatures (Prasad, 1984). This contact is defined by Prasad (1984) as disconformity with the Berach Granite and the Hindoli Group of rocks. These rocks could have been the most prominent sources for sediments to the Vindhyan Basin. Similarly, the occurrences of the Khairmalia volcanics in the vicinity, considered as a basal volcanics, which is now included within the Vindhyan Supergroup, might have been one of the active sources of the sediments during the deposition of the Vindhyan in this sector. Apart from these, the Aravalli-Delhi Supergroups which are exposed in the Aravalli-Delhi mountain chain at the western margin of the basin could also have contributed sediments. Since chemical characterization of all possible sources was beyond the scope of this work, we concentrated on a few pre-Vindhyan magmatic rocks which could have had significant contributions to the sediment budget for the Vindhyan Basin. The geochemical data for these rocks are presented in Table 3.1 and their implications are discussed in the following sections.

3.2.1.1 *The Berach Granites*

The Berach Granites are considered as basement inliers within the Aravalli supracrustals, and believed to have undergone a very low-grade metamorphism during the Proterozoic tectonothermal events (Roy and Jakhar, 2002). The Berach

Granites belong to the Mewar Gneissic Complex and form part of the Archean basement of the Aravalli Supergroup. Described as Chittor Granites by Hackett (1881), Gupta (1934) correlated them with the Bundelkhand Granites and Gneisses occurring in Central India. Gupta (1934) identified that these represent the pre-Aravalli land surface on which the rocks of Aravalli Supergroup lie with a definite erosional unconformity. The geochronological studies on the Berach Granites using the Pb-Pb isochron analysis by Weidenbeck et al. (1996) provided a minimum age of crystallization of 2440 ± 8 Ma, which is similar to the estimated age for the Bundelkhand granites and gneisses given by Mondal et al. (2002).

The texture of these granites varies from coarse porphyritic to highly foliated gneissic type in thin sections. Minerals found in these are quartz, feldspar, biotite and ferromagnesian minerals parallel to the foliation. Two samples (CGB-07-03 and CGB-07-06) of this granite were collected from the Berach River section near Chittorgarh. One of the samples was slightly weathered (CGB07-03) as is evident from its low contents of Na and Ca (Table 3.1). The major difference between the Berach granites and the other Archean granites in the nearby region such as Untala and Gingla is in the amount of SiO_2 , which is lower in Berach. A comparative study between the Berach granites and the data generated on Bundelkhand granites and gneisses (Hussain et al., 2004) suggests that although the chemical compositions are similar, the chondrite normalized Rare Earth Elements (REE) patterns of Berach granites are somewhat different from that of the Bundelkhand granites (Fig. 3.1 A). Further, the multi-element spiderograms normalized to the primitive mantle (PM), in which the elements are arranged according to their incompatibility, are presented in Fig 3.2. The samples from the Berach granites show typical enrichment in Pb and depletion in Sr values compared to their Bundelkhand counter parts (Fig. 3.1A). These observations suggest that though compositionally similar, these two granites have evolved in different tectonic settings, with the Berach granites representing a magmatic arc (subduction zone) setting.

The $\epsilon_{Nd}(0)$ values for the two Berach granite samples are -32 and -30 with T_{CHUR} age of 3.16 and 2.65 Ga and T_{DM} ages of 3.08 and 2.69 Ga (Table 3.1). These model ages are older than the crystallization age of the granites, i.e. 2.5 Ga. Model ages essentially reflect the age of mantle extraction for the samples, hence are older than their crystallization ages.

3.2.1.2 Mafic igneous rocks

The Khairmalia volcanics are reported from the western margins of the Vindhyan Basin. These are described as intermediate amygdaloidal andesitic flows including pyroclastics which occur unconformably over the Berach Granite and over the Pre-Aravalli metamorphics (i.e. Bhilwara Supergroup) (Prasad, 1984). The thickness of the flows is 40 to 100 m. The Khairmalia volcanics are mainly fine grained and dark purple, pink, greenish or greenish brown in colour. The amygdales are of millimeter to centimeter in size, filled with silicate-chloritic, calcite, siderite, chert and quartz. Although the precise age of emplacement of these rocks is not yet known.

Raza et al. (2009) carried out detailed geochemical studies on the Khairmalia volcanics and suggested that these represent Continental Flood Basalt (CFB) except for one sample which showed signatures of Ocean Island Basalt (OIB). They also worked on the Jungel volcanics from the Son Valley and identified them as OIBs. Five samples of mafic igneous rocks were collected from Khairmalia volcanics southwest of Chittorgarh between Badi Sadri and Dholapani, separated by 30 km. The results of geochemical analyses are given in Table 3.1.

Based on total alkali and silica (TAS) diagram (Fig 3.3) these rocks are classified as andesite to dacite, with two of the samples falling within the field of basalt. It is highly likely that these rocks came from the same outcrops that are sampled by Raza et al. (2009). However, in the present study these have been identified as metavolcanics with evidences of metamorphic recrystallization textures.

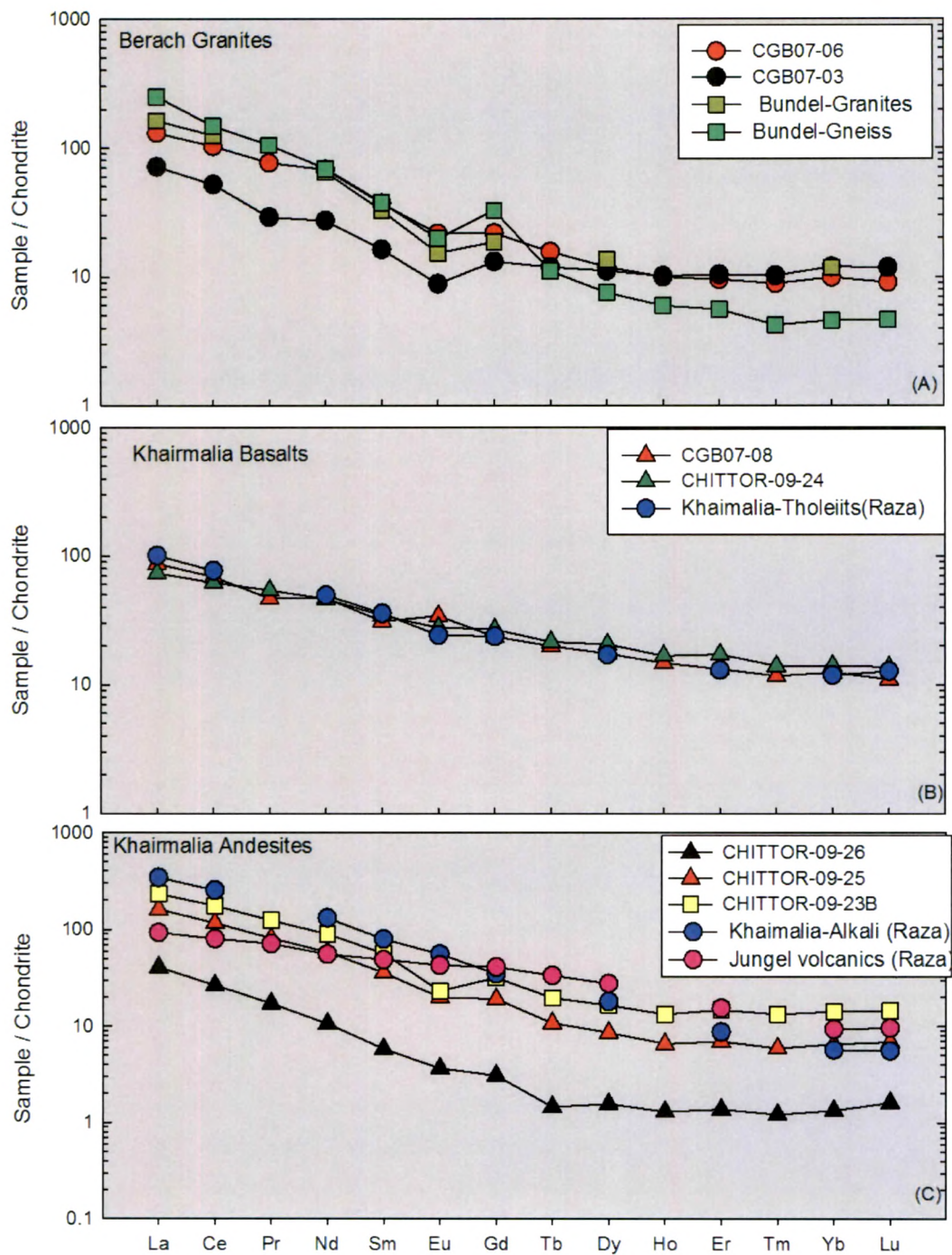


Fig. 3.1: Chondrite normalized REE patterns for various pre-Vindhyan granites and mafic igneous rocks. Data sources: Table 3.1, Hussain et al. (2004) and Raza et al. (2009).

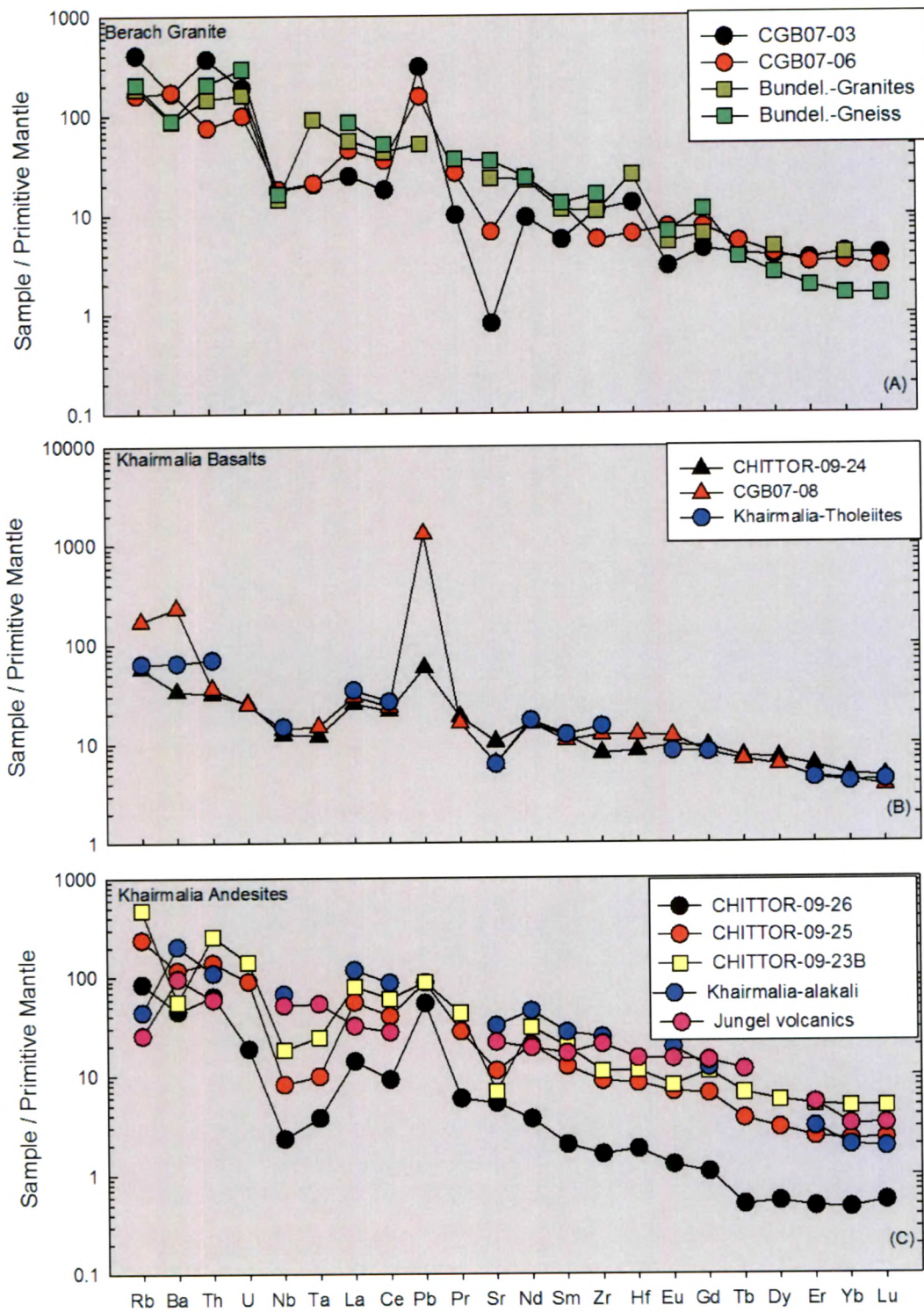


Fig. 3.2: Primitive Mantle normalized multi-element content variations in pre-Vindhyan granites and mafic igneous rocks. Data sources: same as in Fig. 3.1.

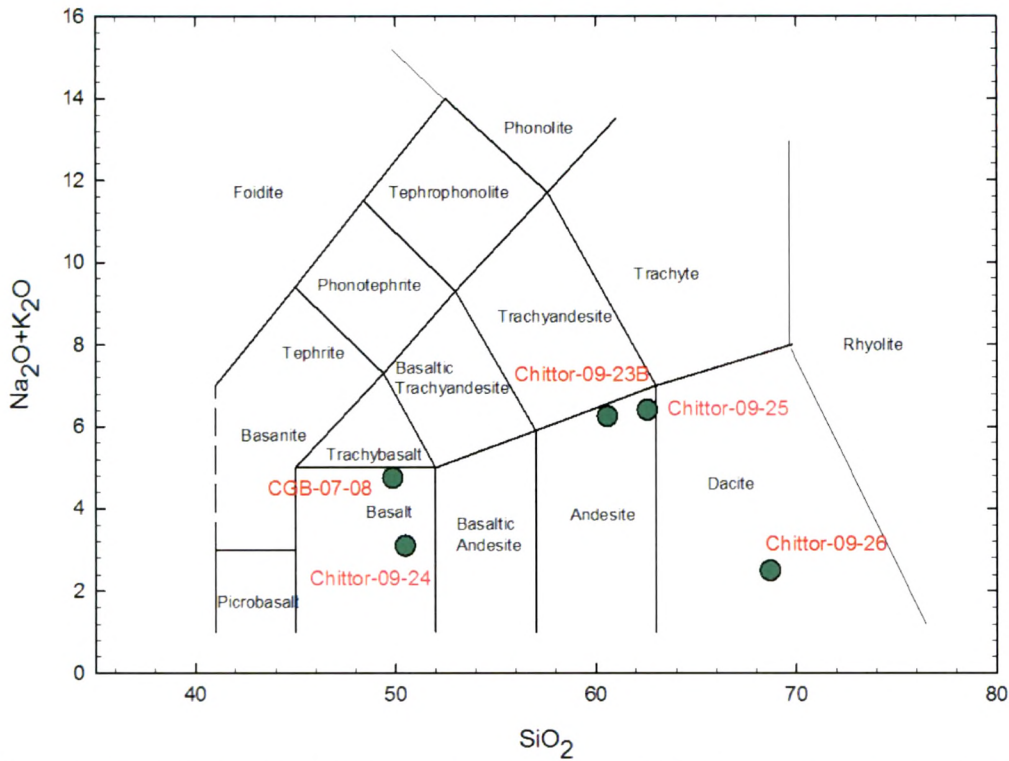


Fig. 3.3: Total Alkali- Silica diagram and classification of the Khairmalia volcanics. Classification scheme after Lee Bas et al. (1990).

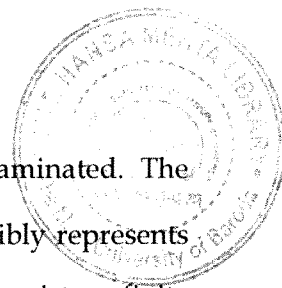
For comparison, the average values of REE concentrations in Khairmalia tholeiites and alkali basalts and those in the Jungel volcanics (Raza et al., 2009) have been plotted along with our data from Khairmalia metavolcanics in Fig. 3.1 B & C. One can see that the two of our mafic metavolcanic samples, identified as basalts (Fig. 3.3), are similar to the Khairmalia tholeiites of Raza et al. (2009) (Fig. 3.1B). Similarly, most of our samples classified as andesite and dacite (Fig. 3.3) have higher total REE contents and show LREE enrichment and appear to be different from Jungel volcanics (Fig. 3.1C).

Further to identify the source characteristics, multi-element variation diagrams were utilized, where trace and rare earth element contents were plotted after normalizing

them to primitive mantle (PM) compositions. Samples with affinity towards andesite and dacite show enrichments in large ion lithophile elements (LILE) and depletion in Nb, Ta, and Sr and enrichments in Pb (Fig. 3.2 B & C). Such features are typical for island/magmatic arc igneous rocks (Winter, 2001) and therefore, hint at a subduction zone setting during Khairmalia magmatism. We envisage that a subduction zone setting existed at the western margin of the Vindhyan Basin during Paleoproterozoic (2500-2200Ma) and that the Khairmalia volcanics represent the mature arc magmatism. Such a scenario is supported by several previous studies (Sarkar et al. 1989; Mishra et al. 2000; Leelanandam et al.; 2006).

Ahmad et al. (2008a) carried out geochemical studies on the Proterozoic mafic volcanic rocks from the Aravalli-Delhi orogeny and suggested that all the metavolcanic rocks within the supracrustal belts of Aravalli, Bhilwara, Jharol and Delhi were of typical tholeiitic in composition except for the rocks in Basantgarh area of Delhi belt, which were cal-alkaline in composition. The Bhilwara and Aravalli samples showed enriched LREE, while Delhi belt samples showed flat to fractionated REE patterns. The incompatible element ratios were similar in Bhilwara and Aravalli volcanics, while Delhi belt samples showed large variations. Comparison of trace element patterns of these rocks with those of the Khairmalia volcanics reveals that the metavolcanics of the Delhi Supergroup have similar chemical affinities (e.g. depletions of Nb & Ta) and going by conclusions made by Ahmad et al (2008a) both should represent island arc settings, though the locations of the subduction zones and their timing could have been different.

The measured $^{87}\text{Sr}/^{86}\text{Sr}$ ratios in these rocks are highly radiogenic (0.718 to 1.969) and so are the initial ratios, which clearly point to incorporation of radiogenic Sr during metamorphism. The measured $^{143}\text{Nd}/^{144}\text{Nd}$ isotopic ratios vary from 0.510919 to 0.512015 (corresponding $\epsilon_{\text{Nd}}(0)$ varies from -33.5 to -12.2; Table 3.1), which confirm the radiogenic nature of Nd in them. The Nd model ages (T_{DM}) vary from 3.22 to 2.22 Ga. It appears that there have been different episodes of this activity with rocks having higher model ages representing magmas affected by



continental derived material at the source or were crustally contaminated. The sample that has the lowest $^{87}\text{Sr}/^{86}\text{Sr}$ (0.71769) and $\epsilon_{\text{Nd}}(0)$ (-12.2) possibly represents the least contaminated lava within the Khairmalia volcanics. There exists a finite probability that some of our metavolcanics may actually represent pre-Khairmalia magmatism.

3.2.2 Vindhyan Sedimentary Sequences

The chemical compositions of the clastic sediments have been widely used as provenance indicators (McLennan et al., 1995, 2003), since these are directly controlled by their original source rocks. Chemistry of siliciclastic sediments has also been used for understanding the weathering histories and the past climate changes (e.g., Nesbitt & Young, 1982; Fedo et al., 1995). These also help to understand secondary processes such as hydraulic sorting and diagenesis (e.g. McLennan et al., 1993) and tectonic history of the depositional environments (Bhatia, 1983; Bhatia & Crook, 1986; Naqvi et al., 1988). Chemistry of sediments also plays an important role in the evaluation of the composition of the continental crust (Condie, 1993). Therefore, geochemistry of the sedimentary rocks/sediments is essential for unraveling the mysteries for the evolutionary processes of the planet Earth.

The composition of sedimentary rocks is controlled by the source rock compositions and the sedimentary processes responsible for sediment generation and its deposition in a basin. Further, diagenesis of sediments, which is responsible for conversion of sediments into sedimentary rocks, also plays a crucial role in determining the chemical compositions of the sedimentary rocks. Some of the geochemical signatures of the source rocks get obliterated by diagenetic processes, in such scenario isotopic ratios come in handy in provenance determination.

The geochemical studies on the finest fraction of sediments (i.e. clay size fraction) are believed to yield good results for understanding the provenance of the sediments since they faithfully record the sedimentary history of the basin. Shales (mudstones), due to their impermeability, retain the minerals from the source rocks (Blatt, 1985; Graver and Scott, 1995) and hence preserve the near original composition of the sources. These rocks record the elemental abundances of the relatively immobile elements (e.g. REE, Th, Nb, Sc, Zr etc.), transferred quantitatively through the sedimentary processes from the parent rocks into the clastic sediments (Taylor & McLennan, 1985; Condie, 1991). According to these workers the abundances as well as the ratios of these elements remain intact during the diagenesis as well as low grade metamorphism. The provenance signal get well represented in case of the mud/shale due to effective mixing of the sources during suspension transport comparative to the sand size, which, in general transported as bed load. Therefore, geochemical study of finer clastic sediments (i.e. shales/pelites) is useful in deciphering the source compositions of the sediments in a basin.

Daly (1909) first identified that Ca/Mg ratios varied over the geological history. Subsequently, numerous geochemical investigations were carried out to identify secular trends in major and trace elements in siliciclastics as well as carbonate rocks. The parameters controlling these secular variations are the mixed responses of sediment recycling and preservation of the changes in the composition due to weathering/diagenesis as well as the evolution of continental crust (McLennan and Hemming, 1992). Sedimentary processes tend to mask the signatures of the provenance and direct correlation with the source rocks is not straightforward. In such a scenario combination of elemental geochemistry and isotopic studies specifically of Nd isotopic ratios have proved to be useful.

The Nd isotopic ratios and rare earth element (REE) concentrations have widely been used in shales for understanding the sedimentary provenance. Since shales are believed to be true representatives of the parent materials because of their fine grained and well-mixed nature. It is believed that the REE concentration of the

Upper Crust is represented by average shales, with low organic content, which show uniform REE pattern with narrow range of Sm/Nd ratio (typically varying between 0.10 and 0.12; Taylor and McLennan, 1985; McLennan et al., 1989). As discussed earlier the REE content of shales remain unchanged during weathering, re-working, re-suspension, and re-deposition and hence the relative abundances of Sm and Nd do not change during deposition and very early diagenesis of shales due to their group chemistry. However, some workers have demonstrated that diagenesis can significantly mobilize/fractionate REEs (Milodowski and Zalasiewicz, 1991; Ohr et al., 1994; Lev et al., 1999; Lev and Filer, 2004). It may lead to disparities between the whole rock geochemical signature of shales and that of the presumed parent material. In this case a preferential loss of the REEs during diagenesis can significantly alter the Sm/Nd ratio and hence the Nd-isotopic signature of the sediments relative to the source rock (McLennan et al., 1989; Bock et al., 1994; Hannigan and Basu, 1998).

3.2.2.1 *Petrography of Sandstones*

The Vindhyan sedimentation in Rajasthan started with the deposition of the Khardeola Sandstone in which volcanic clasts have been reported (Prasad, 1984). Our petrographical study on these sandstones reveals that these do not show any signature of metamorphism. However, in some of the samples we observed sub-parallel fractures in quartz grains with associated high relief. We believe that it might be due to the effect of tectonics associated with the nearby faults (in the GBF zone) on these grains. The most dominant mineral after quartz is feldspar, which are mostly orthoclase. These rocks also contain opaque minerals, predominantly reddish brown in colour, which are most likely hematite (Fig. 3.4). The immature status of these sandstones is evident from the presence of abundant lithic fragments, with large amount of accessory phases of Fe bearing minerals.

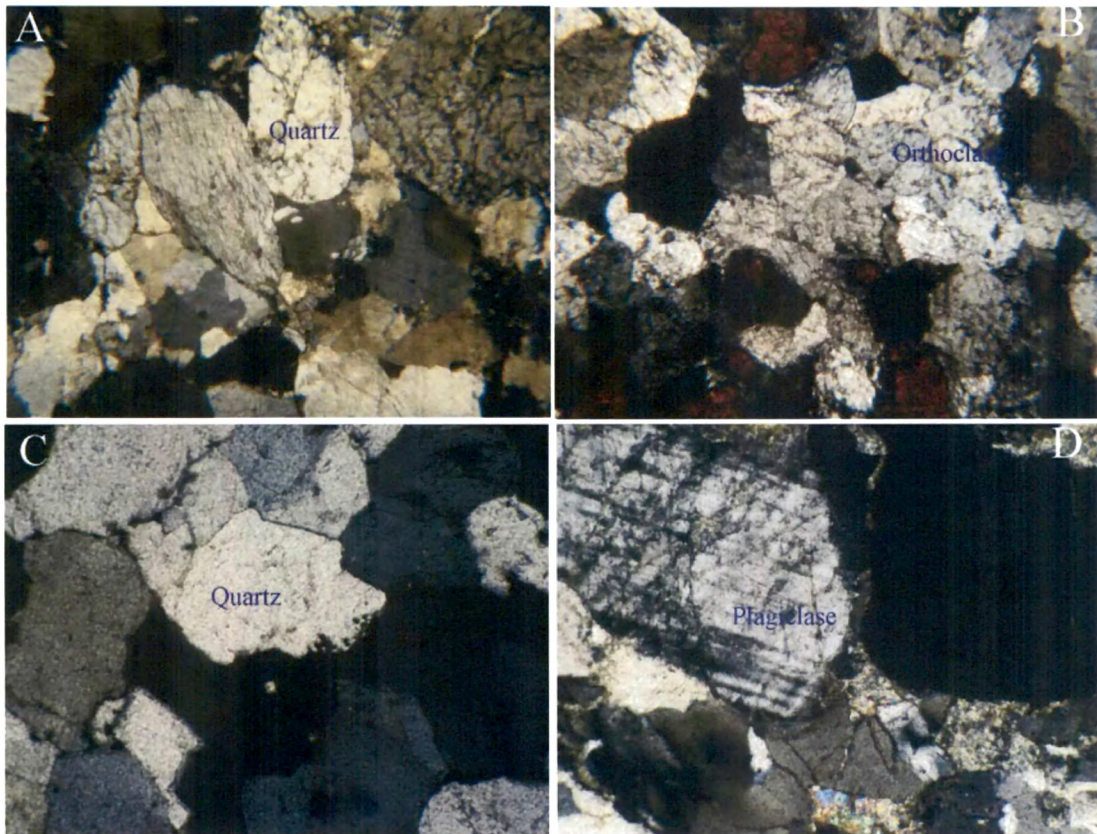


Fig. 3.4: Photomicrographs of thin sections of the Lower Vindhyan sandstones under crossed polars: A) Khardeola Sandstone; B) Bhadesar Quartzite; C) Sawa Sandstone; D) Sawa Sandstone/Porcellanite.

The Bhadesar Quartzite/Sandstone Formation, which is considered equivalent to the Khardeola Formation by Srivastava and Gyanchand (1984) and Soni et al. (1987), is included in the Hindoli Group of rocks by Prasad (1984). The petrographical examination of samples of Bhadesar Formation collected from hillocks of Thukrawa village near Bojunda town reveals that these too contain lithic fragments of volcanic materials, and feldspars. Also, the fractured nature of grains (Fig 3.4b) is very much like those observed in the Khardeola sandstone.

The Sawa Sandstone Formation is gritty in nature. It contains, apart from quartz, plagioclase feldspars and iron oxides with minor lithic fragments (Fig 3.4 C&D).

These observations hint at inclusion of igneous material within this formation. A thin porcellanite formation has been reported to be occurring between this and the overlying Sawa Shale Formation. In the field, however, we found it difficult to identify the porcellanite lithology.

The Kaimur Sandstone contains almost uniform, sub-rounded quartz and orthoclase feldspar grains with low amount of cements (Fig 3.5A) suggesting maturity. Up in the stratigraphical column, the Taragarh Sandstone of the Rewa Group, contains angular quartz grains and plenty of lithic clasts (Fig 3.5.B). The grains are finer compared to the underlying Kaimur Sandstone and the overlying Bundi Hill Sandstone of the Bhandar Group (Fig 3.5C). The texture of the Bundi Hill Sandstone has similarity with the Kaimur Sandstone but have smaller mineral grains. The Shikoda Sandstone (i.e. Maihar Sandstone) occurring above the Lower Bhandar Sandstone contains a lot of angular clasts within a dirty matrix (Fig. 3.5 D).

The petrographical studies suggest that the sandstone formations from the Lower Vindhyan have signatures of immaturity which is evident from the presence of plagioclase feldspars, lithic clasts and opaques. This suggests that the location of the sources could not have been far off from the place of deposition. Similarly, in the Upper Vindhyan the Taragarh Sandstone of the Rewa Group also shows the incorporation of igneous material from the nearby sources as the angularity of the grains hints at a short distance transport for the quartz grains.

3.2.2.2 Clues from Major Elements

The sandstone and shale formations from the Lower Vindhyan (Semri Group) are plotted in the chemical classification diagram of Heron (1988) (Fig 3.6). It is noted that most of the Vindhyan shales/mudstones plot in the field of wacke suggesting that the shales are slightly coarser than a typical shale. The Binota Shale of the Semri Group of the Lower Vindhyan is found to be Fe-rich and falls in Fe-sand field (Fig. 3.6). These observations suggest that the deposition of the Lower Vindhyan mud

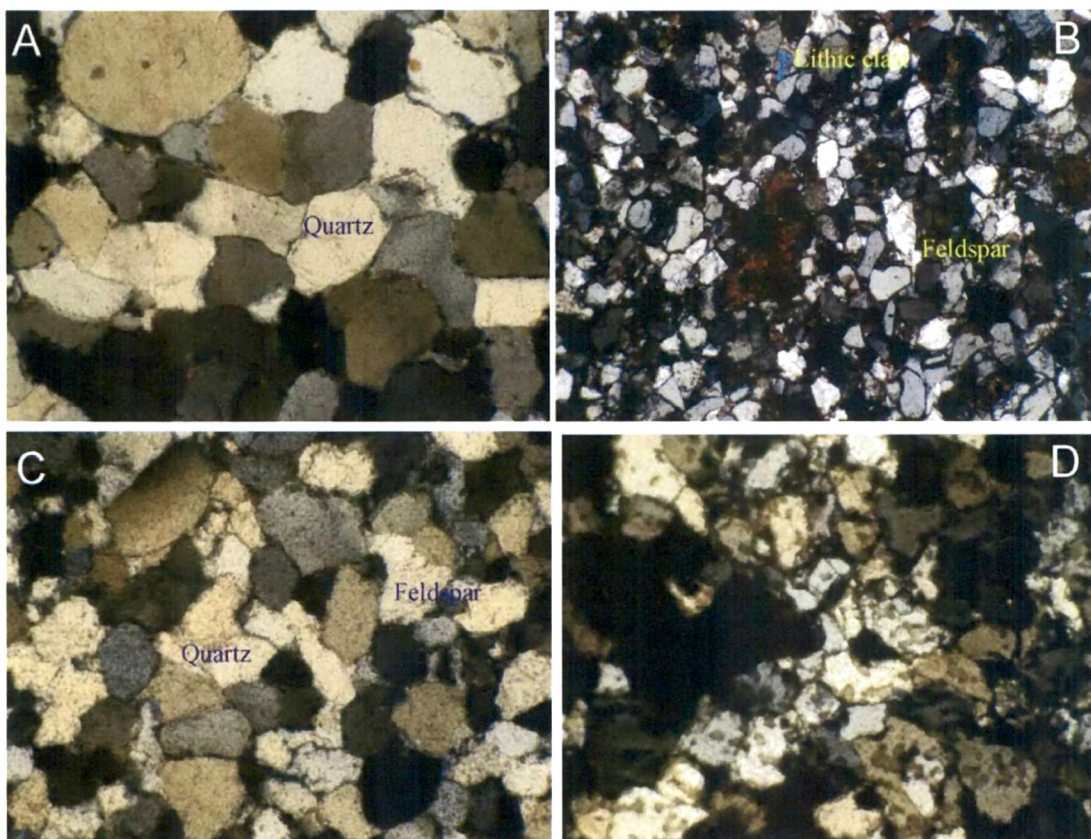


Fig. 3.5: Photomicrographs of thin sections of Upper Vindhyan sandstones under crossed polars; A) Kaimur Sandstone; B) Taragarh Fort Sandstone; C) Bundi Hill Sandstone and D) Shikooda Sandstone. Scale: 1cm = 500 μ m.

rocks did not take place in a deep water regime and not far away from the provenances. The latter is reflected in the lack of sorting of grains. The sandstones of the Lower Vindhyan, except for the Sawa Grit Formation, fall in less mature fields (Fig. 3.6), which is a result of the presence of lithic and feldspathic fragments in them.

The Kaimur sandstones are composed of >95% of SiO_2 , and Al and Fe contents are below the detection limits. The composition itself suggests that it is a Quartz Arenite. Our petrographical studies also indicate it to be a super mature sandstone with the presence of well rounded quartz grains and no feldspar grains (Fig 3.5). Most of the sandstones from the Rewa and Bhandar Groups are of subarkose and sublitharenite type. The Sawa Grit Formation of the Semri Group and the Shikooda Sandstone of

the Bhandar Group are typical quartz arenites and contain > 95% of quartz. The Taragarh Sandstone contains lithic fragments while the Indergarh Sandstone plots at the boundary of Fe-sands and quartz arenite. The survival of the lithic/rock fragments and feldspar in the sandstones as well as within the coarse-grained shales suggest that the sources of these rocks were near the depositional sites within the basin.

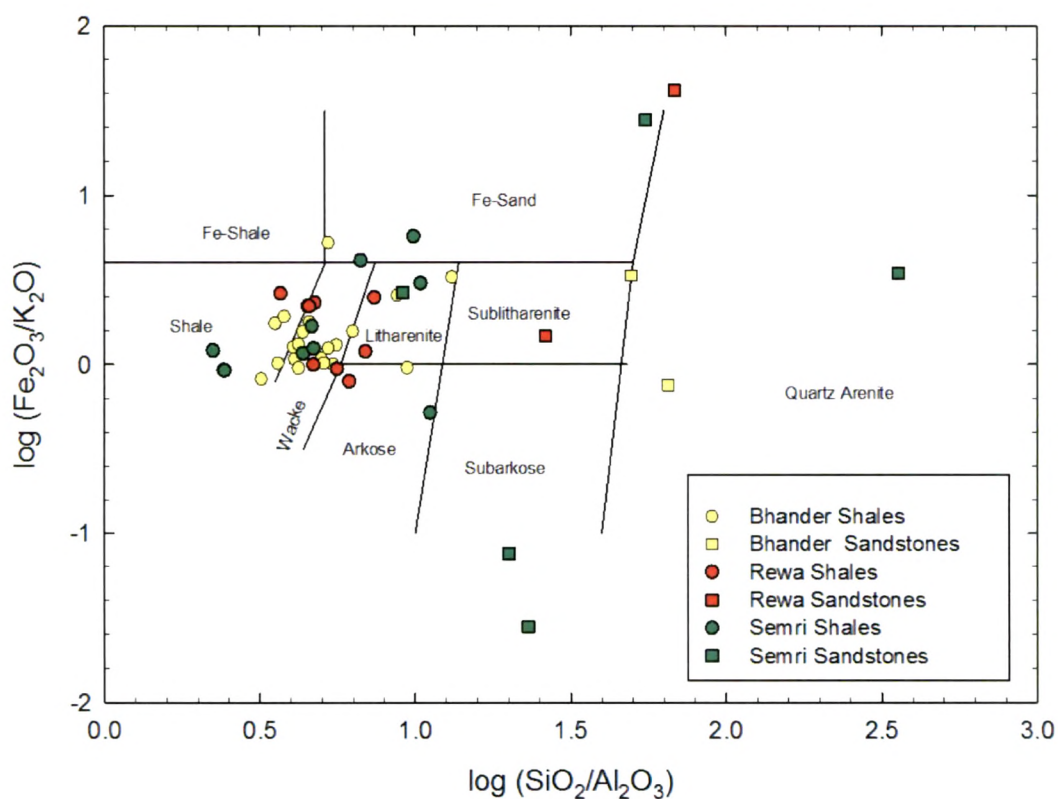


Fig. 3.6: Chemical classification of shale and sandstone formations of various groups of Rajasthan Vindhya Group using the scheme of Heron (1988).

The Chemical Index of Alteration (CIA) proposed by Nesbitt & Young (1982) has been most widely used in understanding of weathering in the source area. This index is defined as follows using molecular proportions:

$$\text{CIA} = [\text{Al}_2\text{O}_3 / (\text{Al}_2\text{O}_3 + \text{CaO}^* + \text{Na}_2\text{O} + \text{K}_2\text{O})] \times 100$$

where CaO^* is the amount of CaO incorporated in the silicate fractions of the rocks and a correction should be carried out for carbonates and apatite contents.

The CIA value of the Khardeola Sandstone is calculated to be 97 while the samples from the Bhadesar Quartzite (CGB-07-12) have values ranging from 40 to 70. The low value of 40 could be explained by higher content resulting from K-metasomatism (Fedo et al., 1995). The Sawa Sandstone and Porcellanite formations have CIA values varying between 70.2 and 87.7, suggesting a moderate to high degree of weathering at the source regions prior to the derivation of these sediments. The CIA calculated data for the Khardeola/Bhadesar formations support that the source areas have experienced high degree of weathering. On the A-CN-K (Al_2O_3 - CaO^* - Na_2O - K_2O) plot of Nesbitt & Young (1984), in which the oxides are represented as molar proportions and the CaO^* represents the carbonate free CaO, the sandstones from the Semri Group plot near the field of illite clay minerals along the A-K axis (Fig. 3.7). This suggests high degree of weathering in the source region, however, the large spread could be a result of involvement of multiple sources.

The sediments from the Upper Vindhyan formations are also plotted on A-CN-K diagram in Fig 3.8. The CIA values for the shales from the Upper Vindhyan vary between 59.5 to 81.9 and the sandstones between 76.7 and 96.9. These observations also suggest moderate to high degree of chemical weathering in the source region of these sediments prior to their deposition. On the A-CN-K diagram (Fig. 3.8) all the sandstones and shales, except a few, fall along the A-K axis suggesting the presence

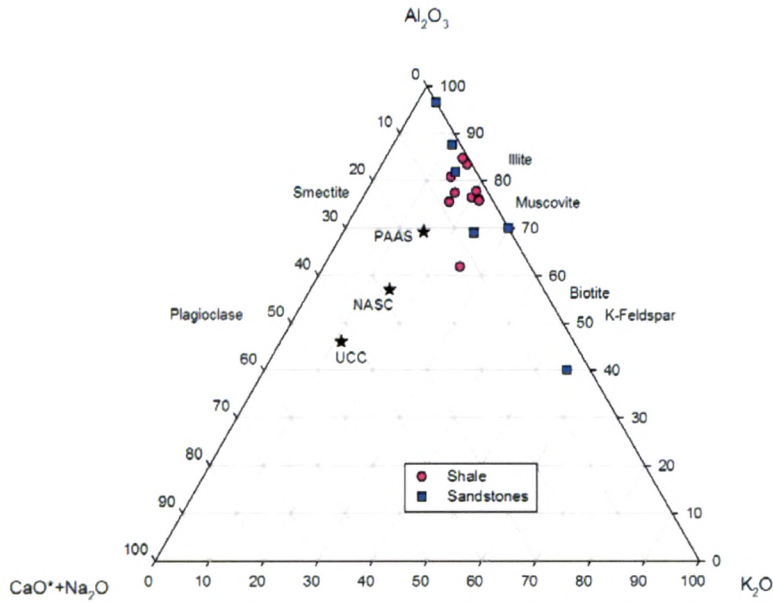


Fig 3.7: Shales and sandstones from the Lower Vindhyan (Semri Group) plotted on A-CN-K diagram of Nesbitt & Young (1984). Also shown are the compositions of PAAS (Post Archean Australian Sediments), NASC (North American Shale Composite) and UCC (Upper Continental Crust).

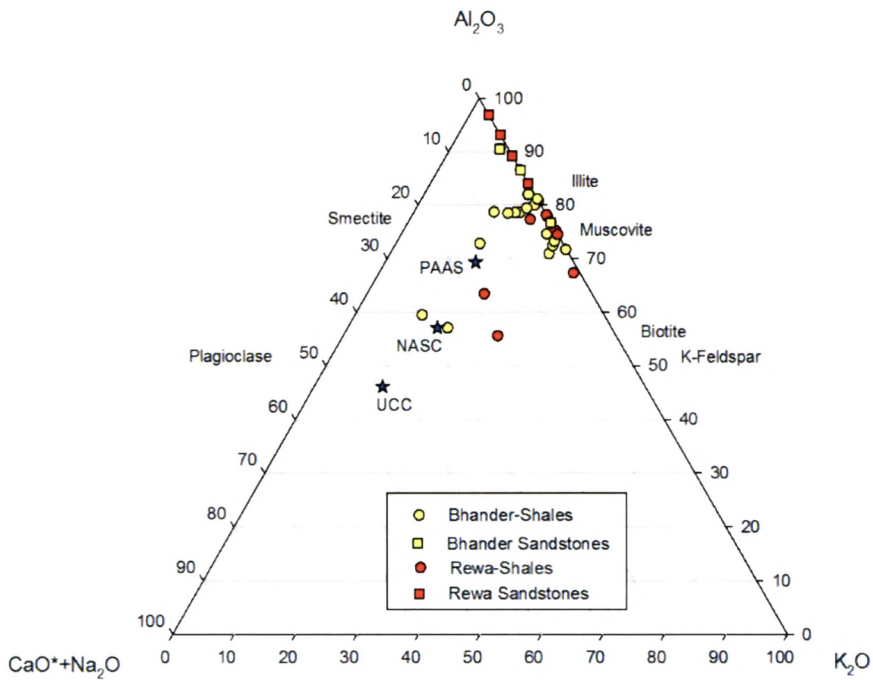


Fig. 3.8: Shales and sandstones from the Upper Vindhyan plotted on A-CN-K diagram of Nesbitt & Young (1984).

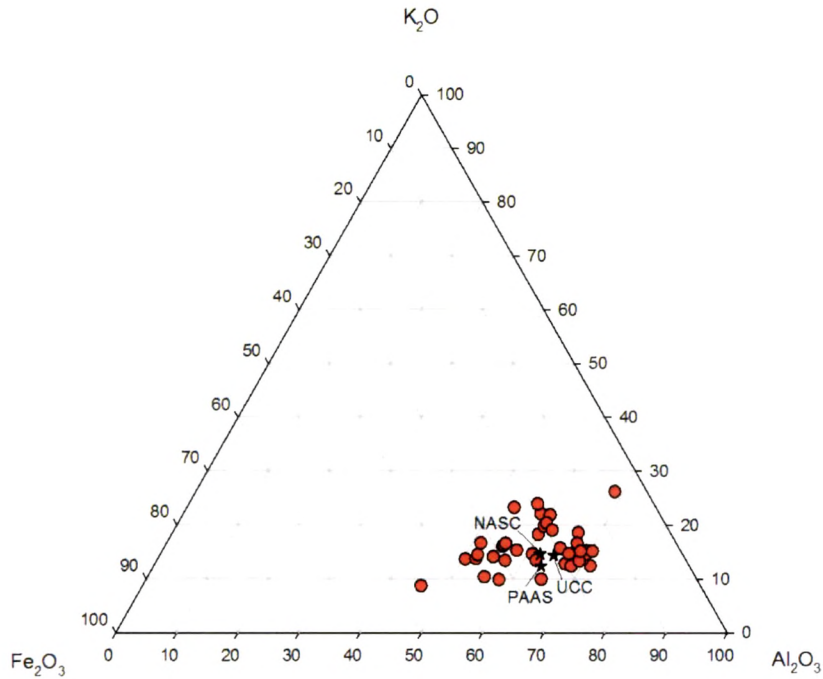


Fig. 3.9: Al_2O_3 - K_2O - Fe_2O_3 diagram for the shales from the Vindhyan of Rajasthan.

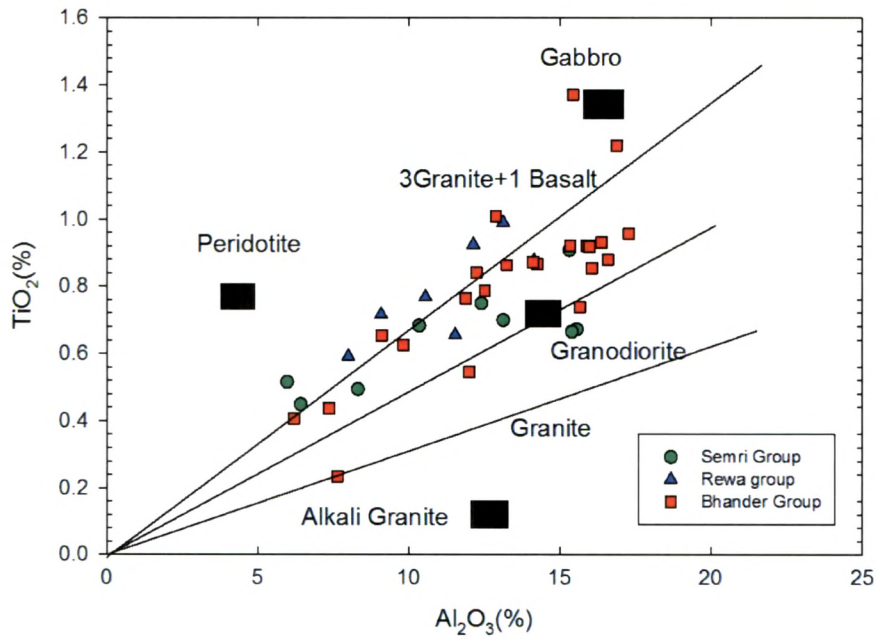


Fig. 3.10: TiO_2 vs. Al_2O_3 plot of McLennan et al. (1980) for sedimentary rocks on which data from the Vindhyan sediments of Rajasthan are plotted. The 'granite' and '3Granite+1 Basalt' lines are from Schieber (1992).

of illite/muscovite. The near absence of Al in the Kaimur Group of sandstone samples restricts us reconstructing the weathering history of the sediment sources.

The computed CIA data in conjunction with the A-CN-K compositional triangular diagram provide valuable information about weathering and tectonic history. The weathering and post depositional diagenetic changes could be ascertained by plotting weathering trends in the A-CN-K plots. No clear trend has been observed for shales of Vindhyan of Rajasthan, except their spread along the A-K axis. This suggests that their sources had undergone high degree of weathering, as during early stages of weathering the samples follow the trend parallel to A-CN line due to loss of Ca and Na from the plagioclase feldspar and later shifting of the trend towards A-apex due to breakdown of K-feldspars (Nesbitt & Young, 1982).

The molecular proportion of Al_2O_3 - K_2O and Fe_2O_3 of the shales are plotted in the compositional space in Fig. 3.9. The majority of the data plotted fall close to Al_2O_3 suggesting clay minerals control the compositions (Wronkiewicz and Condie, 1987). The shales from Rajasthan Vindhyan also show significant variation in iron content (Fig. 3.9).

The chemical resistant behaviour of Al and Ti during weathering has also been used to identify the source signatures by plotting a bivariate plot between TiO_2 vs. Al_2O_3 (McLennan et al., 1980; Schieber, 1992), which has been reproduced in Fig. 3.10. In this plot the data of the Rajasthan Vindhyan fall closer to the mixing line of '3 granite+1 basalt' line of Schieber (1992) and the 'granodiorite' field. Even some samples fall closer to the 'gabbro' field.

3.2.2.3 Clues from Trace Elements

Concentration variations of trace elements have been very useful in understanding provenance, weathering, transportation, diagenesis and metamorphic history of sedimentary rocks. The low mobility of trace elements like Ti, Zr, Y, Nb, Th, Sc and

rare earth elements (REEs) in fluids make them good tracers for understanding the sources of sediments. Trace element geochemistry including the REEs in the fine grained sediments i.e. mud and mudstones (shales) have been extensively used in deciphering history of sediments. The REEs, due to their group behaviour, immobility in natural waters, and almost nonexistent inter-element fractionation, faithfully preserve the source compositions (McLennan et al., 1989). Elements like Th and Sc have similar behaviour in sedimentary environments and hence considered useful for provenance studies (Taylor and McLennan, 1985). The increase of Th/Sc ratio in sediments subsequent to the Archean-Proterozoic transition has been attributed to derivation of sediments from more differentiated felsic material compared to undifferentiated mafic material in Archean (McLennan and Hemming, 1992). Similar trends also have been observed in La/Sc and La/Yb ratios and are believed to be controlled again by felsic material. Various workers have tried to utilize the Sm/Nd ratio over the geological time scale to understand the compositional of the Upper Crust from mafic to felsic (Miller and O'Nions, 1985; Goldstein and Jacobsen, 1988; Dia et al., 1990). However, contrary to a predicted decrease in this ratio it was found to have increased in sedimentary rocks (Goldstein and Jacobsen, 1988; Depaolo, 1988), which suggests a complex evolutionary history for the Upper Crust. Hence, there exist drawbacks in such type of work while relating the trends in sediment compositions to the possible changes in the source rocks.

Chondrite normalised patterns of REE, more specifically of the light rare earth elements (from La to Nd) have been extensively used in sedimentary provenance studies (McLennan et al., 1980). The chondrite normalized REE patterns of shales and sandstones from all the four groups of the Vindhyan Supergroup are presented in Fig. 3.11 and Fig. 3.12. The chondrite normalized patterns are almost similar for all the shales with typical negative Eu anomaly (Fig. 3.11) except for the Nimbahera and Suket Shale of the Semri Group these show slightly depleted LREE patterns (Fig. 3.13). From these patterns it is clear that these shales show homogenous nature reflecting mixed source signatures. The negative Eu anomaly seen in the Vindhyan

shales is quite common in sediments that have been formed after stabilization of the continental crust. The sandstones from all the four groups of the Vindhyan Supergroup show similar LREE enriched patterns as shales except that these have overall lower REE contents and not so pronounced Eu anomalies (Fig. 3.12). From the REE patterns various sandstones within the various groups can be differentiated based on the extent of LREE enrichment. For example, the Bundi Hill Sandstone (Sample No. Satur-23; Fig. 3.12A) has higher REE content compared to that in the Shikooda Sandstone (BUNDI-09-05; Fig. 3.12A). The REE patterns for the Indergarh Sandstone (BUNDI-09-08) collected, near Indergarh town in Bundi district, is quite similar to that of the sample of same formation collected near Rawatbhata town in Chittorgarh district (CHITTOR-09-03), separated by more than 100 km. This suggests that the sources of the sediments to both the places may not have been very different.

For comparison, normalized REE patterns of shales and sandstones were also plotted against the Post Archean Australian Sedimentary Rocks (PAAS: McLennan et al., 1989) in Fig. 3.13 and 3.14 respectively. The REE patterns of Nimbahera Shale and Suket Shale show prominent LREE depletion (Fig. 3.13C) and so do a few formations of the Bhandar Group. This might be due to changes in sources or lesser input from felsic igneous components. The rest of the samples show either a flat or LREE enriched pattern suggesting that the sources for the Vindhyan sediments represented an average, post Archean continental crust.

To further understand the sources of Vindhyan sediments, their normalized trace element contents were plotted in multi-element spidergrams. Normalization was done using compositions of the primitive mantle (PM) and PAAS (Fig. 3.15 to Fig. 3.18). In these diagrams the elements are arranged according to their decreasing incompatibility in mafic igneous systems. The shales are plotted in Fig. 3.15 and 3.16 and sandstones are plotted in Fig. 3.17 and 3.18. The most striking features in the PM normalized diagram plots are: 1) depletion in Nb and Ta; 2) enrichment in Pb; and 3) depletion in Sr (Fig. 3.15 & 3.17). Such patterns are typical of crustal rocks but

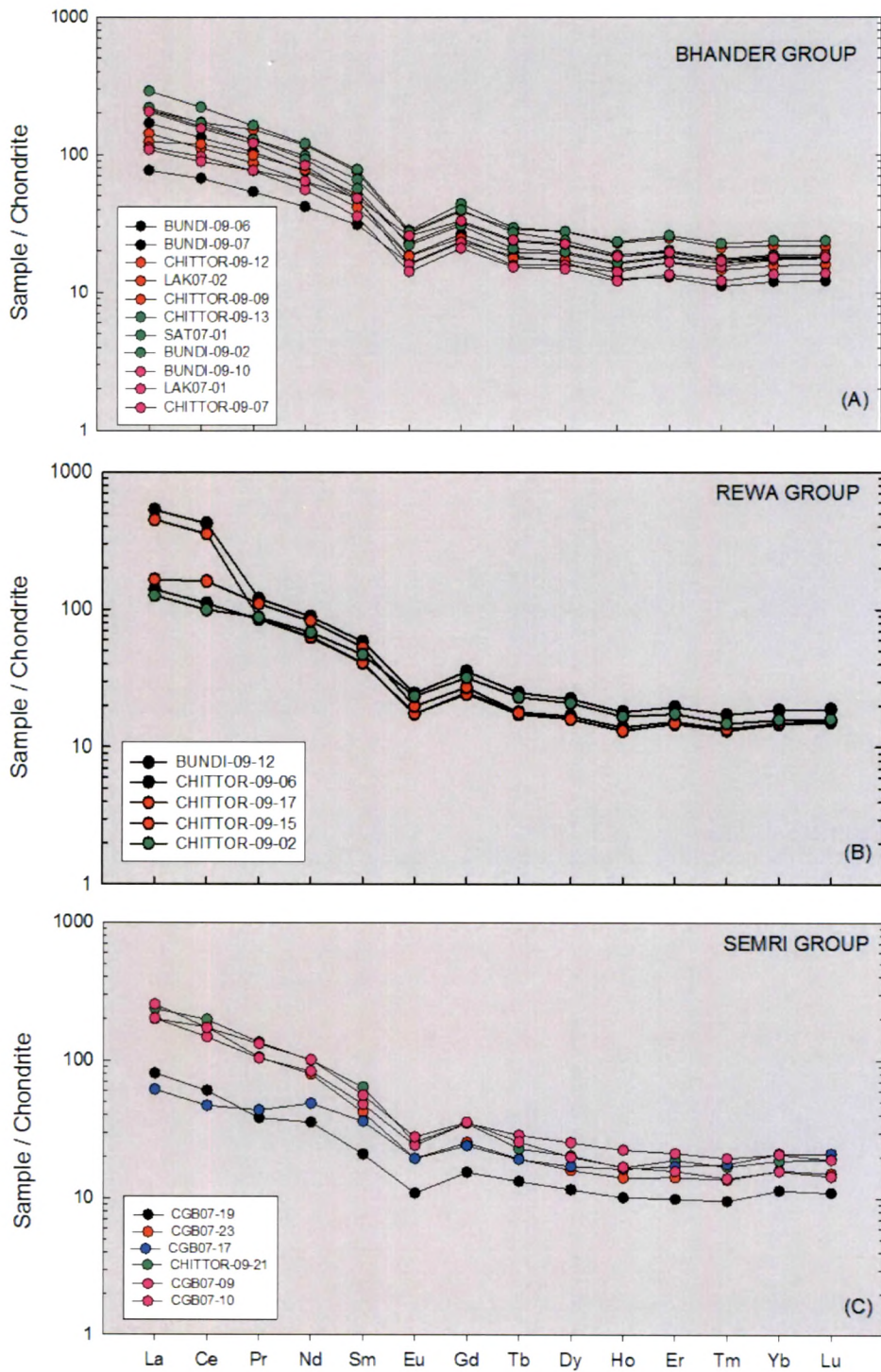


Fig. 3.11: Chondrite normalized REE patterns of shales from the Vindhyan of Rajasthan.

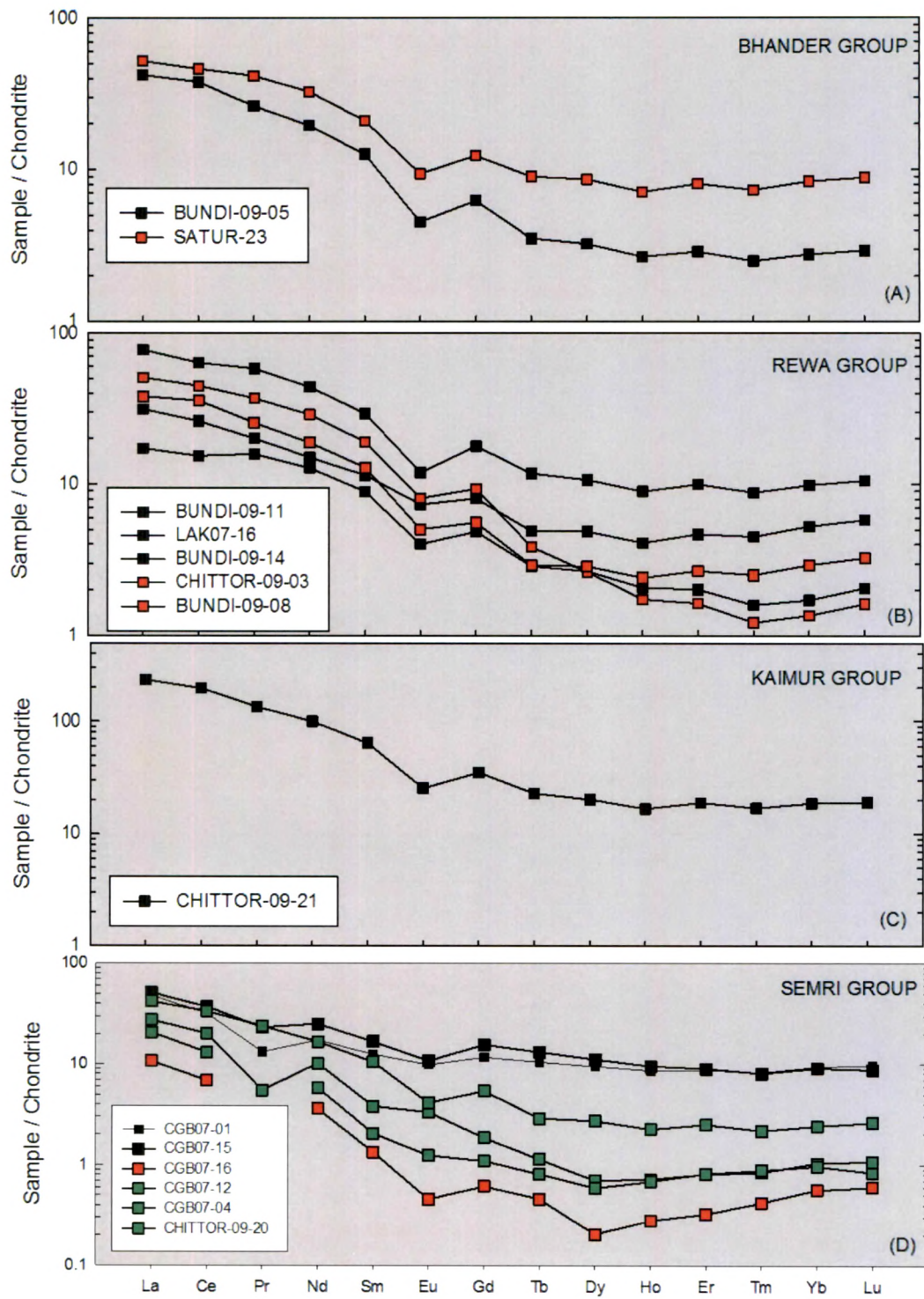


Fig. 3.12: Chondrite normalized REE patterns of sandstones from the Vindhyan of Rajasthan.

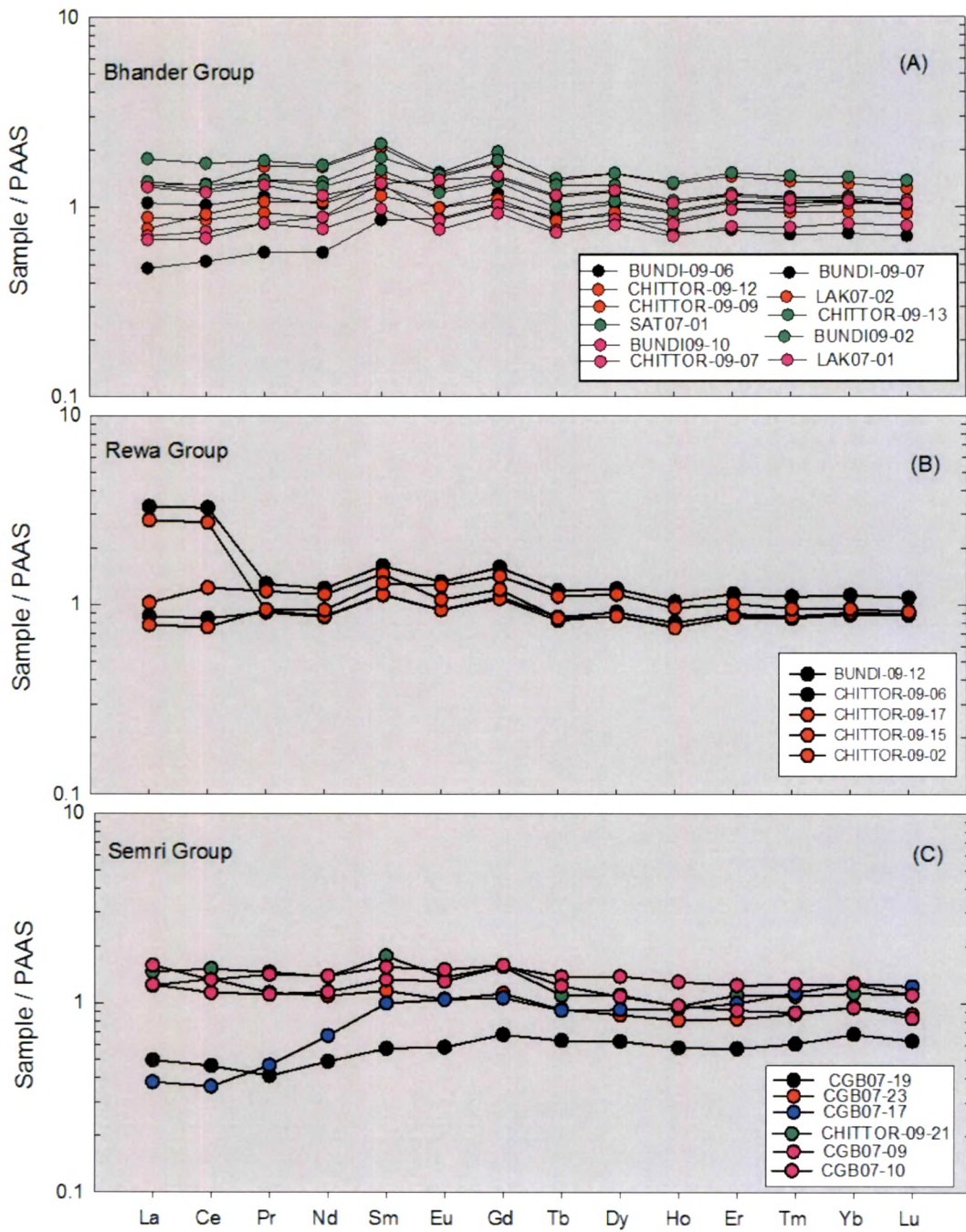


Fig. 3.13: PAAS normalized REE patterns for shale formations of the Vindhyan Supergroup, Rajasthan.

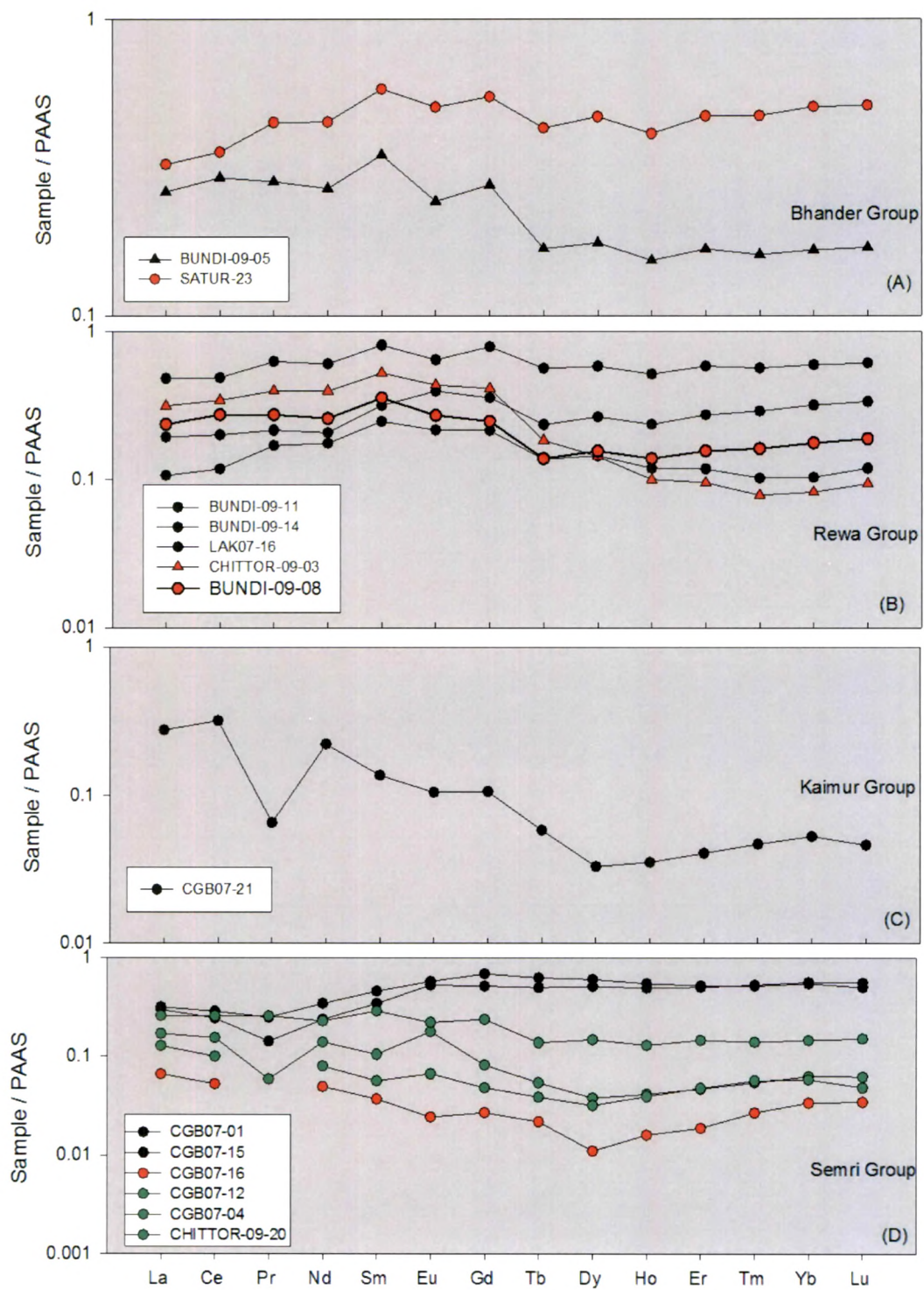


Fig. 3.14: PAAS normalized REE patterns for sandstone formations of the Vindhyan Supergroup, Rajasthan

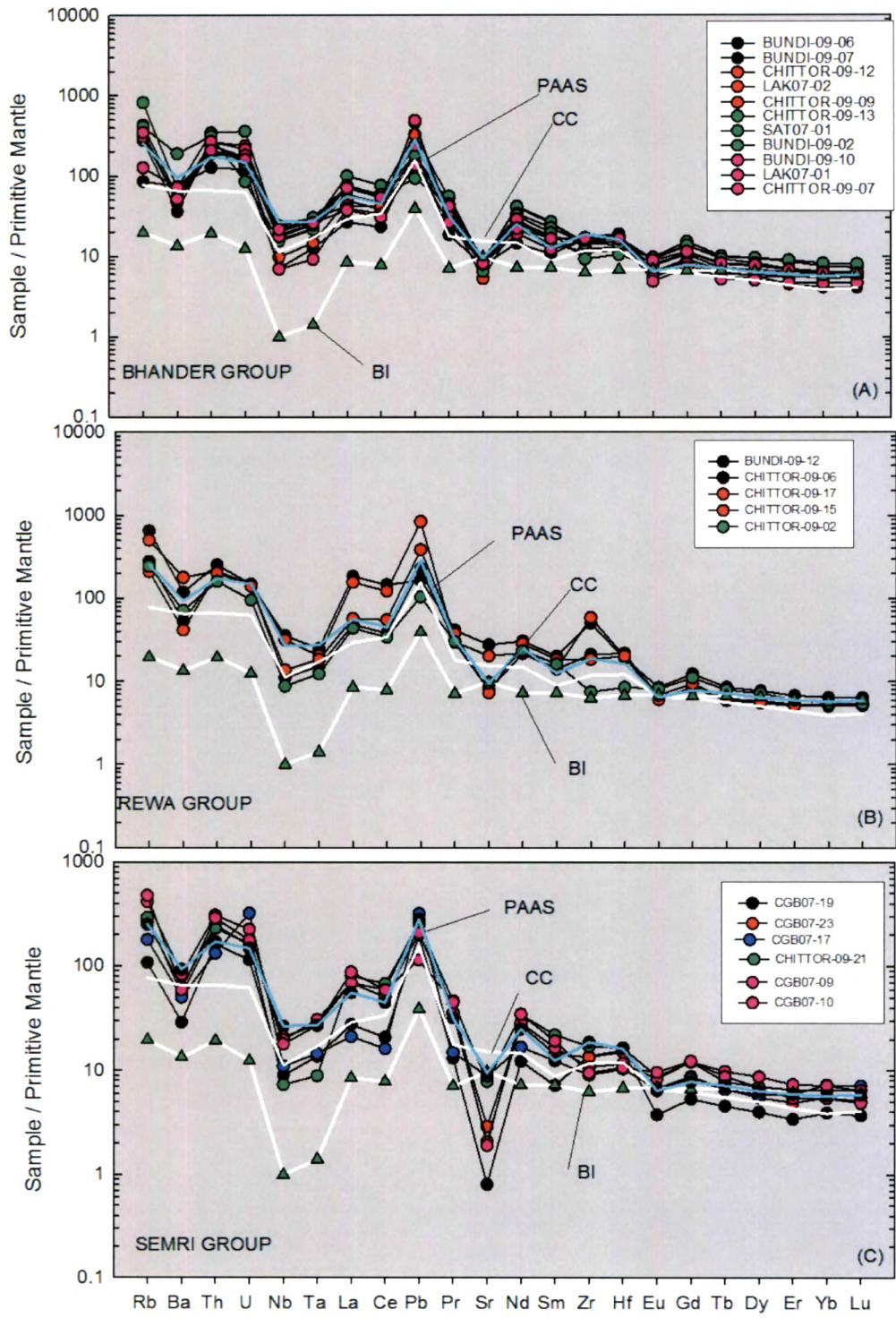


Fig. 3.15: Primitive Mantle normalized multi element spidergrams for the Vindhyan Shales. Also plotted are the patterns for PAAS, Average Continental Crust (CC) and average compositions of Barren Island lavas (BI: a modern volcano in the Andamans).

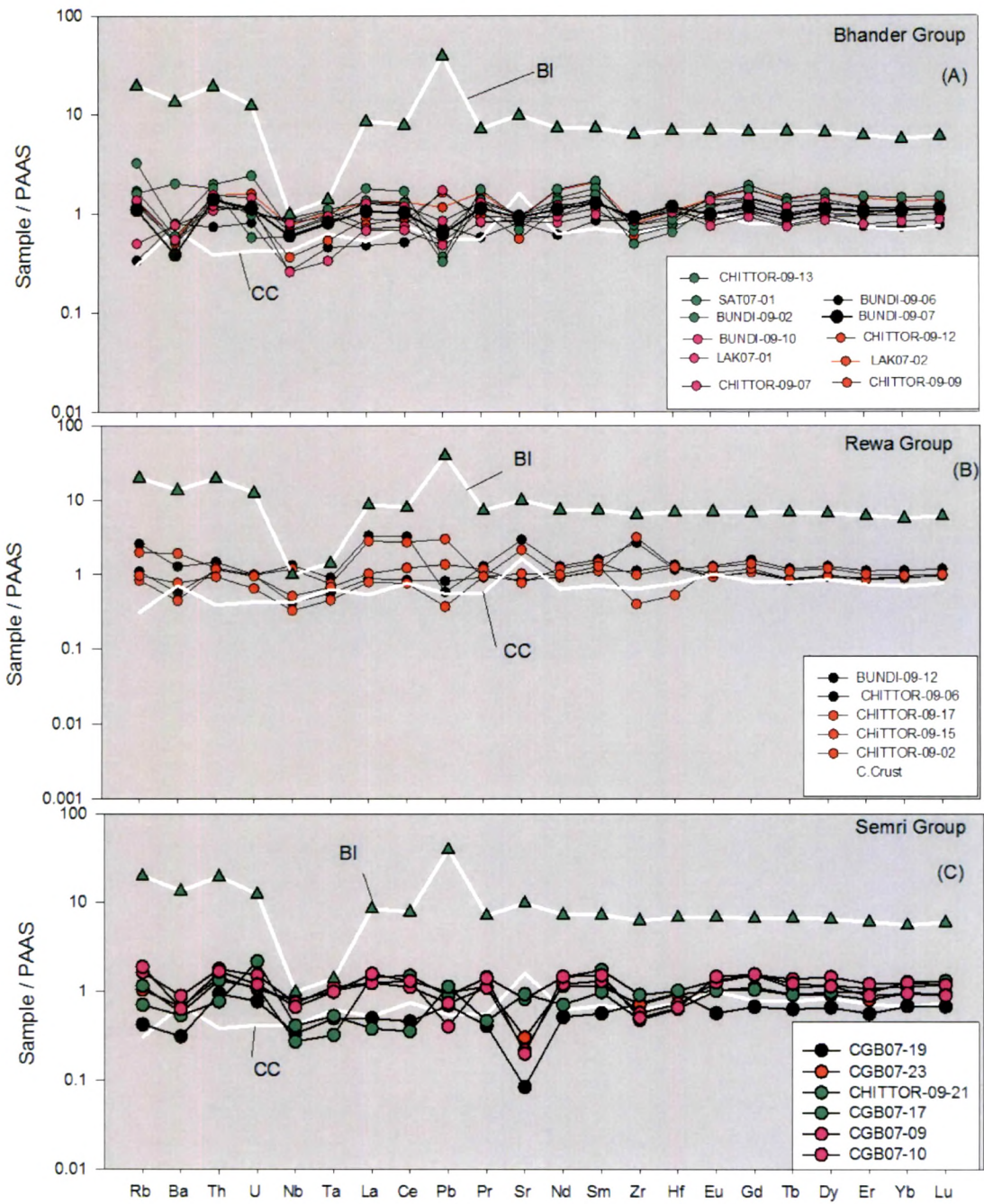


Fig. 3.16: PAAS normalized multi element spiderograms for the Vindhyan shales.

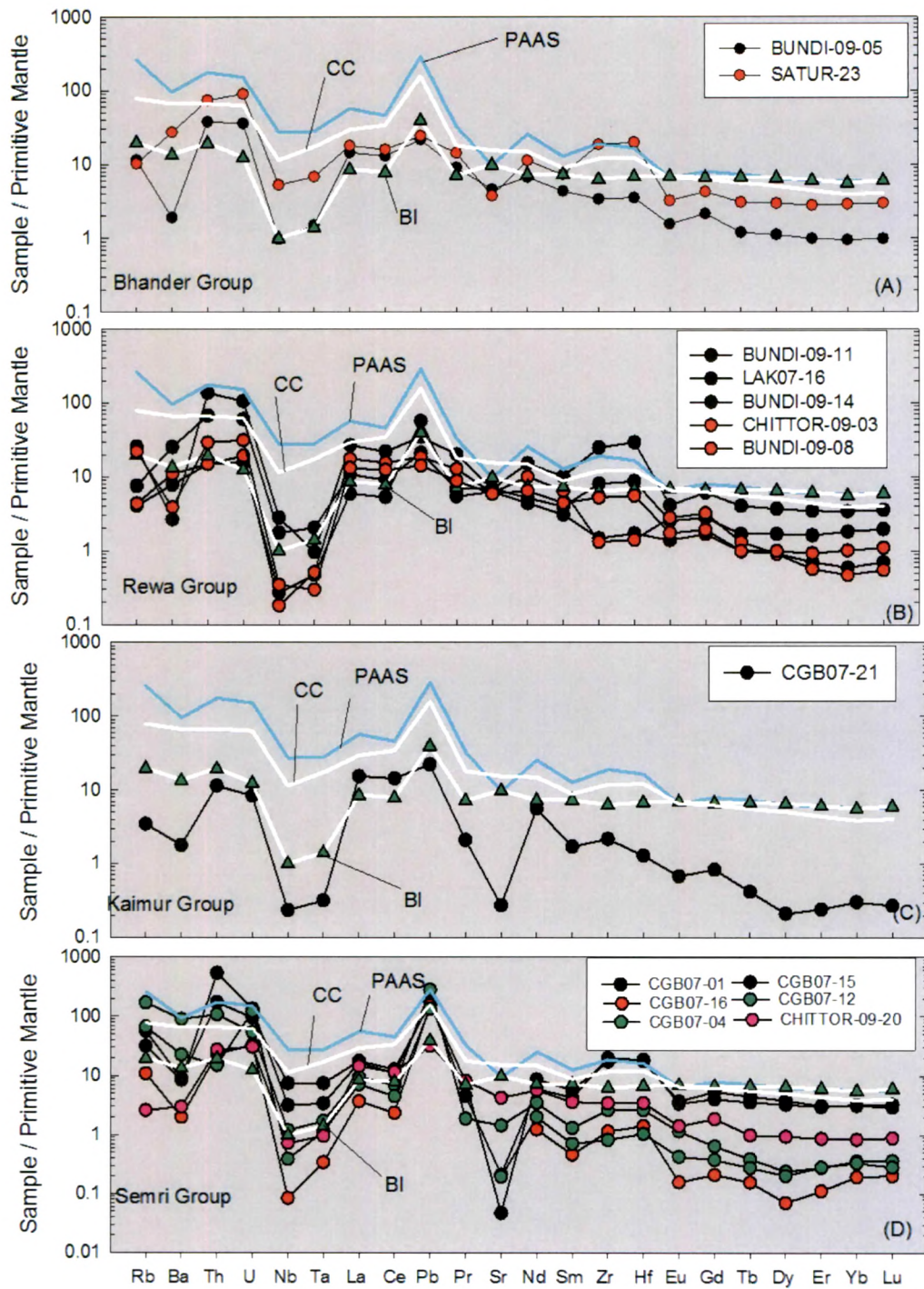


Fig. 3.17: PM normalized multi-element spidergrams for the Vindhyan sandstones.

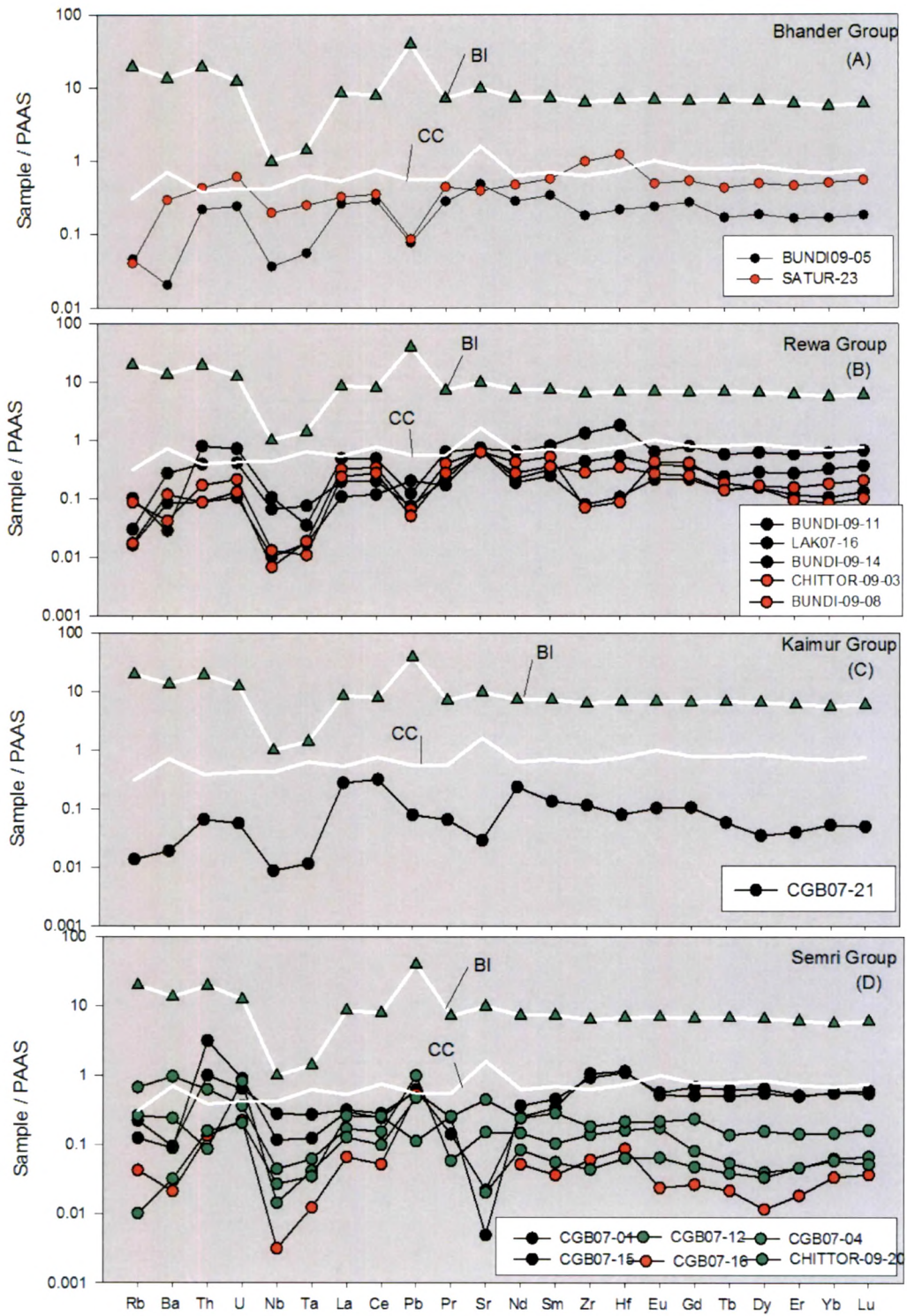


Fig. 3.18: PAAS normalized multi-element spiderograms for the Vindhyan sandstones.

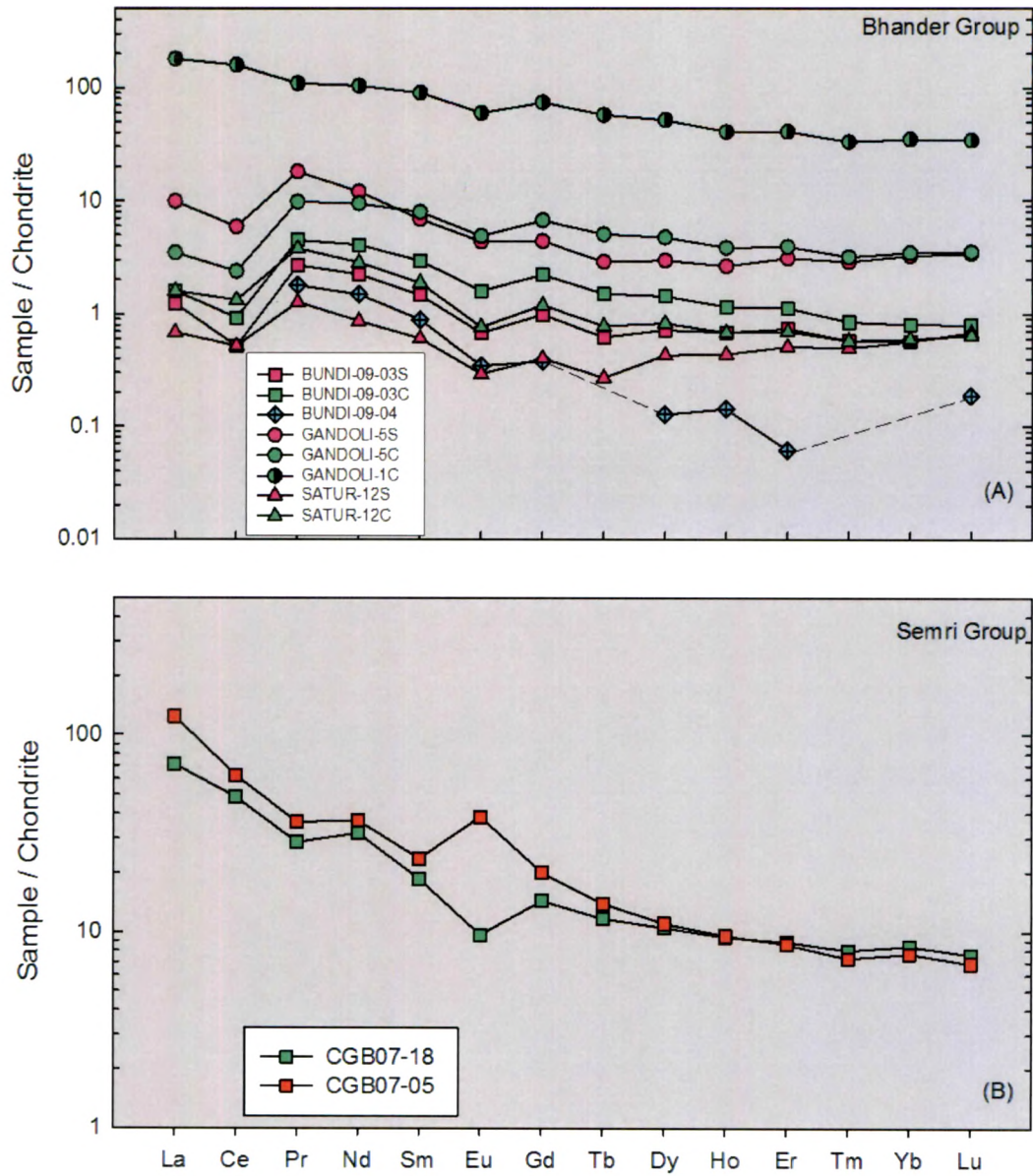


Fig. 3.19: Chondrite normalized REE patterns for carbonate (C) and silicate (S) fractions of limestone/dolostones of the Vindhya of Rajasthan.

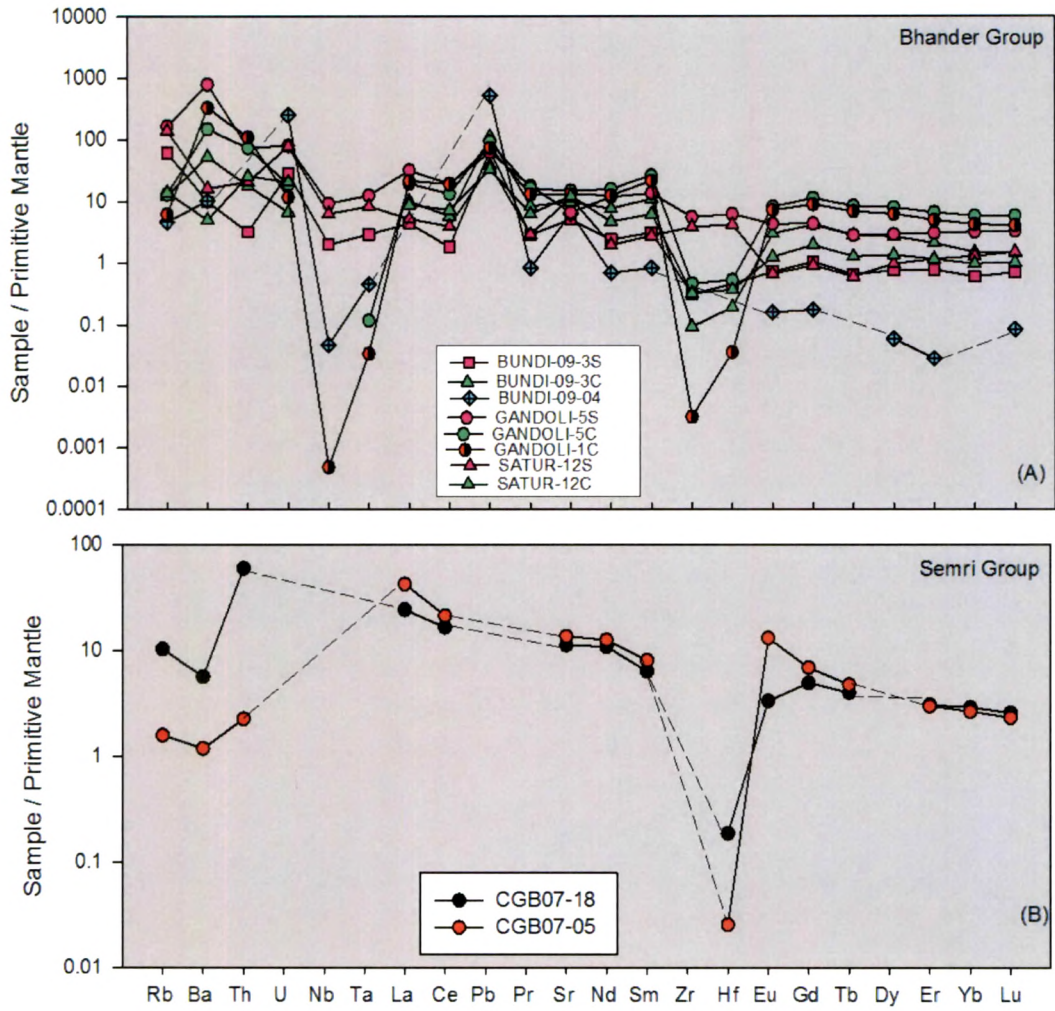


Fig. 3.20: The PM normalized multi-element spiderograms for carbonate (C) and silicate (S) fractions of the carbonate formations of the Vindhyans of Rajasthan.

more pronounced in material derived from subduction zone magmatism (Winter, 2001). For comparison with the modern day subduction zone magmatism an average composition (N=28) of lavas from Barren Island Volcano, Andaman Sea (Luhr & Haldhar, 2006) have also been plotted along with an average composition of continental crust (Taylor & McLennan, 1985). The typical shape of the patterns in all formations across the Vindhyan is similar to that of the Barren Island lavas. There are quite a few samples of shales that show depletion of several elements compared to PAAS (Fig. 3.16) and almost all the sandstones show large depletions in most elements compared to PAAS and Barren Island lavas (Fig. 3.18). The prominent depletion features that are characteristic of subduction zone mafic magmatism persisted even on PAAS normalized plots (Fig. 3.18), which clearly suggests that Vindhyan sandstones had contributions from subduction zone igneous rocks that existed in close proximity of the basin. We, therefore, postulate that a subduction zone setting existed in the vicinity of the basin, and sediments for the basin derived from magmatic arc that contained mafic igneous rocks like Khairmalia volcanics.

Limestone formations of the Vindhyan Supergroup are important members as they record changes in the depositional environment and patterns. Some of the limestones are impure and contain siliciclastic sediments. To shed some light on the source of non-carbonate matrix, these rocks also are analyzed for their trace element contents. Figure 3.19 and 3.20 show chondrite normalized REE patterns and PM normalized trace element patterns in these rocks. These limestone formations have high REE contents in both carbonate and silicate fractions (Fig. 3.19), which suggest incorporation of REE into carbonate matrix during deep burial diagenesis and or recrystallization. Interestingly, the silicate fractions in these limestone show Nb, and Ta depletions and Pb enrichments (Fig. 3.20) similar to those observed in shale and sandstone formations, which suggest that the clastic sediment sources did not change much even when the carbonate was getting deposited.

Trace element ratios such as Nb/Ta, Zr/Sm and Ce/Pb can also be used as tracers for sediment sources (Miller et al., 1994). These ratios in the Vindhyan sediments of

Rajasthan also support their derivation from island or magmatic arc igneous rocks and their derivatives (Fig. 3.21 and 3.22). To further characterize the sources of siliciclastic sediments in the Vindhyan Supergroup of Rajasthan a bivariate plot of Chondrite normalized ratios: La/Yb versus Yb/Gd has been utilized (Fig. 3.23). A three component mixing envelope is generated using the Khairmalia Tholeiites, older metavolcanics from the Hindoli Group and the Berach Granite as end members. We observed that most of the Vindhyan sediments from Chittorgarh and Bundi districts fall within this envelope, which suggests that the surrounding rocks to the west and south of the Vindhyan Basin in Rajasthan played a major role in supplying sediments for the supergroup. Sediments from mafic igneous rocks dominated the Upper Vindhyan.

An attempt was made to decipher existence of any temporal change in contribution from felsic and mafic components to the Vindhyan using the elemental ratios La/Th and Th/Yb (Fig. 3.24). In general, La/Th increases and Th/Yb decreases with the increase in incorporation of mafic/basic igneous materials (McLennan et al., 1980; Wang et al., 1986). Our observations (Fig. 3.24) suggest that the contributions from mafic igneous rocks started to rise around the upper part of the Semri Group and become very strong during the deposition of the Kaimur Group (La/Th=11 and Th/Yb=6.5) and in the Rewa Group (La/Th=3.8 and Th/Yb=6.2).

All the geochemical results from Vindhyan sequences of Rajasthan suggest that these were possibly deposited in a foreland basin developed adjacent to a subduction zone. The presence of Khairmalia Andesite, an arc derived lava flow, at the base of the Vindhyan in Chittorgarh region supports the above hypothesis. The subduction zone or zones might be located within the Aravalli craton. The materials for the Vindhyan were clearly derived from the Aravalli-Delhi Supergroups, along with other basement rocks which were exposed on topographically higher regions. Such a scenario is also supported by the field based sedimentological studies on the Vindhyan basin that indicate that basin was open from the west (Banerjee, 1974). In fact, the Porcellanite Formation in the Semri Group in the Son Valley has also been

identified as a direct product of arc volcanism, and it has been proposed that the eastern margin of the Vindhyan Basin in the Son valley was developed as a foreland basin with southerly dipping subduction of oceanic plate attached to the Bundelkhand craton under the Bhandara craton in the south (Chakrabarti et al., 2007).

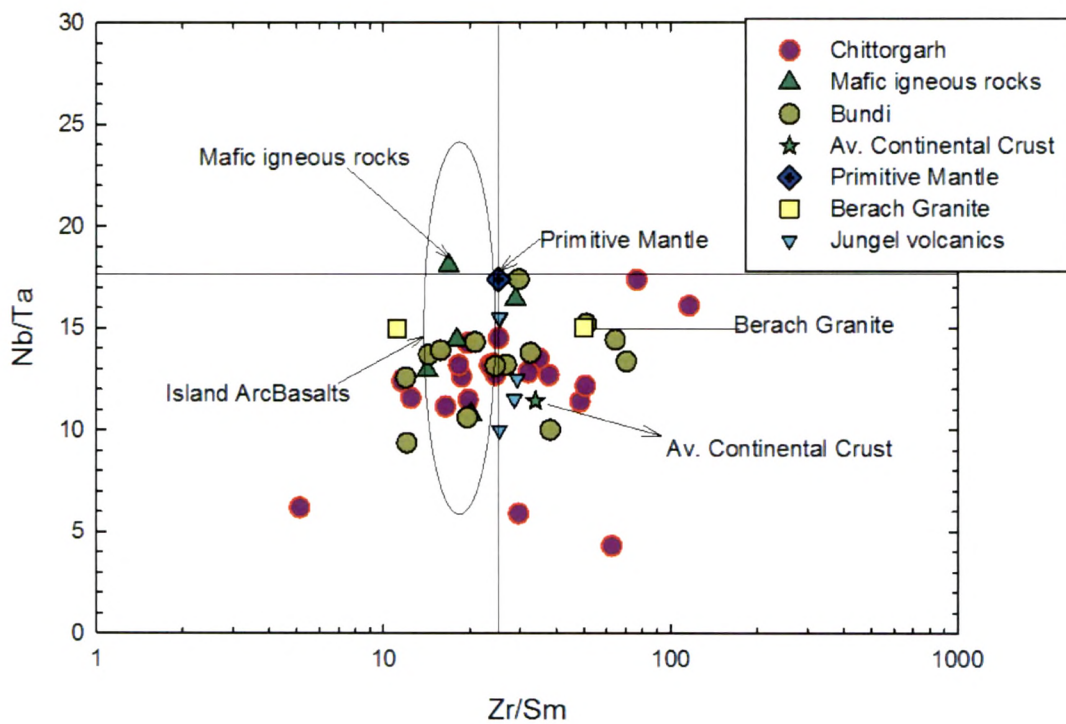


Fig. 3.21: Nb/Ta vs. Zr/ Sm variation in Vindhyan sediments and pre-Vindhyan mafic igneous rocks, Berach Granite and Jungel volcanics. Fields are after Foley et al. (2002).

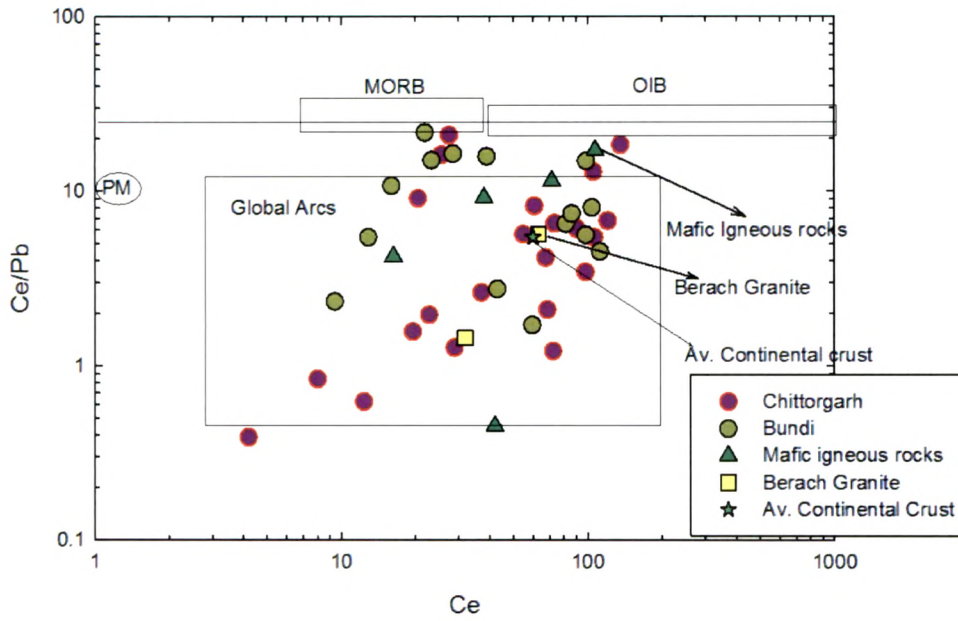


Fig. 3.22: Ce/Pb versus Ce in Vindhyan sediments from various sectors of the basin. Also plotted are the data from pre-Vindhyan granite, mafic igneous rocks and average continental crust. Fields are after Foley et al. (2002).

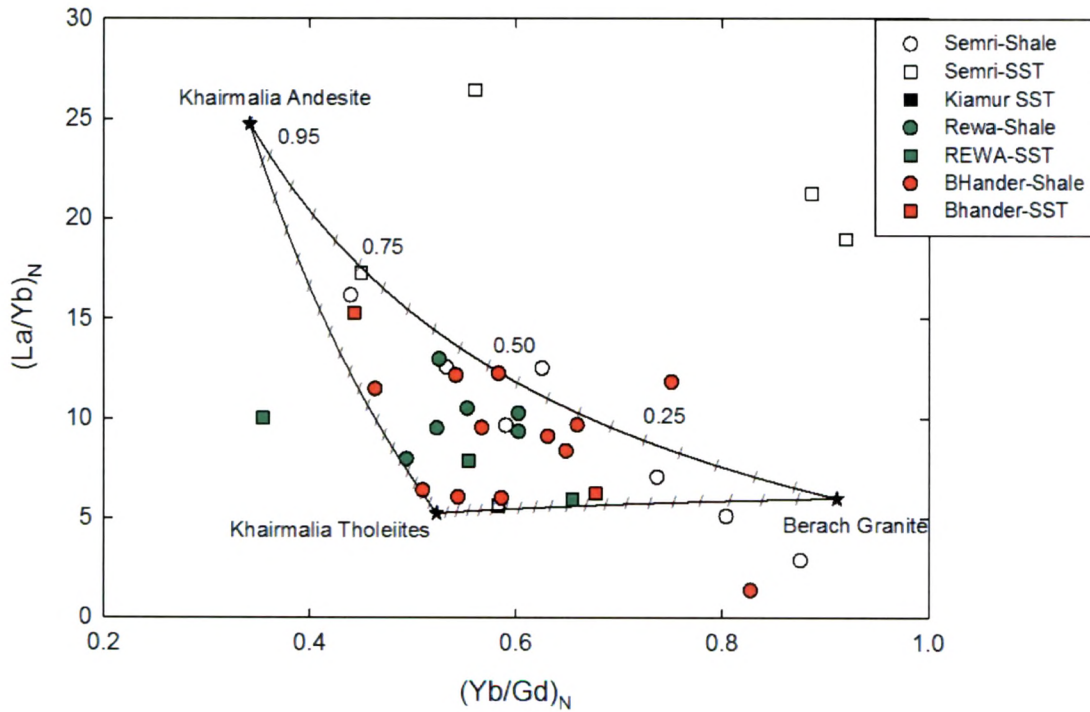


Fig.3.23: Chondrite normalized La/Yb versus Yb/Gd plot for Vindhyan sediments superimposed on model curves for mixing between three end members.

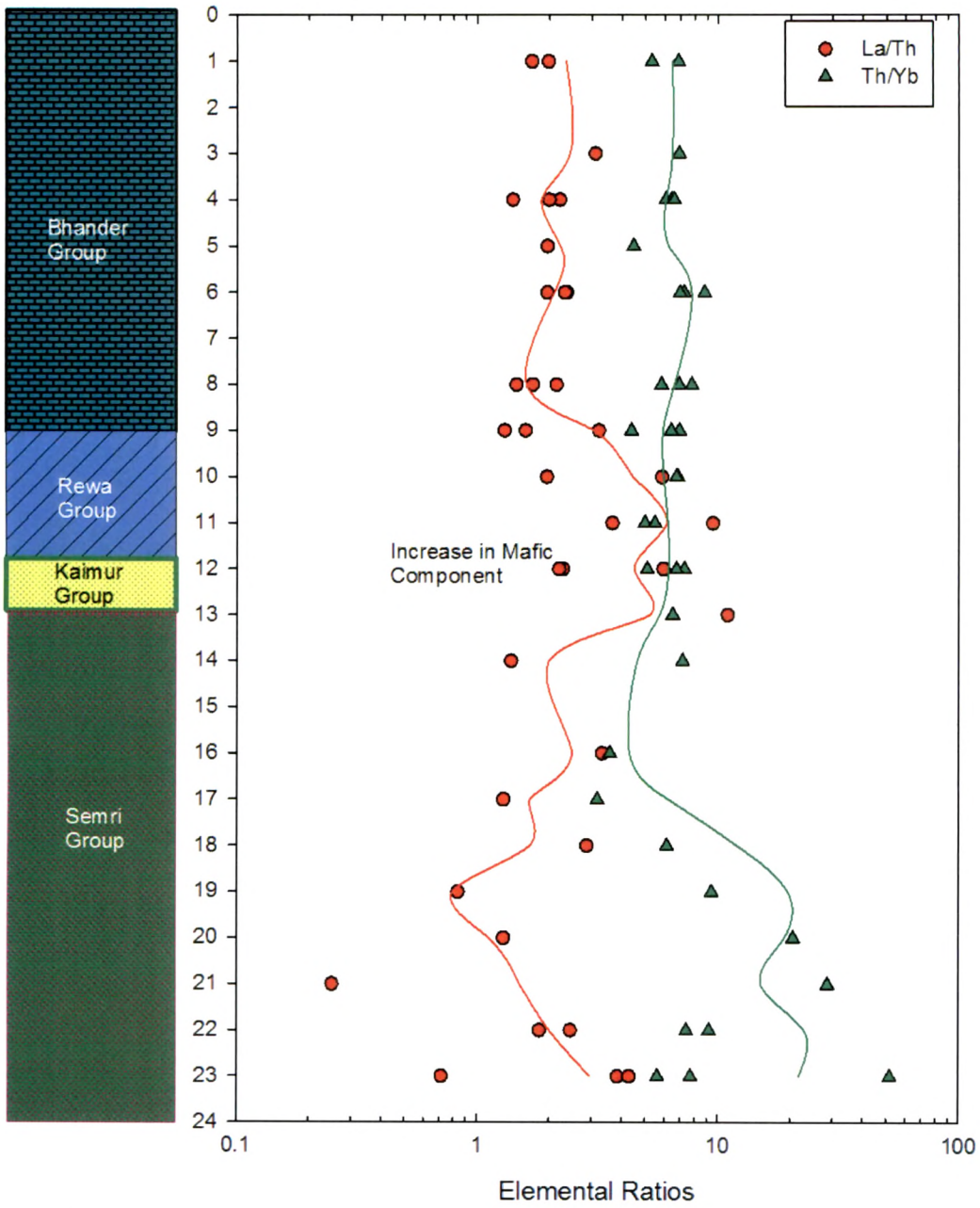


Fig. 3.24: La/Th and Th/Yb profiles along the stratigraphical column of the Vindhyan Supergroup, Rajasthan. The scale along the depth/height profile is arbitrary. The lines are drawn using a 3-points average statistics.

3.2.2.4 *The Radiogenic isotope studies*

The radiogenic isotopic studies of Nd and Sr have been used in deciphering the source compositions of the detrital sedimentary rocks, using their chemical properties as well as the advantages of the radioactive decay of ^{147}Sm to ^{143}Nd and ^{87}Rb to ^{87}Sr . McCulloch and Wasserburg (1978) suggested that the Sm/Nd ratios of shale and other sediments are constant and similar to their parent rocks and it does not change appreciably during sedimentary processes (as discussed earlier in trace elements section) and hence Sm-Nd model dates of sedimentary rocks relative to Chondritic Uniform Reservoir (CHUR) or Depleted Mantle (depleted in large ion lithophile elements) are ages of mantle extraction of the original igneous source rocks from which the first sediments were derived. This aspect of the Nd-isotope systematics helps us in understanding the provenance. The Rb/Sr ratios in shale are highly variable due to the absorption of Rb by clay minerals and mostly higher than their parent rocks, and Sr isotopes are less reliable, particularly for very old rocks, in provenance determination. The Sm-Nd model dates of sedimentary rocks can be seen as time elapsed since the Nd separation from CHUR or DM. Hence the model ages are “crustal residence ages” and could be used for understanding crust mantle interaction through the time. The crustal residence ages of the Proterozoic and Phanerozoic shales are generally older than their depositional ages suggesting that the recycled crustal material which separated from CHUR or DM long before the formation of their parent rocks, got incorporated in shales. These ages decrease whenever young volcanic materials get mixed with older terrigenous sediments (Faure, 1986).

The Sr-isotope data from the Vindhyan Supergroup suggest that the highly radiogenic Sr is present in almost all the siliciclastic formations, while in limestones and dolostones it is moderately radiogenic. The observed $^{87}\text{Sr}/^{86}\text{Sr}$ variation is between 0.70818 (Blawan Dolostone) and 1.07899 (Khardeola Shale). A histogram of

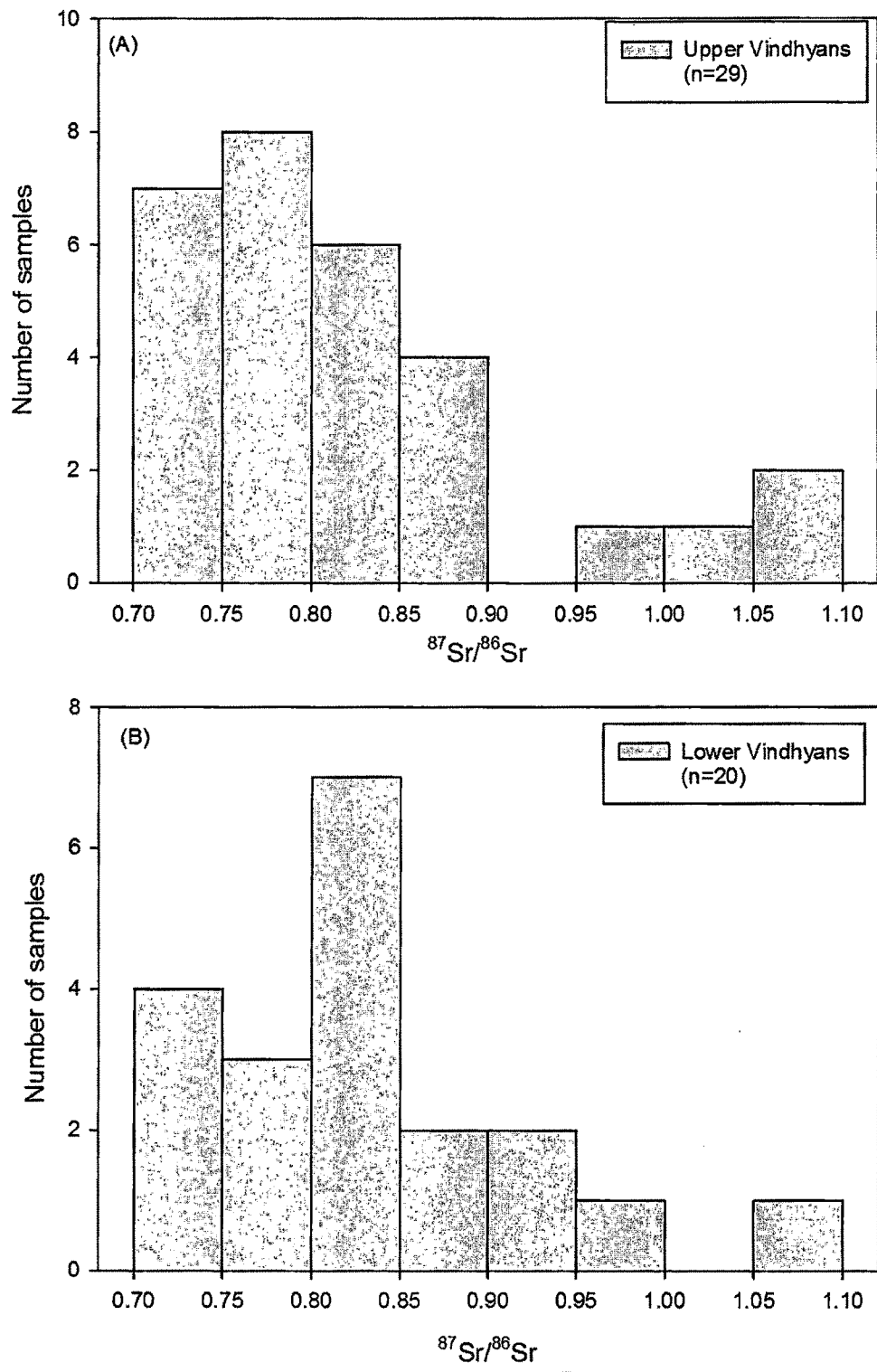


Fig. 3.25: Histograms showing frequency distribution of $^{87}\text{Sr}/^{86}\text{Sr}$ ratios in the Upper Vindhya (A) and the Lower Vindhya (B) of Rajasthan.

$^{87}\text{Sr}/^{86}\text{Sr}$ ratios variations in the Vindhyan of Rajasthan is presented in Fig. 3.25 (A: Upper Vindhyan and B: Lower Vindhyan). From the frequency distribution pattern one can observe that the ratios are highly radiogenic and values for the Lower and the Upper Vindhyan overlap. Therefore, extractions of any valuable information about provenance is difficult. The $^{87}\text{Sr}/^{86}\text{Sr}$ ratio, in sedimentary rocks, is readily affected by diagenesis and other fluid mediated post-diagenetic processes due to the reactive nature of Rb & Sr, hence the primary $^{87}\text{Sr}/^{86}\text{Sr}$ rarely preserved.

$\epsilon_{\text{Nd}}(0)$ of sediments in the Semri Group varies from -34.0 to -12.9, with the mean at -22.2, whereas that of the Kaimur Group falls in a narrow range between -18.2 and -17.1 with the mean at -17.7. The sediments from the Rewa Group have $\epsilon_{\text{Nd}}(0)$ values varying between -17.8 and -14.6 with the mean at -16.2 and the variation in the Bhandar Group is between -20.2 and -14.2, with the mean at -17.3. The range of values in the Rewa and the Bhandar groups are overlapping. There are significant changes in the values of $\epsilon_{\text{Nd}}(0)$ at the boundaries between various groups. Interestingly, it is difficult to differentiate the average ϵ_{Nd} values of the Rewa (-16.4) and the Bhandar groups (-16.8) in the Chittorgarh sector, while in the Bundi sector they are different: ϵ_{Nd} -16.0 and -17.4, respectively. The main mode of $\epsilon_{\text{Nd}}(0)$ variations in the Vindhyan of Rajasthan is at -17, and more than 70% of samples fall in the range of -20 to -14 (Fig. 3.26A).

The variations of average ϵ_{Nd} in various groups also reveal an important aspect of the depositional conditions in the Vindhyan Basin. The observation that there is an appreciable change in average ϵ_{Nd} with time suggests that each group (e.g. Semri, Kaimur, Rewa and Bhandar) of rocks had distinct sediment sources, which in turn implies that either there were distinct breaks in sedimentation in the basin or there were major tectono-climatic changes in the provenances subsequent to the deposition

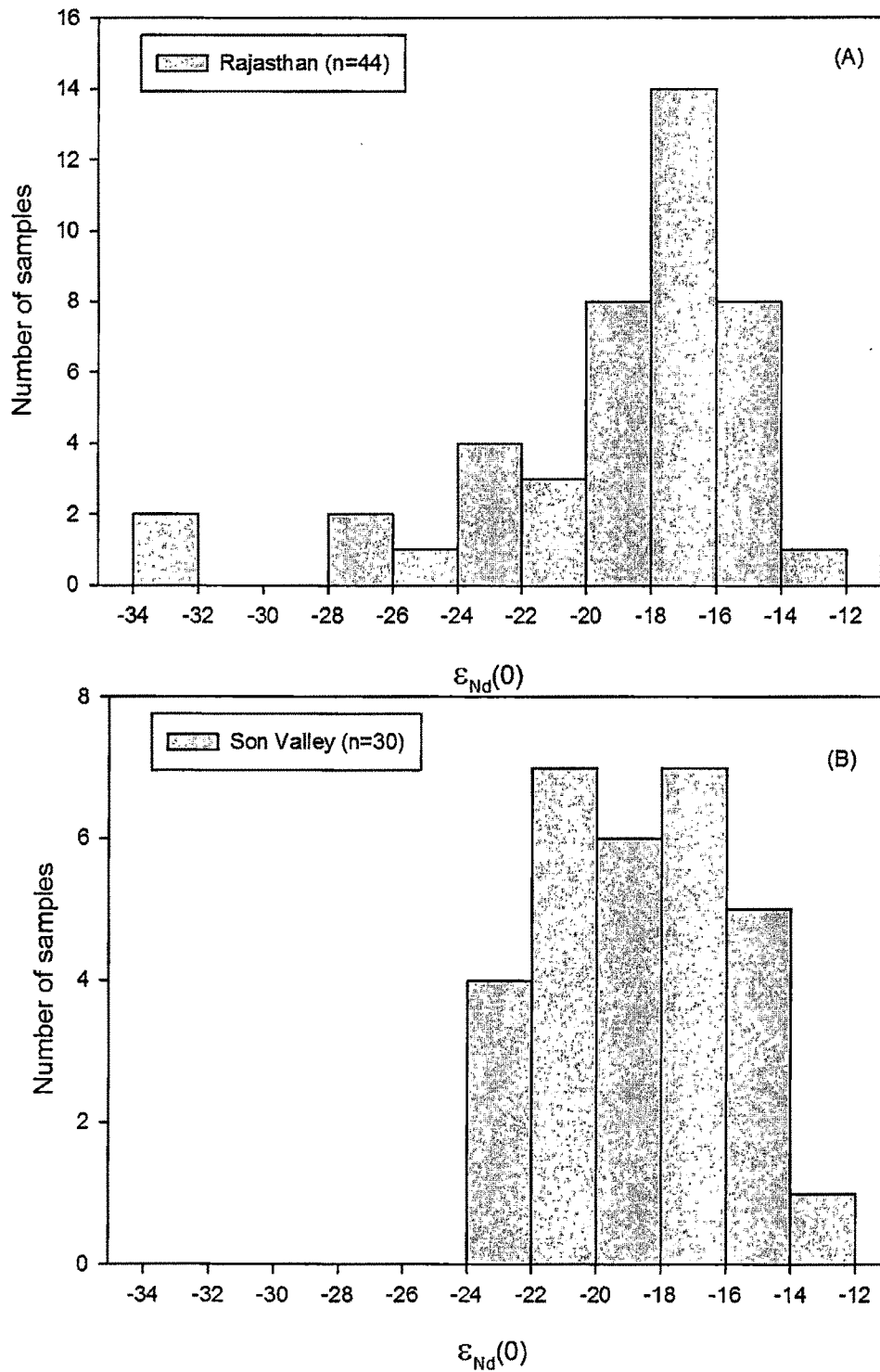


Fig. 3.26: Histograms showing frequency distributions $\epsilon_{Nd}(0)$ in the Vindhyans of Rajasthan (A) and the Son Valley (B). Data source for the Son Valley: Chakrabarti et al. (2007).

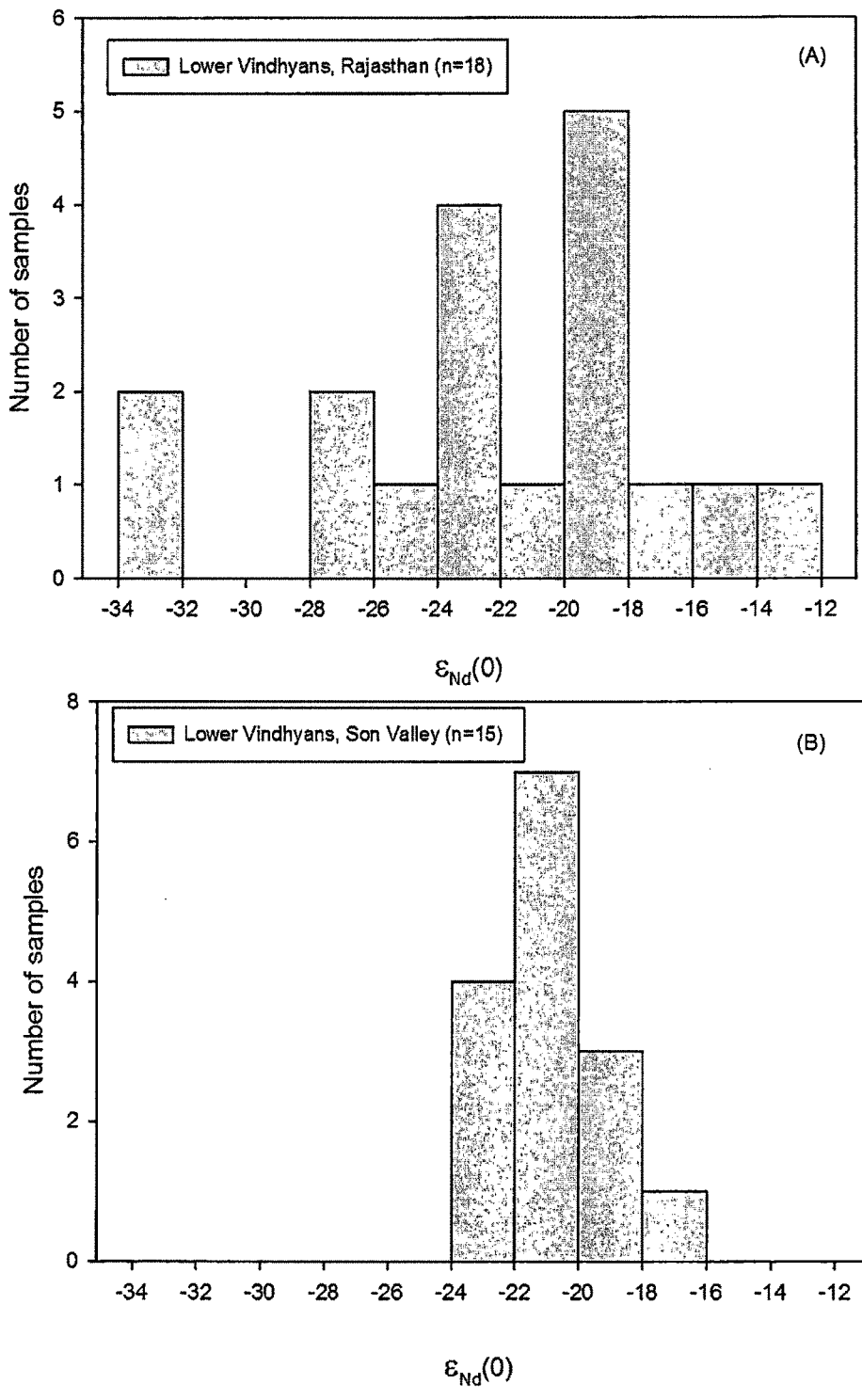


Fig. 3.27: Histograms showing frequency distributions $\epsilon_{Nd}(0)$ in the Lower Vindhyan formations of Rajasthan (A) and the Son Valley (B). Data source for the Son Valley: Chakrabarti et al. (2007).

of each group of rocks. A closer look at the change in ϵ_{Nd} reveals that all the breaks, except for the one between the Semri Group and the Kaimur Group did not have a basin-wide presence. The distributions of the $\epsilon_{Nd}(0)$ in the Vindhyan of Rajasthan (our data) are compared with that in the Vindhyan of the Son Valley (Chakrabarti et al., 2007) in Fig. 3.26 and 3.27.

We find that Chakrabarti et al. (2007)'s $\epsilon_{Nd}(0)$ for Vindhyan formations in the Son Valley values are comparable to our data from equivalent formations in Rajasthan. Chakrabarti et al. (2007) reported $\epsilon_{Nd}(0)$ values for the Porcellanite Formation in the range of -22.7 to -16.7, which overlaps with the range of values (-25.8 to -19.2) we find in equivalent formations in Rajasthan (Sawa Sandstones, Sawa Shales and Porcellanite). The average values of $\epsilon_{Nd}(0)$ for the Semri Group calculated from Chakrabarti et al. (2007) is found to be -20.5, which is slightly higher than that of the Semri Group in Rajasthan (-22.2). The drastic difference in the epsilon value across the Lower and the Upper Vindhyan transition as observed by Chakrabarti et al. (2007) (from -20.5 to -17.4) is not seen in the Vindhyan of Rajasthan, where it changes from -16.7 in the Suket Shale to -17.1 in the Kaimur Sandstone. This observation corroborates the findings that unlike the Vindhyan of the Son Valley the transition between the Lower Vindhyan and the Upper Vindhyan in Rajasthan is not sharp. The overall variation in $\epsilon_{Nd}(0)$ in Rajasthan (-34.0 to -12.9) is large in comparison to restricted variation in the Son Valley (-24 to -12). The Vindhyan sediments from both the sectors show a prominent mode at $\epsilon_{Nd}(0) = -17$ (Fig. 3.26). In both the sectors this mode appears only in the Upper Vindhyan. The $\epsilon_{Nd}(0)$ of the Lower Vindhyan of Rajasthan show bimodal distribution, with modes at -23 and -19, whereas that of the Lower Vindhyan of the Son valley has a mode at -21. These observations suggest that a majority of the original sediments for the Upper Vindhyan of Rajasthan and of the Son Valley came from similar type of magmatic rocks and that for the Lower Vindhyan in both the sectors came entirely from different types of sources.

Considering that the depositional age of the Lower Vindhya is now well constrained in the Son Valley sector (e.g. Ray, 2006) we calculated $\epsilon_{Nd}(T)$ for various equivalent/correlatable formations of the Semri Group in Rajasthan. The same exercise was also done for the formations of the Upper Vindhya assuming approximate ages for them. The data presented in form of histograms in Fig. 3.28. $\epsilon_{Nd}(T)$ varies from -20.4 to +5.1 in the Vindhya of Rajasthan. If we exclude one sample from the Suket Shale (CGB-07-22A) that has a $\epsilon_{Nd}(T)$ value of -20.4, then the range of $\epsilon_{Nd}(T)$ of the entire Vindhya reduces to -14.4 to +5.1. $\epsilon_{Nd}(T)$ goes on increasing as one follows the stratigraphic younging direction in the Lower Vindhya, e.g. it increases to +2.4 in the Suket Shale from -9.9 in the Sawa Grit Formation. Such a change clearly points to the increased addition of sediments from juvenile material. The value of +3.1 in the Sawa Sandstone clearly indicates influence of young igneous sources.

$\epsilon_{Nd}(T)$ for the rocks of the Upper Vindhya were calculated assuming the following the depositional ages: 1) Kaimur Group: 1200Ma (the age of Bijaygarh Shale), 2) Rewa Group: 1000Ma (younger than the Kimberlite intrusion) and 3) Bhandar Group: 750 Ma for the lower part and 650 Ma in the upper part (based on Sr-isotope stratigraphy). These assumptions are based on existing reliable geochronological information (Ray, 2006). The value $\epsilon_{Nd}(T)$ for the Kaimur Group varies from +3.9 to +5.1 (av. +4.5), for the Rewa Group from -8.8 to -1.5 (av. -6.0) and for the Bhandar Group from -12.7 to -3.5 (av. -7.8). Positive $\epsilon_{Nd}(T)$ values clearly indicate a significant presence of juvenile mantle derived material in these sediments, whereas the high negative values indicate large continental crustal contribution.

The $f_{Sm/Nd}$, which is a measure of Sm and Nd fractionation with respect to Sm/Nd of CHUR, is -0.45 and -40 for the two Berach granite samples and for the mafic igneous

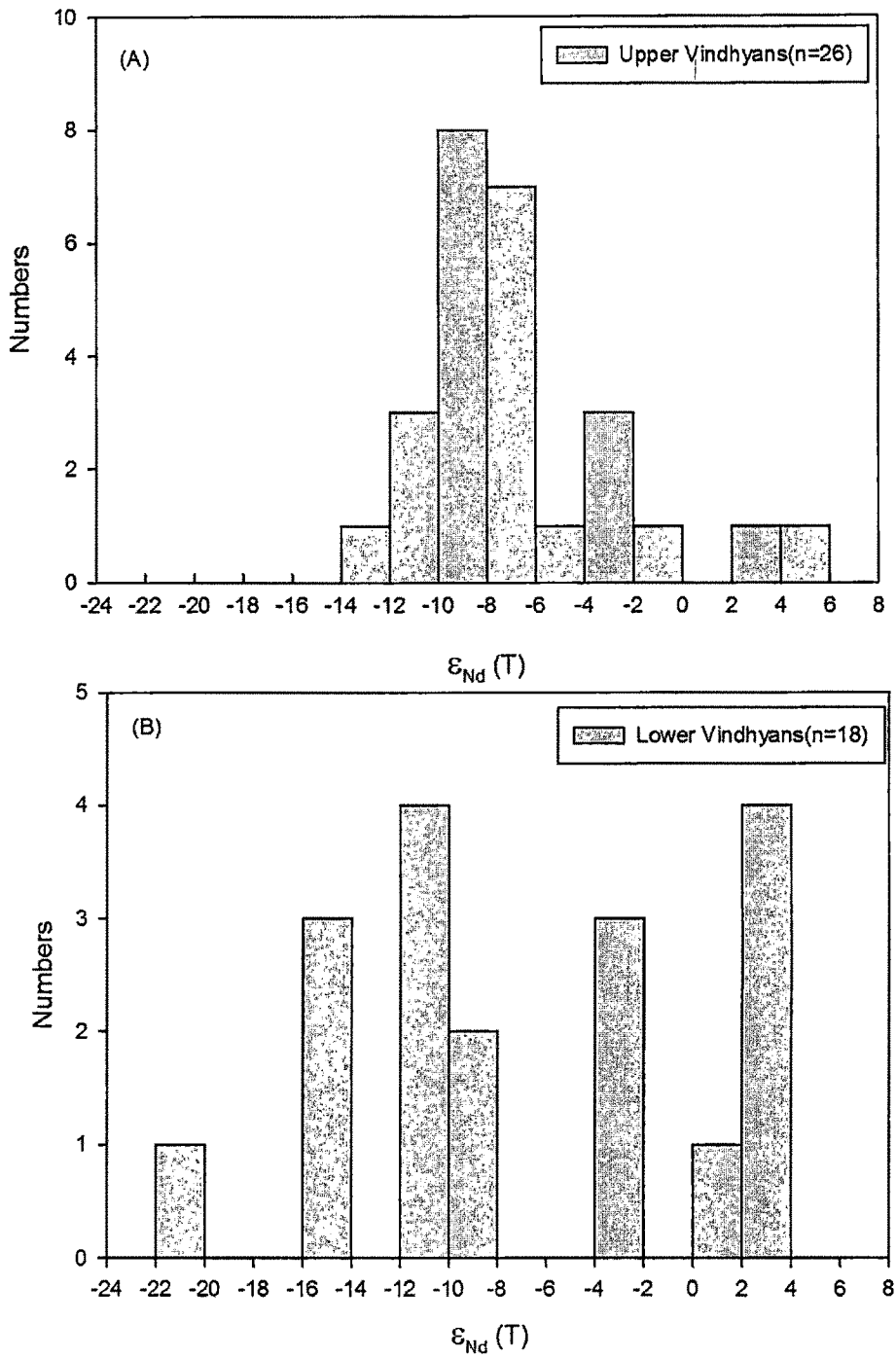


Fig. 3.28: Frequency distributions diagram for $\epsilon_{Nd}(T)$ in the Upper Vindhyan (A) and the Lower Vindhyan (B) of Rajasthan.

rocks it varies between -0.45 and -0.25. It varies between -0.64 and -0.25 (av. -0.41) in the Semri Group and decreases to -0.69 in the Kaimur Group. In the Rewa Group the value varies between -0.56 and -0.30 (av. -0.42) and in the Bhandar Group between -0.62 and -0.24 (av. -0.50). These variations suggest that the source of material remained almost same for most part of the deposition of the supergroup, except for abrupt changes across the transitions between groups.

The calculated model ages (T_{DM}) for the Vindhyan formations from Rajasthan are plotted in histograms in Fig. 3.29. T_{DM} age of a sedimentary rock essentially represents an average mantle extraction ages of the original igneous protoliths from which the sediments have been derived, and therefore are older than the age of deposition. The distribution of T_{DM} in the Lower Vindhyan shows a prominent mode at ~1500 Ma. The distribution pattern shows that there is a general decrease in T_{DM} from the Lower to the Upper Vindhyan. The decrease/increase in T_{DM} or an increase/decrease in ϵ_{Nd} corresponds to an increased/decreased contribution of radiogenic Nd to the sedimentary sequences. The increase in ϵ_{Nd} can be attributed to incorporation of juvenile material or termination of contributions from old crustal sources. In general, the addition of juvenile sediments is associated with tectonic activity, in the form of crustal uplift or renewed volcanism (Andersen and Samson, 1995). It is generally observed that the Archean and early to mid-Proterozoic sediments have T_{DM} ages close to their stratigraphic ages, and in the case of younger sediments these ages are much older (as much as 2.0 Ga) than their stratigraphic ages (O'Nions et al., 1983).

T_{DM} distributions in Rajasthan and that in the Son valley (Fig. 3.30) show a prominent mode at ~2300 Ma, which could be attributed to derivation of sediments from two prominent igneous sources; one from a >2300 Ma source and other from a <2300 Ma source. Interestingly, T_{DM} values of this mode are observed predominantly in the formations of the Lower Vindhyan. In Rajasthan, this value could be attributed to the mixing of sediments derived from the ~2500 Ma old basement rocks (e.g. Berach granite) with those derived from younger igneous rocks, the ~1850 Ma

old Hindoli Group and/or the Khairmalia volcanics, whereas, in the Son Valley the sediments appear to have been derived from the ~2500 Ma old basement (e.g. Bundelkhand Granite) and the ~1630 Ma old rhyolitic volcanics that formed the Porcellanite Formation.

Interestingly, the model age (T_{DM}) of the Kaimur Sandstone of Rajasthan is found to be the lowest (~1.3 Ga) while that of the same in the Son Valley is 2.5 Ga (Chakrabarti et al. 2007). The T_{DM} of the Kaimur Sandstone of Rajasthan appears to be close to its depositional age (~1200 Ma) as inferred from the available geochronological data (see Table 2.4).

The second and the highest mode in the T_{DM} distribution in Rajasthan is observed at ~1500 Ma (Fig. 3.29), which is seen only in this part of the Vindhyan, and mostly in the Upper Vindhyan. This age can be interpreted as mixing of sediments derived from various igneous sources: 1) the ~1850 Ma old Hindoli volcanics which is most prominent in the Pb-Pb age distribution of detrital zircons from the uppermost Vindhyan sandstone formation (Malone et al., 2008), and 2) other magmatic events as observed in the age distribution of detrital zircons (1020, 1140, 1260 and 1380 Ma, Malone et al., 2008) whose sources might be located within the Aravalli-Delhi fold belt. It might also be possible that the mixing of sediments from the Malani Igneous Suite (~750 Ma) and from the Hindoli Group of rocks or other unidentified sources whose zircons have been observed by Malone et al. (2008) could have generated the T_{DM} at 1500Ma in the Upper Vindhyan younger than 750 Ma. If true, this goes against the claim by Malone et al. (2008) that the Vindhyan Basin did not receive sediments from the Malani Igneous Suite (MIS) and therefore, is older than 1000 Ma. Here, it is to be noted that the population density curves (vs. age) in Fig. 15 of Malone et al. (2008) contain a small peak below 1000 Ma and therefore, their conclusion about the non-inclusion of material from MIS is not unequivocal. Furthermore, the appearance of zircons in sediments from magmatic sources depends on several processes including the distance between the source and basin,

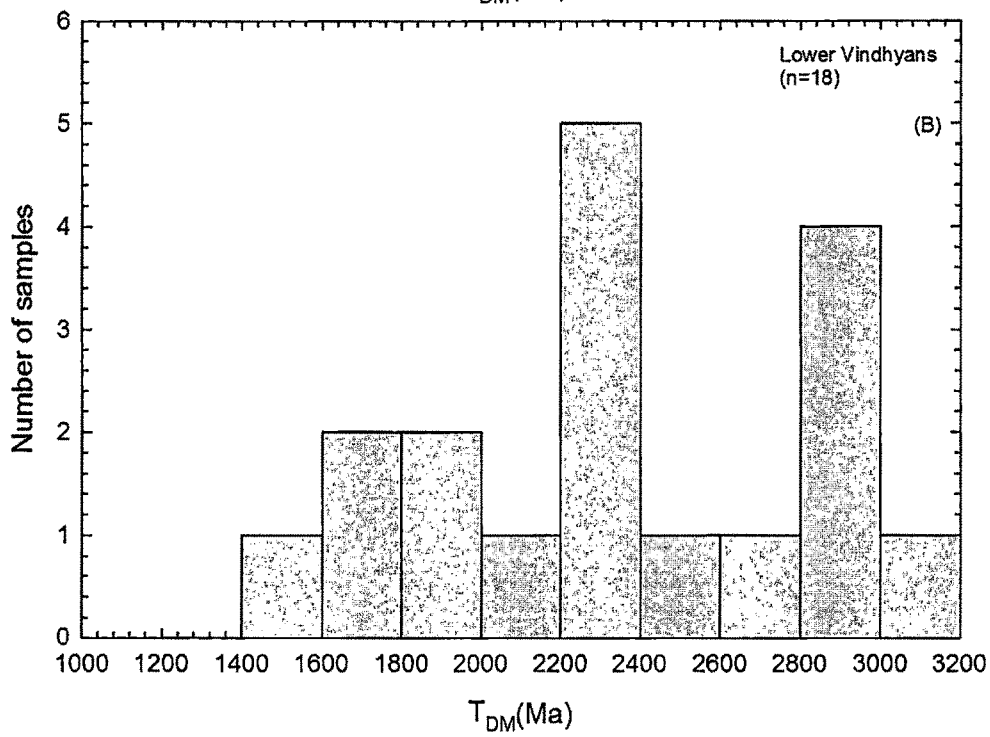
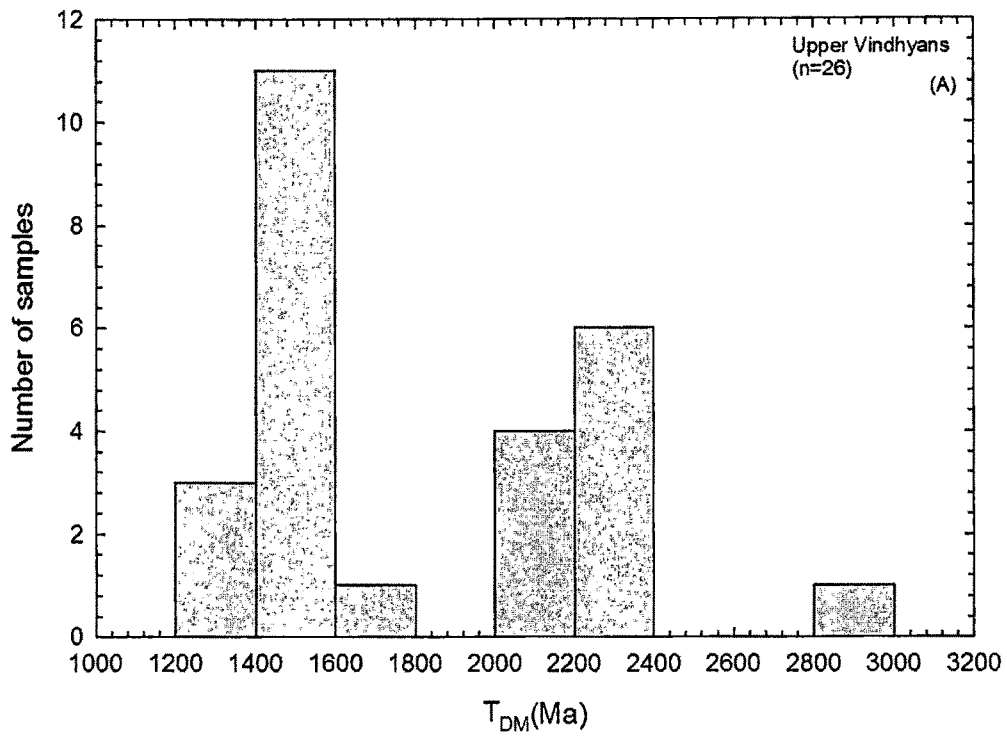


Fig 3.29: T_{DM} frequency distributions in the formations of the Upper Vindhya (A) and the Lower Vindhya (B) of Rajasthan.

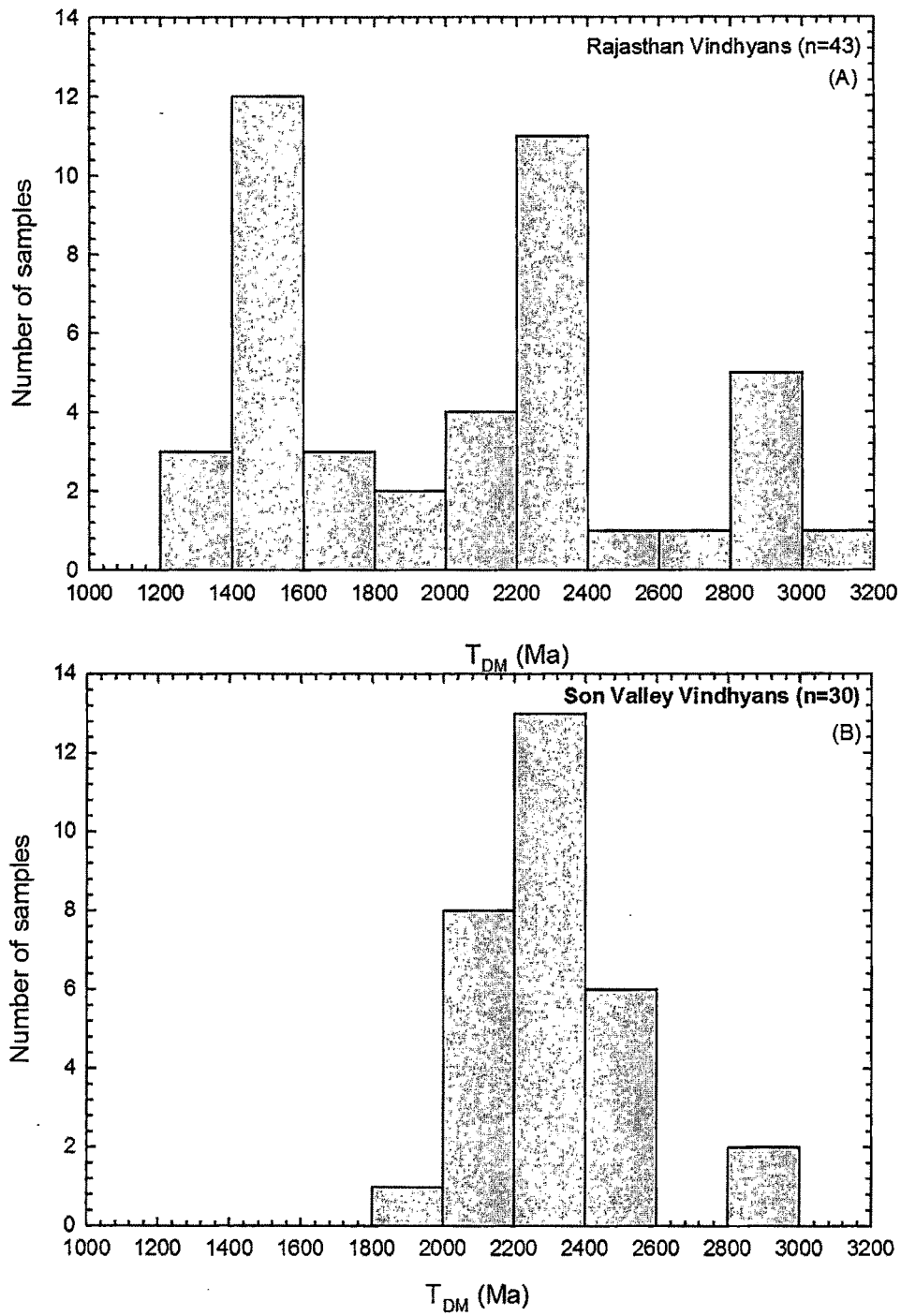


Fig. 3.30: Histograms showing T_{DM} distributions in the Vindhya of Rajasthan (A) and of the Son Valley (B).

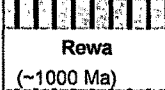
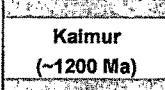
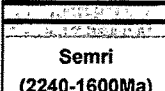
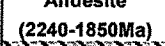
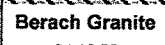
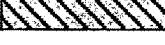
		Chittorgarh			Bundi			Son Valley		
		$\epsilon_{Nd}(0)$	$\epsilon_{Nd}(T)$	$T_{DM}(Ma)$	$\epsilon_{Nd}(0)$	$\epsilon_{Nd}(T)$	$T_{DM}(Ma)$	$\epsilon_{Nd}(0)$	$\epsilon_{Nd}(T)$	$T_{DM}(Ma)$
Upper Vindhya		-16.8	-9.7	2.3	-17.4	-6.6	1.6	-15.6	-9.8	2.3
	Bhandar (<620 Ma)									
		-16.4	-7.1	2.2	-16	-5.3	1.5	-17.8	-8.13	2.1
	Rewa (~1000 Ma)									
Lower Vindhya		-17.7	4.5	1.3				-17.6	-5.8	2.2
	Kaimur (~1200 Ma)									
Lower Vindhya		-20.8	-6.7	2.4				-20.5	-14.3	2.4
	Semri (2240-1600Ma)									
Archeans		-12.2	2.2	2.22						
	Khairmalia Basalt									
		-26.3	-5.7	2.85						
	Andesite (2240-1850Ma)									
Archeans		-32	-1.3	2.7				-34	2.3	2.5
	Berach Granite ~2440 Ma									
Archeans		-30.2	-6.4	3.1						

Fig. 3.31: The variation of the average values of the $\epsilon_{Nd}(0)$, $\epsilon_{Nd}(T)$ and T_{DM} across the stratigraphical column and the basin.

hence the absence of zircons from MIS cannot be claimed as direct evidence against a younger age for the Upper Vindhyan. It is quite possible that the high mountain ranges of the Aravallis to the east of MIS created a barrier for any sediment (zircon) contribution from it to the Vindhyan Basin.

One of the most important observations in the T_{DM} distributions is that the formations in the Son Valley have $T_{DM} \geq 1800$ Ma, whereas that in Rajasthan is as low as ~ 1200 Ma (Fig.3.30). This observation means that either the sources in the west (Rajasthan) did not contribute sediments to the deposition of Vindhyan in the east (Son Valley), or that there existed a physical barrier within the basin which did not allow sediments to move from west to east.

Fig. 3.31 presents the three important parameters ($\epsilon_{Nd}(0)$, $\epsilon_{Nd}(T)$ and T_{DM}) related to the Nd-isotope systematics across the stratigraphical column in various sectors of the Vindhyan Basin. As discussed earlier the average values of ϵ_{Nd} for various groups are distinct and vary widely across the basin. The T_{DM} of the Upper Vindhyan are younger in the Bundi sector compared to that in the Chittorgarh sector and the Kaimur Group has the youngest model age of ~ 1.3 Ga. Comparing our results from Chittorgarh with that of Chakrabarti et al. (2007) from Son Valley we find that except for the Kaimur Group rocks average T_{DM} values are identical in both the sectors (Fig. 3.31) even though the ϵ_{Nd} values for the Rewa and the Bhandar groups are different in both the sectors. The Lower Vindhyan in both the sectors are geochemically correlatable through identical ϵ_{Nd} and T_{DM} . These observations suggest that the Vindhyan in both the sectors, to a large extent, are contemporaneous and had similar type of sediment sources. Upper Vindhyan in Bundi sector, however, appear to have contributions from much younger sources as reflected in their T_{DM} values.

3.2.3 Geochronological studies

An attempt was made to date possible datable horizons within the Rajasthan sector of the Vindhyan Basin. For this purpose, the porcellanite layer sandwiched between the Sawa Sandstone and Sawa Shale (Prasad, 1984) was chosen to constrain the age of the Lower Vindhyan (Semri Group). Petrography of these samples did not reveal any volcanoclastic material, hence, we believe that most likely these represent the Sawa Sandstone. Detrital zircons were separated from these samples and analyzed for their ^{207}Pb - ^{206}Pb ages following the method described in the previous chapter. For dating the Upper Vindhyan, Sr-isotope stratigraphy technique was utilized in the topmost limestone formation, i.e. Balwan Limestone. The implications of these results are discussed below along with the Nd model ages.

3.2.3.1 Detrital Zircon Geochronology of the Sawa Sandstone

The results of our study (Table 3.6) suggest that there is no correlation between the age of the grains and their morphological types. A probability distribution of the grains with their respective ages are presented in Fig. 3.32. Most of the grains are concordant and their ^{207}Pb - ^{206}Pb ages show a bimodal distribution. As expected, the oldest zircon population present in the rock was found to have been derived from the ~2.5 Ma old basement granites and older crustal rocks present in this part of the Indian shield. The zircons showing mode at ~1.9 Ga are apparently derived from magmatic activities of these ages (Hindoli Group), and can be linked to the timing of the base metal mineralization (Roy and Jakhar, 2002). On the basis of this work the youngest event recorded by the zircons is a 1616 Ma event and the youngest mode is at 1660 Ma (Ray et al., 2007). This clearly suggests that parts of the Sawa Sandstone may actually be correlatable with the Deonar Porcellanite Formation in the Son Valley. This would mean that, even though there is no lateral continuity of the Lower Vindhyan of the Son Valley into Rajasthan, the formations of Semri Group in the west were deposited contemporaneously with those in the east within the

Vindhyan Basin. These observations suggest that Vindhyan sediments were depositing simultaneously in western as well as in eastern parts of the basin. Such an inference is also supported by ϵ_{Nd} and T_{DM} data from both the sectors.

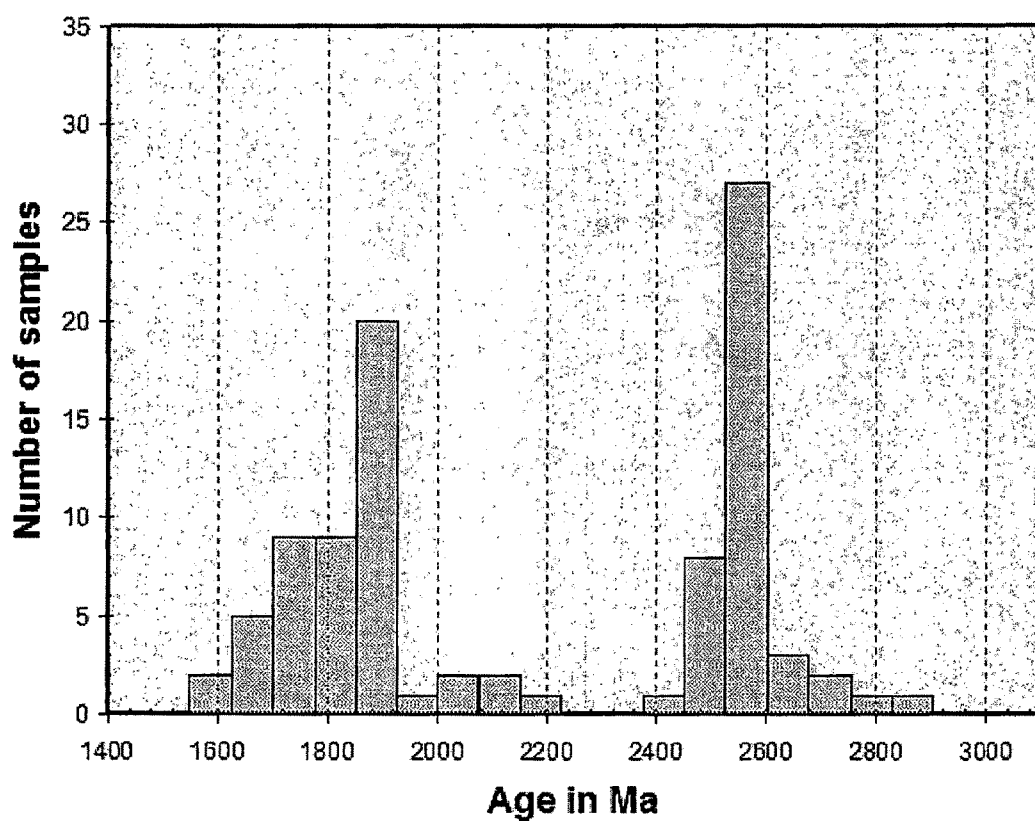


Fig. 3.32: Histogram showing distribution of ^{207}Pb - ^{206}Pb ages for detrital zircons from the Sawa Formation, Semri Group, Chittorgarh.

3.2.3.2 *Nd model ages (T_{DM})*

The calculated Nd-model ages of the sediments discussed earlier can give clues to the ages of the sediments. Since, the model ages are the ages derived from the Nd isotopic ratios, which have been behaving like close system after their incorporation in the basin, the age calculated reflects an age which is resultant of mixing of the sources ages. Therefore, the age calculated may be older than the actual depositional age of the sediments because of the differential mixing of older and younger material, which were originally derived from the Earth's mantle. In any case these ages could not be younger than their actual depositional age or rather than the youngest igneous material added to the sediments. But the distribution of the model ages through the stratigraphical column may give some relative age information of any sedimentary basin.

As already discussed the average T_{DM} values of the Vindhyan of Rajasthan vary from 1.3 to 2.4 Ga, with the youngest age coming from the Kaimur Group. The T_{DM} of ~ 1.3 Ga for Kaimur suggest that the age of the sedimentation in this group is younger than 1.3 Ga and contributions from a younger igneous activity (1200 <Age<1300 Ma) could have been responsible for such a low model age. The Semris in both the sectors have average T_{DM} of 2.4 Ga, which means that the Vindhyan sedimentation did not start until 2.4 Ga. Following the same line of argument we infer that the Rewa and Bhandar groups of rocks are younger than 1.5 Ga in the Bundi sector, however, considering the T_{DM} of the Kaimur Group we can safely conclude that the Upper Vindhyan of Rajasthan are younger than 1.3 Ga.

3.2.3.3 *Sr-isotope stratigraphy*

Strontium isotope stratigraphy is a relative dating method for limestones formed out of ocean water. This method can be very useful to provide first order depositional age brackets in sedimentary sequences where absolute ages are meager. This method

is based on the use of $^{87}\text{Sr}/^{86}\text{Sr}$ in unaltered marine carbonates and the $^{87}\text{Sr}/^{86}\text{Sr}$ evolution curve for the global seawater (e.g. McArthur, 1994, Veizer et al., 1999, Burke et al., 1982). By tying $^{87}\text{Sr}/^{86}\text{Sr}$ of discrete stratigraphic levels to the global seawater evolution curve tied to the geomagnetic polarity time scale or absolute ages; approximate time gaps and relative depositional ages can be estimated. Since the evolution curve in Precambrian is not robust, the ages obtained through this method should be treated as minimum ages. Such a method can only work if Sr in the samples has remained unaffected by diagenesis and subsequent alteration. Therefore, care must be taken to recover samples from the least altered portions of a rock or isotopic analysis. We make an attempt to use this method to constrain the age of the Lakheri and the Balwan Limestones of the Upper Vindhyan of Rajasthan.

The $^{87}\text{Sr}/^{86}\text{Sr}$ data generated on these limestones are presented in Table 3.11. The ratios obtained for the Lakheri Limestone was higher than the value reported by Ray et al. (2003) (0.70678), and hence deemed to be useless for stratigraphic purpose. In the case of the Balwan Limestone Formation, however, we were able to get much lower $^{87}\text{Sr}/^{86}\text{Sr}$ values (e.g. 0.70676 and 0.70684) normalized to NBS 987 value of 0.71025. The lowest value of 0.70676 for the Balwan carbonates was projected onto the Sr-evolution curve of Shields and Veizer (2002) and a minimum age of 620Ma was obtained. This means that the Balwan Limestone is at least 620 million years old and that it could have been deposited prior to this date but later than 650 Ma (Sr stratigraphy age for the Lakheri Limestone, Ray et al., 2003). This age estimate for the Balwan Limestone is in tune with the biostratigraphic inferences made by Kumar and Pandey (2008) for the same formation.

The fossil findings of the Neoproterozoic age from the Sirbu Shales (Srivastava, 2009) and the Balwan Limestone (Kumar and Pandey, 2008) support the Neoproterozoic age for the Bhandar Group. Here, we would like to emphasize that the minimum age of 620Ma of the Balwan Limestone, which is the second topmost lithounit (below Dholpur Shale) of the Vindhyan in Rajasthan, indicates that the deposition of the Vindhyan Supergroup was over much before the Precambrian-Cambrian transition.

It is also highly likely that these sediments could have recorded the events of Cryogenian period (750-600Ma) of the Neoproterozoic. With these new information we have made an attempt to correlate the Vindhyan of Rajasthan with those in the Son valley (Fig. 3.33).

3.2.4 Provenance of the Vindhyan Sediments

The geochemical investigations of the Vindhyan sediments from the Rajasthan reveal that the provenance of these sediments lie in the pre-Aravalli, Aravalli, Hindoli and Delhi Supergroup of rocks exposed to the west or southwest of the Vindhyan Basin. The identification of magmatic arc type multi-element patterns (typical Nb-Ta-Sr depletions and Pb enrichment) within various formations of the Vindhyan Supergroup and their similarity to the patterns observed in the Khairmalia volcanics and other mafic igneous rocks in the vicinity, hints at the existence of a subduction zone to the west of the basin prior to the initiation of deposition. It is highly likely that this part of the Vindhyan Basin probably was formed as a result of subduction zone related tectonic events.

Sediments of the Semri Group show increased incorporation of mafic igneous material as one goes up stratigraphically. The association of Sawa Grit/Sandstone with volcanoclastics (porcellanite) and high positive $\epsilon_{Nd}(T)$ of some of the formations clearly points to direct contribution of volcanic/volcanoclastic sediments to the Vindhyan Basin, but mostly prior to and during the deposition of Kaimur Formation (~1.3 Ga). It is highly likely that the youngest zircon populations seen in the Sawa Grit/Sandstone Formation (~1616 Ma) represents the felsic volcanism in the eastern part of the basin (or its equivalents in the west) that formed the Deonar Porcellanite Formation. The trace element chemistry of sediments also suggests input from subduction zone magmatic sources such as the Khairmalia type andesites in almost all the formations in Rajasthan. Chemical and isotopic compositions clearly indicate that the major igneous sources for the sediments were the Berach Granites and the

mafic igneous rocks, that occur in the basal part of the Aravalli Supergroup (Ahmad et al., 2008b) and the Khairmalia type volcanics that occurred just before the deposition of the Vindhyan (Fig. 3.34). We also observe sediment contributions from much older ($T_{DM} > 2.5$ Ga) mafic igneous rocks ($f_{Sm/Nd} > -0.4$) (Fig. 3.34) to the Lower Vindhyan. Such sources could be komatiites of Aravalli craton (Ahmad et al. 2008b). From Fig. 3.34, one can also see that apart from the above sources there were other igneous sources, with low $f_{Sm/Nd}$ and low T_{DM} (< 1.3 Ga), which contributed sediments to the Vindhyan Basin, especially during the deposition of the Upper Vindhyan. Such sources, most likely, were felsic (highly differentiated) in nature and we believe that these are the granitic and rhyolitic rocks of 1300 to 750 Ma age and present in the Aravalli craton.

The sedimentation in the Vindhyan Basin appears to have lasted for more than 1 billion years. The lithological boundaries identified in between the groups are found to be times of changes in the chemistry of sediments (Fig. 3.35). The drastic changes in T_{DM} , ϵ_{Nd} and $f_{Sm/Nd}$ across boundary between the Lower Vindhyan and Upper Vindhyan indicate the change in provenance. The difference in the model ages of the Rewa and Bhandar Groups in the Chittorgarh and Bundi districts suggests that the younger sources contributed substantially in the Bundi sector. This could be attributed to the Delhi orogeny in the vicinity.

Various important geochemical and isotopic proxies ($^{87}Sr/^{86}Sr$, $f_{Sm/Nd}$, $\epsilon_{Nd}(0)$, $\epsilon_{Nd}(T)$ and T_{DM}) have been plotted across the stratigraphical column in the Fig. 3.35. The $^{87}Sr/^{86}Sr$ ratios as expected, is highly radiogenic (Fig. 3.35A) and vary widely, hence are not suitable for provenance study. The $\epsilon_{Nd}(0)$ and $\epsilon_{Nd}(T)$ show increasing trends with stratigraphy in the Semri Group, whereas T_{DM} shows a decreasing trend (Fig. 3.35C, D, & E). Combining these findings it can be postulated that higher contribution from juvenile igneous components masked the supply of sediments from older crustal sources towards the top of the Lower Vindhyan.

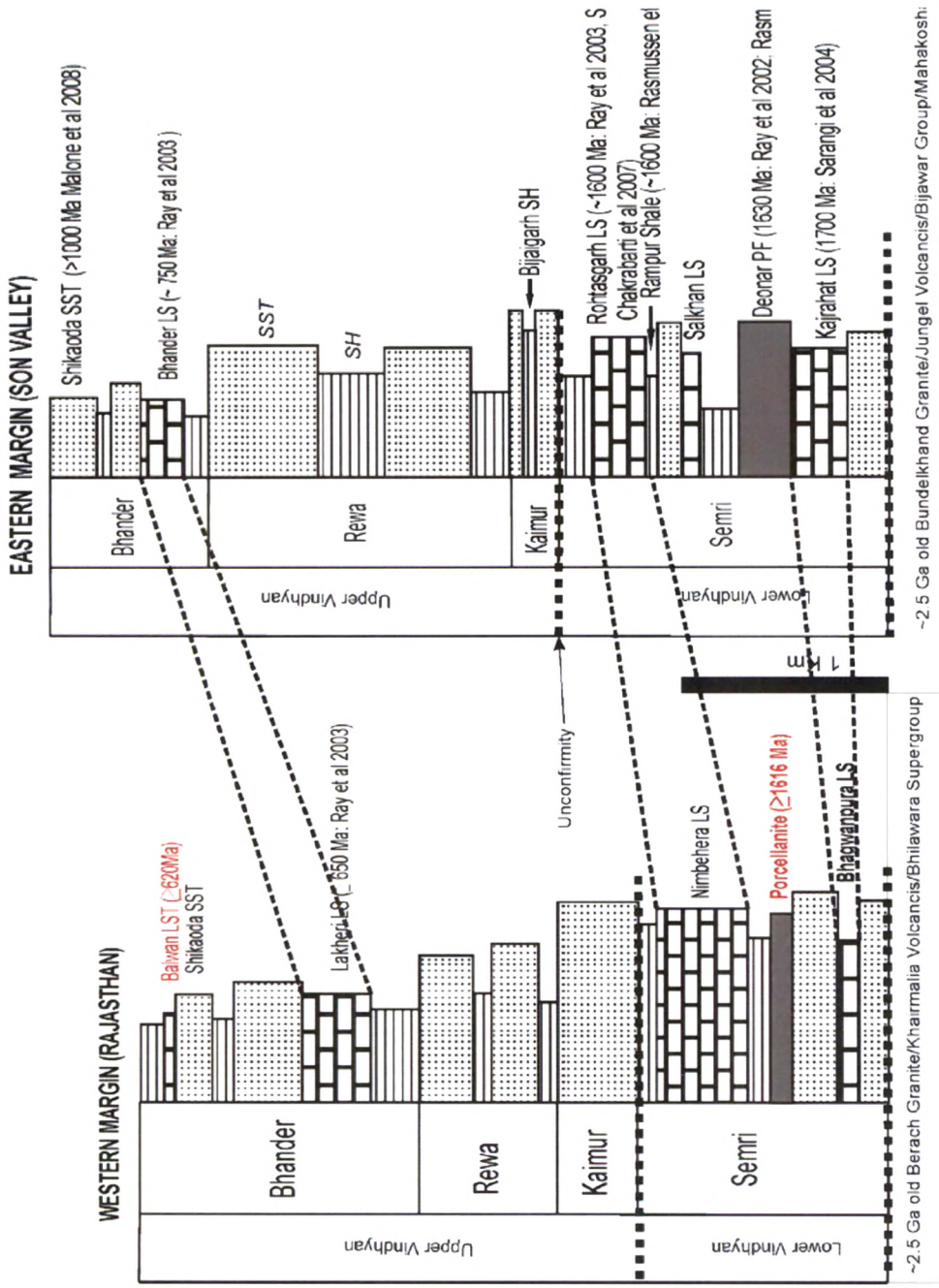


Fig.3.33: Geochronological correlation between Rajasthan and the Son Valley Vindhyan based on the present work. Results from present work are marked in red.

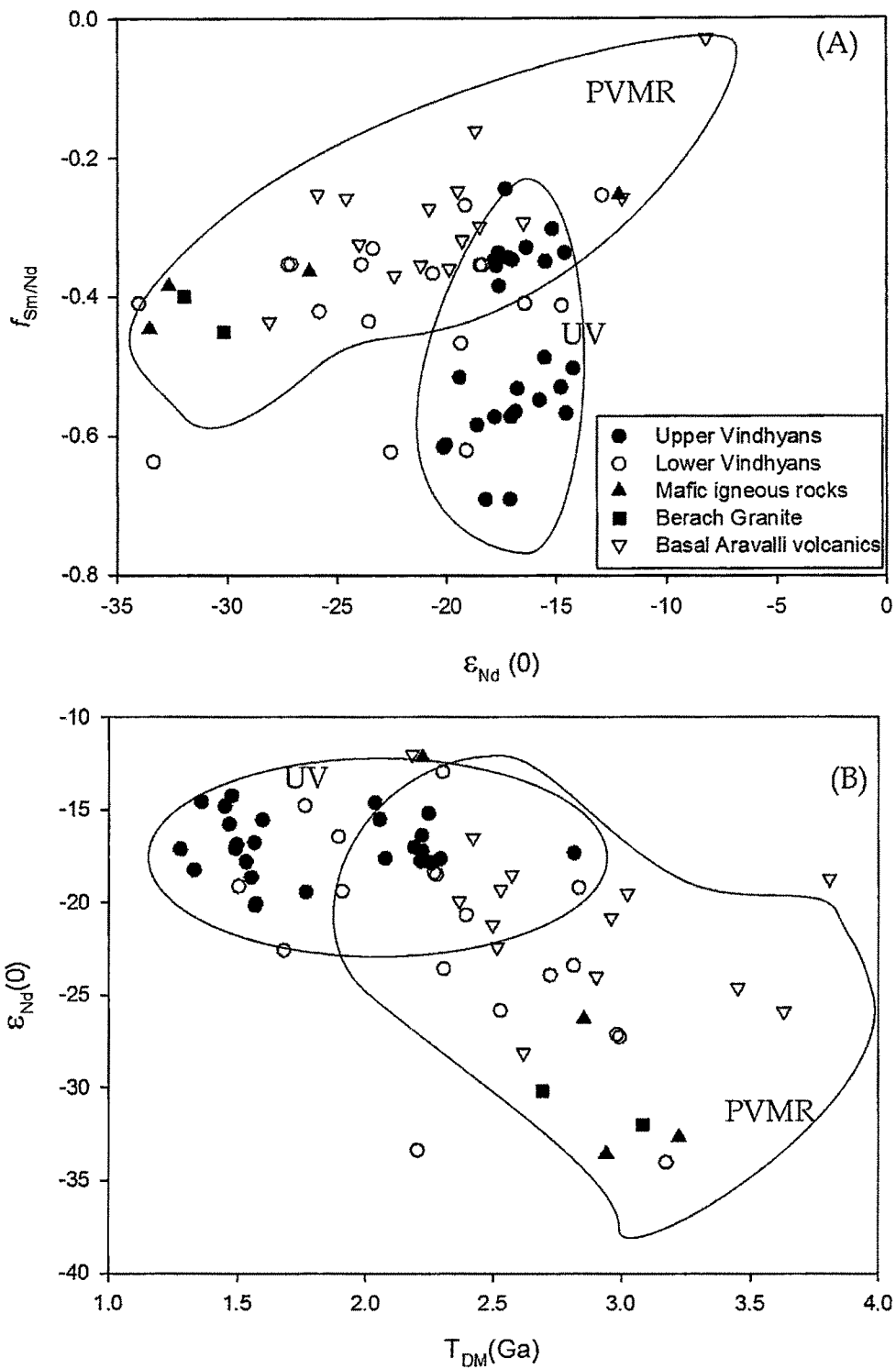


Fig. 3.34: Plots of $f_{Sm/Nd}$ vs. $\epsilon_{Nd}(0)$ (A) and $\epsilon_{Nd}(0)$ vs. T_{DM} (B) showing data for sediments from the Lower and the Upper Vindhyan, pre-Vindhyan mafic igneous rocks, Berach Granite and volcanics from the Aravalli Supergroup. Data source for Aravalli volcanics: Ahmad et al. (2008b). PVMR: Pre-Vindhyan Mafic Rocks; UV: Upper Vindhyan.

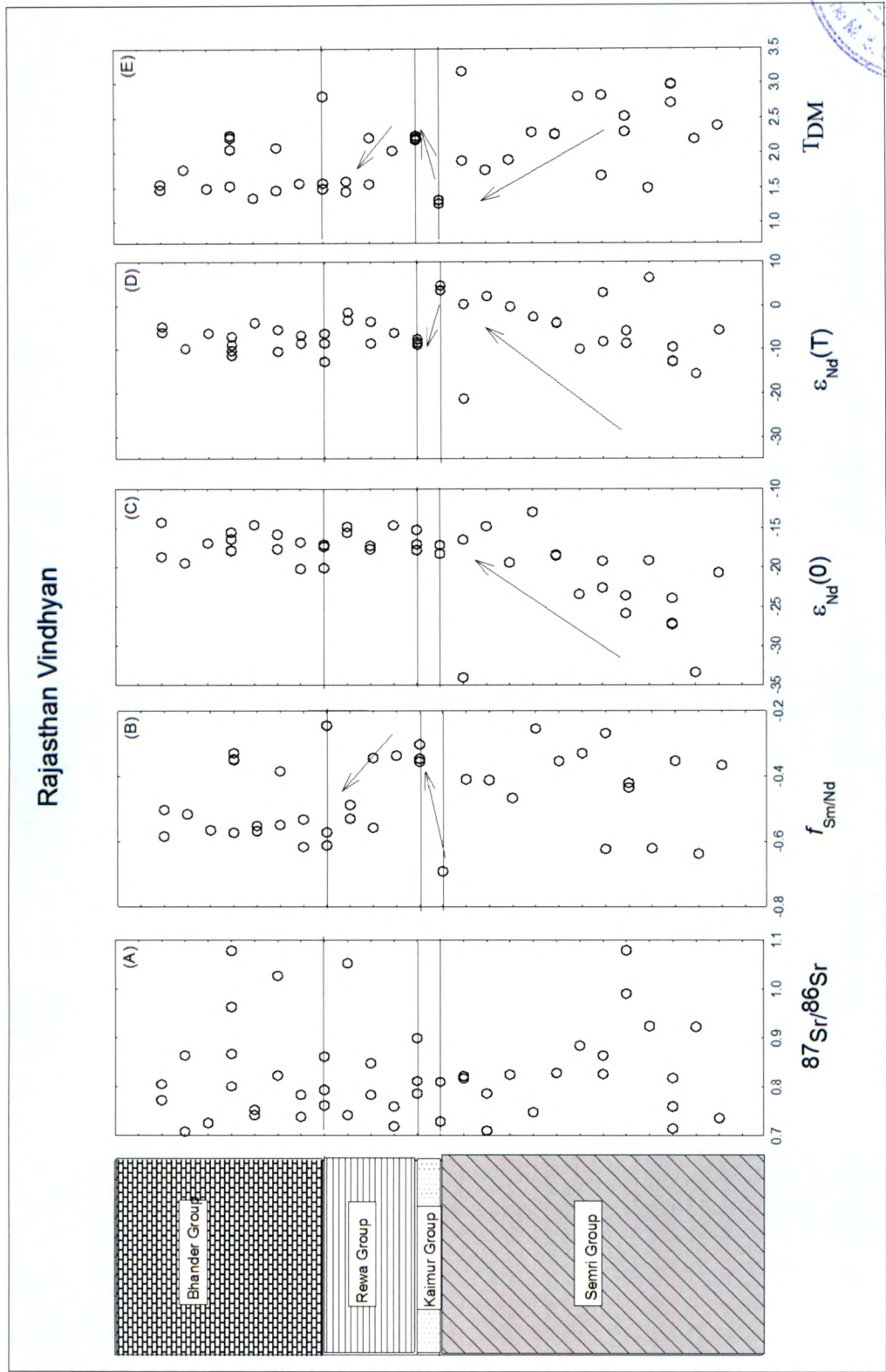


Fig. 3.35: Variation of various geochemical proxies across the stratigraphical column in the Vindhyan Supergroup of Rajasthan.

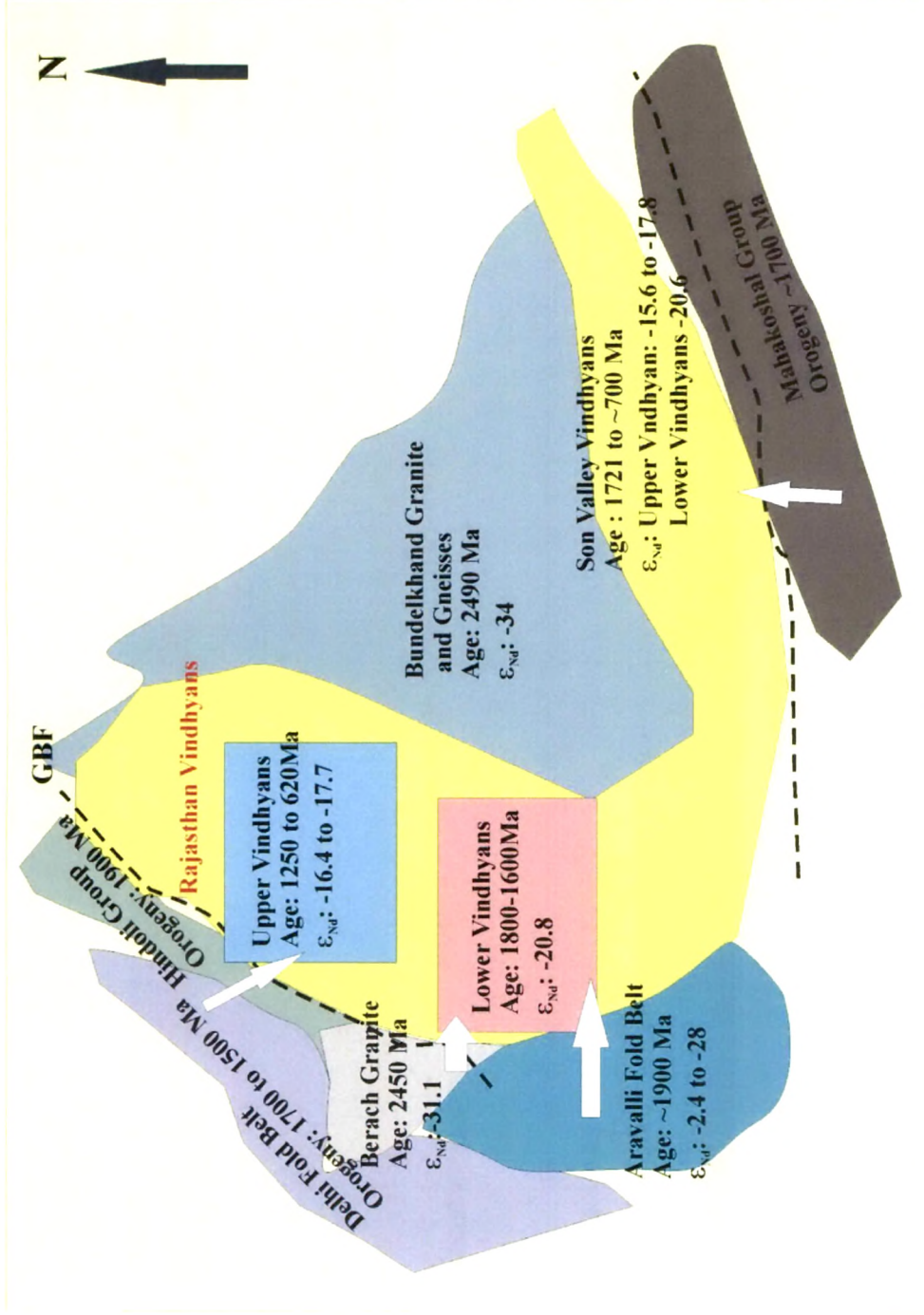


Fig. 3.36: A schematic of Vindhyan Basin during the deposition of Vindhyan Supergroup and the inferred provenances of sediments.

The young model ages and positive $\epsilon_{Nd}(T)$ of the Kaimur Formation clearly demands direct incorporation of young mantle derived components into the sediments. Just prior to the deposition of the Rewa Group all chemical parameters revert back to the average values observed within the Semri Group, possibly meaning similar sediment sources continued to contribute. However, the reduction in $f_{Sm/Nd}$ starting within the Rewa Group hints at contributions from more felsic (or differentiated) sources to the Upper Vindhyan. Based on the above observations and observations made by Chakrabarti et al. (2007) a sketch of the Vindhyan Basin configuration is presented in Fig. 3.36 along with the location of possible source regions for sediments.

3.2.5 $\delta^{13}C$ and $\delta^{18}O$ variations in limestones

Major inquiries related to the evolution of the Earth's atmosphere, climate, the sedimentary cover and the life are believed to be answered through the study of isotopic variations in chemical sediments hence, in the seawater through time. Numerous studies in the recent past have demonstrated the usefulness of carbon and oxygen isotope compositions of Phanerozoic marine carbonate sediments in this regard (e.g., Veizer et al., 1980; Burke et al., 1982; Holser, 1984; Richter et al., 1992; Strauss, 1997; Veizer et al., 1999). Such studies have substantially improved our knowledge about the evolution of our planet during the last 540 million years. Variations of C isotopes reflect a series of complex biogeochemical interactions that document equilibrium between net burial of organic matter and oxidation of their reduced forms (e.g., Berner & Raiswell, 1983; Popp et al., 1997; Kump & Arthur, 1999). The O isotopic variation through time, if considered primary, tells us either that the ancient oceans were warmer compared to their modern counterparts or the isotopic composition of the oceans became progressively higher (Veizer et al., 1999).

In recent times, the use of above isotopic tracers has been extended into Precambrian in an attempt to understand the evolution of Earth's nascent ocean-atmosphere

systems and life (e.g., DesMarais, 1994; Hall & Veizer, 1996; Frank et al., 1997; Jacobsen & Kaufman, 1999). Also, there have been efforts to generate seawater $\delta^{13}\text{C}$ isotopic evolution curve that can be used as tools for stratigraphic correlation, for most part of the Precambrian that lacks biostratigraphic framework. In spite of all the earlier research, not enough data has yet been generated either to carry out isotope stratigraphy or critically understand the co-evolution of life and environment during Precambrian in a global scenario.

To strengthen the existing database and to fill the gaps in our knowledge about various global events that occurred during Earth's early history during the Proterozoic we studied the C and O isotopic records preserved in Lakheri and Balwan Limestone formations of the Upper Vindhyan in Rajasthan that are believed to have been deposited during the Neoproterozoic time (Ray et al. 2003).

3.2.5.1 The Lakheri Limestone

The Bhandar Group in Rajasthan is comprised mostly of sandstones (see Table 2.1) and two limestone formations and four shale formations (Fig.2.2). The Lakheri Limestone that occurs at the bottom part of the Bhandar Group is has a gradational contact with the overlying shale formation (Ganurgarh). In an earlier work Kumar et al. (2002) had observed a negative excursion in $\delta^{13}\text{C}$ variation in these carbonates at Satur near Bundi town hypothesized it to represent one of the Neoproterozoic global glaciations. The authors also had reported a physical evidence for glaciation in form of tilloid bed at the base of the formation near the town of Lakheri, however, this could not be located during the present study. Ray et al. (2003) also reported a negative excursion in $\delta^{13}\text{C}$ but in the equivalent formation in the Son Valley and had hinted at a possible correlation with one of these glacial events.

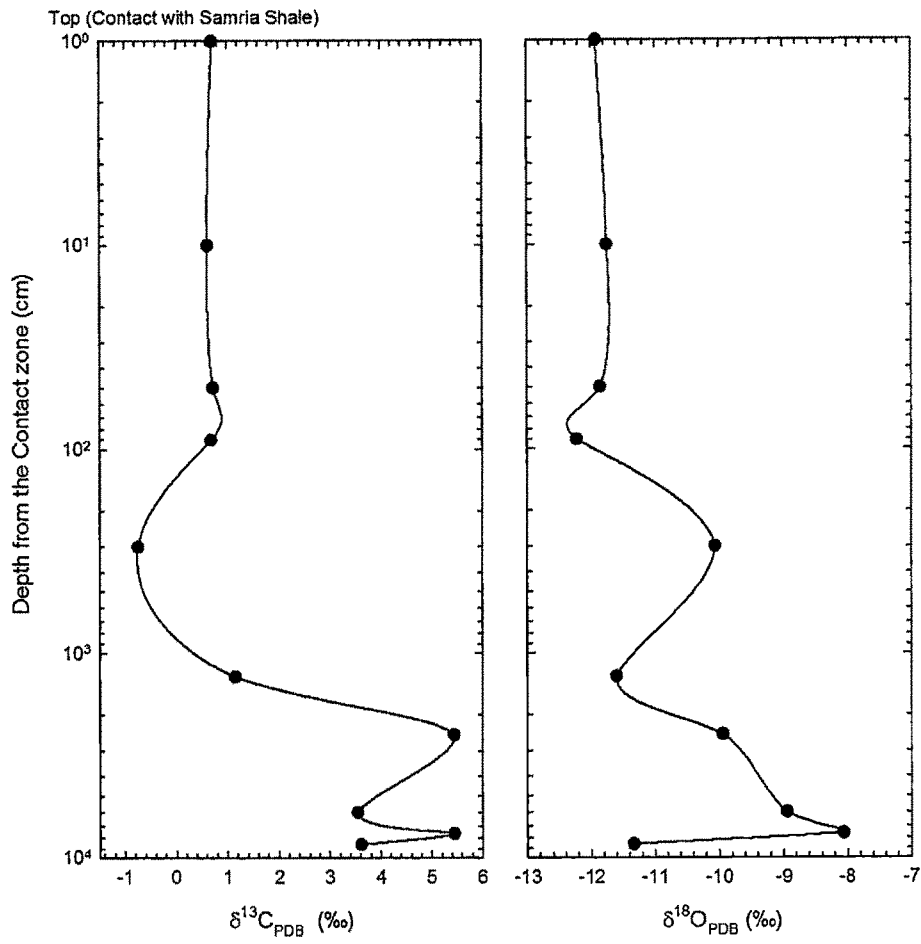


Fig. 3.37: $\delta^{13}\text{C}$ and $\delta^{18}\text{O}$ profiles in the Lakheri Limestone at Gandoli on the Bundi-Indergarh Road.

To contribute to this discussion we decided to carry out carbon isotope studies on this formation at Gandoli, where the entire width of the Lakheri Formation is exposed. The stable isotope data are presented in Table 3.8 and plotted in Fig. 3.37. $\delta^{13}\text{C}$ value appears to decrease with height, from $\sim 5\text{‰}$ to 0‰ , from bottom to top. Although not very significant by itself, this change if combined with the data of Kumar et al. (2002) hints at a large variation from -5.2‰ to $+6\text{‰}$. Such a change (about 11‰) could be attributed either to 1) facies variation within the basin, with the deeper facies having more negative $\delta^{13}\text{C}$ values or 2) to an overall decrease in biology towards the end of deposition.

3.2.5.2 *The Balwan Limestone*

The Balwan Limestone Formation is the topmost carbonate unit of the Vindhyan Supergroup and is exposed only in the Rajasthan sector near Lakheri. It overlies the Shikaoda Sandstone Formation and is exposed in a $\sim 100\text{m}$ thick band along a 15 km section (Fig. 2.4) and truncated by folds and faults on both ends of the length. The formation contains molar tooth structures near the bottom and is stromatolitic at the top. The most interesting aspect of this formation is the presence of a $\sim 20\text{m}$ thick conglomerate band in the middle. The conglomerate is mostly intraclastic and at places contains flat pebbles of the bottom beds of the same formation. Immediately below and above the conglomerate zone the limestone beds contain chert pebbles. We feel that this zone is a result of a storm and/or slope failure close to the shoreline of the basin.

High resolution of carbonate sampling was done in the formation (Table 2.6) and visually least altered components were analysed for C and O isotopic ratios compositions (Table 3.10A). Since there is no apparent positive correlation between the $\delta^{13}\text{C}$ and $\delta^{18}\text{O}$ in the samples (Fig. 3.38) and negative correlation between Mn/Sr and $\delta^{18}\text{O}$ (Fig. 3.39), these isotopic compositions are deemed least altered (i.e. almost pristine) following the arguments given by Veizer et al. (1999). The profiles of $\delta^{13}\text{C}$ and $\delta^{18}\text{O}$ are plotted in Fig. 3.40 for transect 2 (Table 2.6). The profiles of $\delta^{13}\text{C}$ and

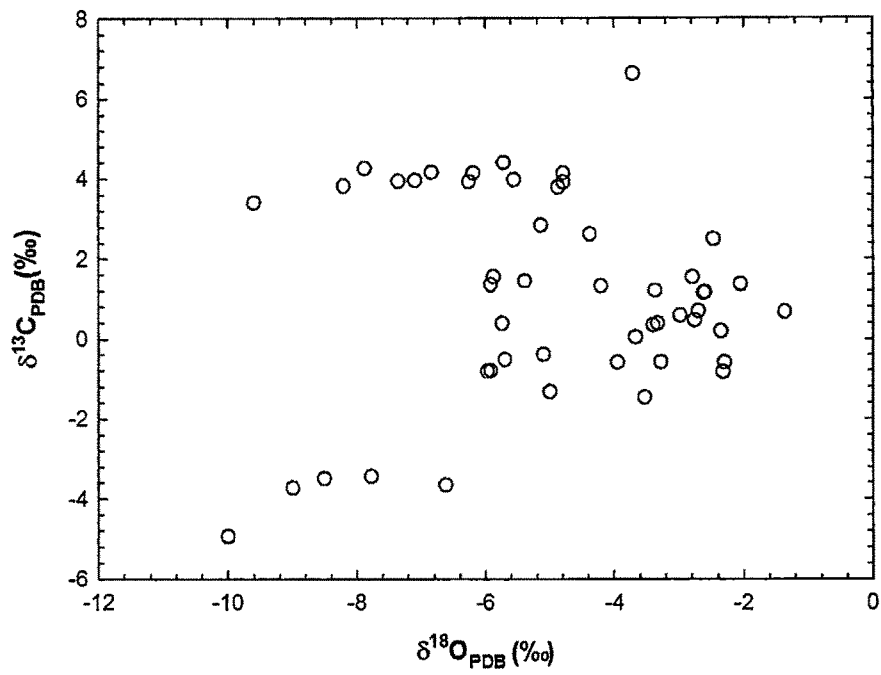


Fig. 3.38: $\delta^{13}\text{C}$ vs. $\delta^{18}\text{O}$ of carbonate components from the Balwan Limestone.

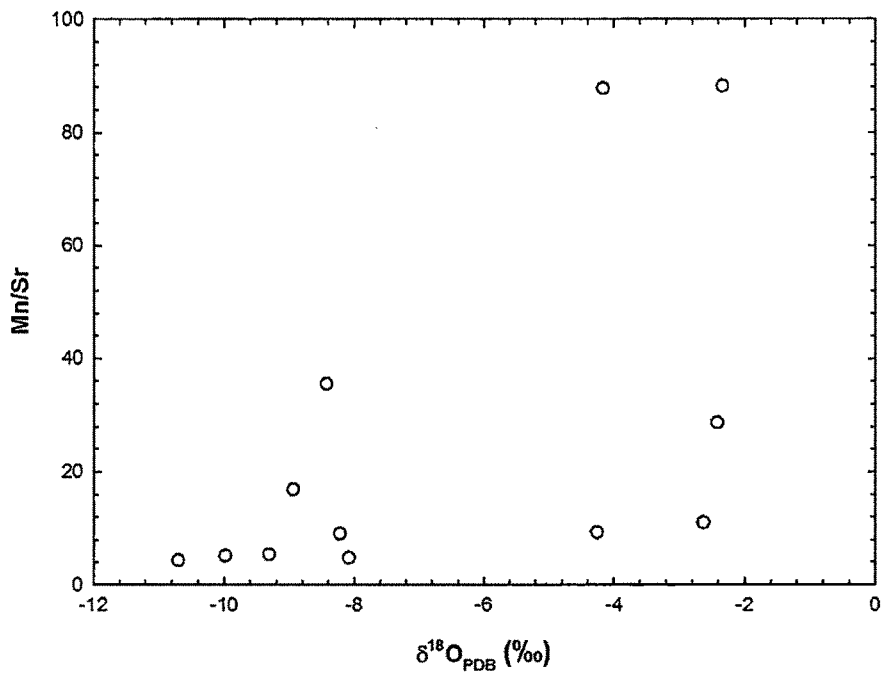


Fig. 3.39: Mn/Sr vs. $\delta^{18}\text{O}$ in carbonate components from the Balwan Limestone.

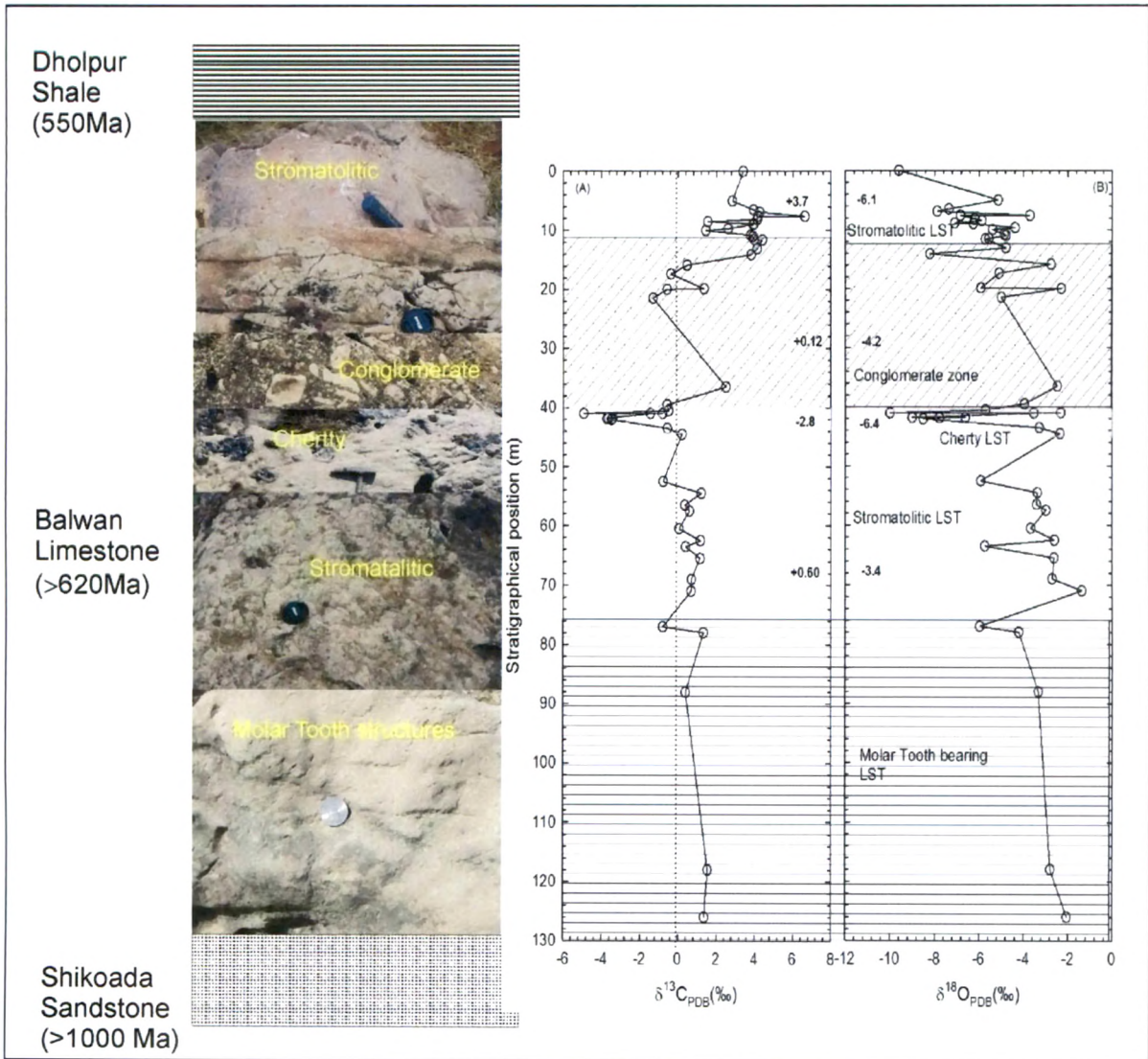


Fig.3.40: $\delta^{13}C$ and $\delta^{18}O$ profiles across the Balwan Limestone near Lakheri Town, Bundi, Rajasthan.

$\delta^{18}\text{O}$ are plotted in Fig. 3.40 for transect 2 (Table 2.6). It was found that the beds below the conglomerate bearing horizon has the lowest $\delta^{13}\text{C}$ composition (-4.9‰) whereas the bed immediate above the conglomerate horizon has the highest $\delta^{13}\text{C}$ (+6.6‰).

As can be seen from the profile in Fig. 3.40, the $\delta^{13}\text{C}$ hovers between values of -1 ‰ and +2 ‰ below the cherty horizon, but becomes more negative (up -5 ‰) within it. It comes back to slightly positive values within the conglomerate zone but becomes highly positive (up +6.6 ‰) in layers above this zone. Such trends are not confined along to one transect, in fact, we have observed this in three transects, along the length of the entire formation, separated by more than a few kilometers (>7km). We, therefore, believe that the negative and positive excursions of $\delta^{13}\text{C}$ in the Balwan Limestone are not a result of any facies variation, instead represent basin wide, if not global, changes in organic matter burial. The negative excursion probably reflects large scale reduction in biology just before the storm or slope failure event and the positive excursion reflects sudden change in biodiversity. Considering the Sr-isotope stratigraphic age for the Balwan Limestone we strongly feel that this storm event could possibly be related to the latest global glaciation event of the Neoproterozoic. However, more research is necessary to substantiate such an inference, since, we have not observed any diamictite horizon within this formation.

3.2.6 Evolution of the Vindhyan Basin in Rajasthan

The geochemical and isotopic studies in the Rajasthan Vindhyan suggest that the sources of the sediments were located in adjoining Aravalli-Delhi fold belt and in the Archean basements. Variations in chemical parameters across the supergroup support classification of the Vindhyan Supergroup into various groups. In general, the boundaries between the four groups are characterized by changes in provenance. The difference in the model ages of the Semri Group and the Kaimur Group in Rajasthan reflects the dynamic nature of tectono-geomorphic setting in this part of

the basin compared that in the Son Valley sector. The protoliths of the Vindhyan sediments, most likely, were located within a magmatic arc setting, the remnants of which may now be located within the pre-Vindhyan fold belts to the west of the basin. The presence of a subduction zone in the Aravalli-Delhi belt during Neoproterozoic and Paleoproterozoic time has also been proposed by earlier workers (Sarkar et al. 1989; Mishra et al. 2000; Leelanandam et al. 2006). Based on the inferences of Chakrabarti et al. (2007) and our results from Rajasthan, and the concept of a Central Indian Suture Zone resulting from a mid Proterozoic collision (Sinha-Roy et al., 1998; Yedekar et al., 1990; Jain et al., 1991; Sinha-Roy and Mohanti, 1988; Sudgen et al., 1990; Raza et al., 1993), a model for the tectono-stratigraphic evolution of the Vindhyan Basin in Rajasthan is proposed below.

The tectonic configuration of the Vindhyan Basin before the deposition began could be understood from the geophysical investigations of Mishra et al. (2000), where they suggested for a collisional zone for the Aravalli and Satpura fold belts during Paleoproterozoic time. This model is a two stage model. During the first stage ~1900Ma, (age of Dharwal granites) due to the Aravalli orogeny, a foreland setting got generated in the eastern flank of the Aravalli mountain chain. Aravalli orogeny also resulted in mafic igneous intrusion, obduction of ophiolites sequences and development of a magmatic arc with andesite volcanism e.g. Khairmalia (Fig. 3.41). These rocks supplied the sediments to the Lower Vindhyan for about 200 million years. The presence of a volcanoclastic sedimentary member (Porcellanite) and evidence for direct input from volcanic ejecta to the Lower Vindhyan sediments and particularly to the Kaimur Group of rocks in the Upper Vindhyan hint at the presence of a very active subduction zone. The initiation of Delhi orogeny in the western flank of the Aravalli Mountain marks the closing of the Lower Vindhyan. After completion of the major Delhi folding at ~ 1400 Ma, the second stage sets in and the Upper Vindhyan start getting deposited. This appears plausible in the light of available geochronological age estimates of the Kaimur Group. The low T_{DM} age of ~1.3 Ga which is similar to the age estimated for the Bijaygarh Shale in the Son Valley supports the inferences that there exists a gap in the sedimentation between

the Lower and the Upper Vindhyan. The low T_{DM} ages of the Rewa and the Bhandar groups (~1.5 Ga and 1.6 Ga) in the Bundi district, which is closer to the Delhi Fold belt, also support the conclusion that the sedimentation in the groups postdates the Delhi orogeny.

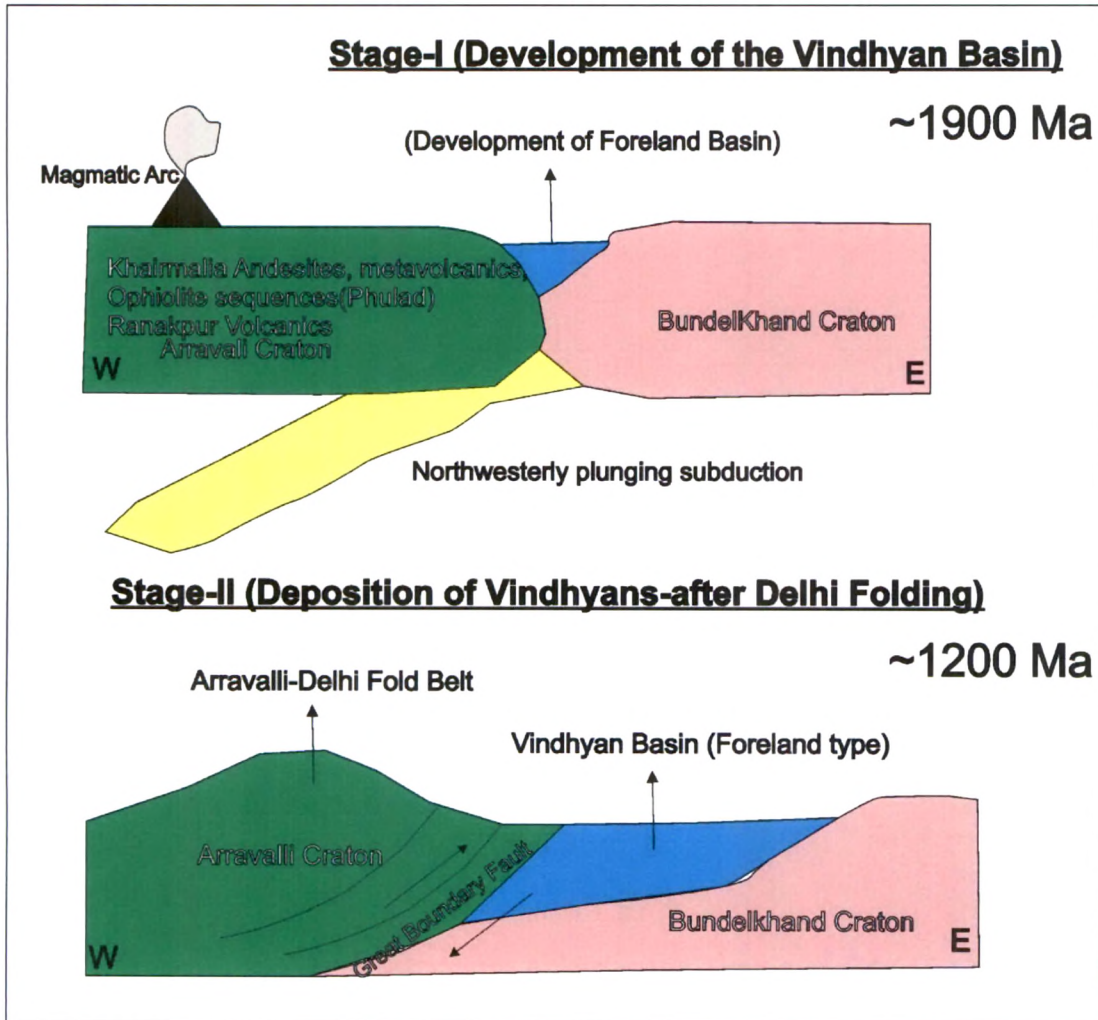


Fig. 3.41: A schematic diagram of our proposed evolutionary model for the Vindhyan Basin in Rajasthan. The collision between the Bundelkhand craton and the Aravalli craton resulted in the formation of the Aravalli-Delhi Mountain Belts subsequent to the subduction of the pre-Vindhyan oceanic crust. The present day GBF and associated faults might be the expressions of this tectonic process.